2014

Hot corrosion behaviour of new candidates for thermal barrier coatings application in turbine simulated environments

Mohammad Hamed Habibi
Louisiana State University and Agricultural and Mechanical College

HOT CORROSION BEHAVIOUR OF NEW CANDIDATES FOR THERMAL BARRIER COATINGS APPLICATION IN TURBINE SIMULATED ENVIRONMENTS

A Dissertation

Submitted to the Graduate Faculty of the
Louisiana State University and
Agricultural and Mechanical College
in partial fulfillment of the
requirements for the degree of
Doctor of Philosophy

in

The Department of Mechanical and Industrial Engineering

by
Mohammad Hamed Habibi
B.S., University of Semnan, 2007
M.S., University of Tehran, 2010
May 2014

To my beloved mother and father,

Mansoureh and Mohammad Hassan

and my supportive sister and brother

Hamideh and Vahid.

Acknowledgements

I would like to express my appreciation and sincere gratuity to Prof. Shengmin Guo, the major professor and committee chairman, for his help, encouragement and great support throughout the research. I would like to thank Prof. Muhammad A. Wahab, Prof. Guoqiang Li, and Dr. Luo, members of my committee, for their time and kind help.

I would also like to thank all my colleagues in the Turbine Innovation and Energy Research Center (TIER) of Louisiana State University for their invaluable discussions, advices and help throughout my dissertation research.

Table of Contents

Acknowledgements iii

List of Figures vii

Abstract x

1. Overview 1
   1.1 Research Objective 2
   1.2 Framework of the Thesis 5

2. Introduction 7
   2.1 High Temperature Environment 7
   2.2 Thermal Barrier Coatings System 9
   2.3 Ceramic Top Coat 9
   2.4 Metallic Bond Coat 11
   2.5 Thermally Grown Oxide (TGO) 11
   2.6 Deposition Methods (APS and EB-PVD) 12
   2.7 Failure Mechanism of TBCs 13
   2.8 Oxidation 14
   2.9 Hot Corrosion- Definition 14
   2.10 Hot Corrosion of Zirconia Based TBCs 15
   2.11 Yttria Stabilized Zirconia (YSZ) 17
   2.12 Disadvantages of Currently Used YSZ 19
   2.13 New Candidates for TBCs 20

3. Evolution of Hot Corrosion Resistance of YSZ, $Gd_2Zr_2O_7$, and $Gd_2Zr_2O_7$+YSZ Composite Thermal Barrier Coatings in Na_2SO_4+V_2O_5 at 1050°C 23
   3.1 Abstract 23
   3.2 Introduction 24
   3.3 Experimental 25
   3.4 Results and Discussion 26
   3.5 Conclusion 39
   3.6 Acknowledgments 40
   3.7 Disclaimer 40

4. Phase Stability and Hot Corrosion Behavior of ZrO_2-Ta_2O_5 Compound in Na_2SO_4-V_2O_5 Mixtures at Elevated Temperatures 41
   4.1 Abstract 41
   4.2 Introduction 41
   4.3 Experimental Procedure 43
   4.4 Results 44

4.5 Discussion 50
4.6 Conclusions 54
4.7 Disclaimer 55
4.8 Acknowledgments 55

5. An Investigation on Hot Corrosion Behavior of YSZ-Ta_2O_5 in Na_2SO_4+V_2O_5 Salt at 1100˚C 56
5.1 Abstract 56
5.2 Introduction 56
5.3 Material and Methods 59
5.4 Results and Discussion 62
5.5 Conclusions 70
5.6 Disclaimer 71
5.7 Acknowledgments 71

6. Evolution of Hot Corrosion Behavior of YSZ-Ta_2O_5 Composites with Different YSZ/Ta_2O_5 Ratios 72
6.1 Abstract 72
6.2 Introduction 72
6.3 Experimental Procedure 76
6.4 Phase Stability and Hot Corrosion Behavior of 0TaYSZ, 10TaYSZ, 20TaYSZ and 30TaYSZ 78
6.5 Phase Stability and Hot Corrosion Behavior of 40TaYSZ, 50TaYSZ, 60TaYSZ and 70TaYSZ 82
6.6 Summary and Conclusion 89
6.7 Disclaimer 90
6.8 Acknowledgments 90

7. The Hot Corrosion Behavior of Plasma Sprayed Zirconia Coatings Stabilized with Yttria, Ceria, and Titania in Na_2SO_4+V_2O_5 91
7.1 Abstract 91
7.2 Introduction 91
7.3 Experimental Procedure 94
7.4 Results 95
7.5 Discussion 100
7.6 Conclusions 105
7.7 Disclaimer 105
7.8 Acknowledgments 106

8. Summary and Conclusions 107

References 110

Appendix A: Letters of Permission to Use Published Material 122

Vita… 127

List of Figures

Figure 2.1 Temperature capabilities of several classes of alloys[1]. 8

Figure 2.2 A schematic diagram of TBC components which is applied to turbine blade and the temperature drop across TBC[9]. 10

Figure 2.3 Schematic cross-sections of TBCs produced by a)APS and b) EB-PVD[16]. 13

Figure 2.4 Acidity and reaction behavior and products for the various ceramic oxides with vanadium compound[19]. 16

Figure 2.5 TBC composition selection is based on durability[1]. 18

Figure 2.6 Phase diagram of the Y_2O_3-ZrO_2 system [17]. 18

Figure 3.1 Temperature profile of hot corrosion test 26

Figure 3.2 XRD patterns of as-received A) conventional YSZ, B) $Gd_2Zr_2O_7$+YSZ, C) $Gd_2Zr_2O_7$ 28

Figure 3.3 Cross-section of APS coatings A) conventional YSZ, B) $Gd_2Zr_2O_7$+YSZ, C) $Gd_2Zr_2O_7$ 29

Figure 3.4 XRD patterns of A) conventional YSZ, B) $Gd_2Zr_2O_7$+YSZ, C) $Gd_2Zr_2O_7$ after hot corrosion in Na_2SO_4+V_2O_5 at 1050ºC 30

Figure 3.5 SEM surface images of A) conventional YSZ, B) $Gd_2Zr_2O_7$+YSZ, C) $Gd_2Zr_2O_7$ after hot corrosion in Na_2SO_4+V_2O_5 at 1050ºC 31

Figure 3.6 EDS spectra from the surface of the coatings A) crystal at region A in Figure 3.5A, B) crystal at region A in Figure 3.5C, C) region B in Figure 3.5C 32

Figure 3.7 Cross-section of A) conventional YSZ, B) $Gd_2Zr_2O_7$+YSZ, C) $Gd_2Zr_2O_7$ after hot corrosion in Na_2SO_4+V_2O_5 at 1050ºC 37

Figure 3.8 Cross section along the crack of a delaminated YSZ coating after hot corrosion in Na_2SO_4+V_2O_5 at 1050ºC 38

Figure 4.1 XRD patterns of as-received A) YSZ, B) 30TaSZ, C) 50TaSZ and D) 70TaSZ 45

Figure 4.2 SEM images of as-received sintered A) YSZ, B) 30TaSZ, C) 50TaSZ and D) 70TaSZ 46

Figure 4.3 XRD patterns of A) YSZ, B) 30TaSZ, C) 50TaSZ and D) 70TaSZ after hot corrosion in $Na_2SO_4 + V_2O_5$ at 1100˚C for 40 hours 47

Figure 4.4 SEM surface images of A) YSZ, B) 30TaSZ, C) 50TaSZ, D) 70TaSZ after hot corrosion in $Na_2SO_4 + V_2O_5$ at 1100˚C for 40 hours. 48

Figure 4.5 XRD patterns of as-received A) 30TaYSZ, B) 30TaSZ 49

Figure 4.6 XRD patterns of A) 30TaYSZ, B) 30TaSZ after hot corrosion in $Na_2SO_4 + V_2O_5$ at 1100˚C for 40 hours 50

Figure 4.7 SEM surface images of A) 30TaYSZ, B) 30TaSZ, after hot corrosion in $Na_2SO_4 + V_2O_5$ at 1100˚C for 40 hours. 51

Figure 5.1 Surface of as received specimen A) before and B) after charging with salt mixuture for hot corrosion 61

Figure 5.2 Surface of YSZ sample after hot corrosion in $Na_2SO_4 + V_2O_5$ at 1100˚C after 40 hours 61

Figure 5.3 XRD patterns of as-received (A) YSZ, (B) TaYSZ. 63

Figure 5.4 XRD patterns of samples after hot corrosion in $Na_2SO_4 + V_2O_5$ at 1100˚C (A) YSZ, after 40 hours and (B) TaYSZ, after 80 hours. 65

Figure 5.5 SEM surface images of YSZ A) after 2 cycles, B) after 5 cycles, C) after 7 cycles, D) after 10 cycles, hot corrosion in $Na_2SO_4 + V_2O_5$ at 1100˚C 67

Figure 5.6 SEM surface images of TaYSZ after hot corrosion in $Na_2SO_4 + V_2O_5$ at 1100˚C after 80 hours. 69

Figure 5.7 EDS spectra from the surface of TaYSZ after hot corrosion in $Na_2SO_4 + V_2O_5$ at 1100˚C after 80 hours (Figure 5.6) (A) crystal at region A in Figure 5.6B, (B) crystal at region B in Figure 5.6B, and (C) matrix in Figure 5.6C. 70

Figure 6.1 XRD patterns of as-received A) 0TaYSZ, B) 10TaYSZ, C) 20TaYSZ and D) 30TaYSZ 79

Figure 6.2 XRD patterns of A) 0TaYSZ, B) 10TaYSZ, C) 20TaYSZ and D) 30TaYSZ after hot corrosion in $Na_2SO_4 + V_2O_5$ at 1100˚C for 40 hours 80

Figure 6.3 SEM surface images of A) 0TaYSZ, B)10TaYSZ, C) 20TaYSZ, D) 30TaYSZ , hot corrosion in $Na_2SO_4 + V_2O_5$ at 1100˚C for 40 hours..... 83

Figure 6.4 XRD patterns of as-received E) 40TaYSZ, F) 50TaYSZ, G) 60TaYSZ and H) 70TaYSZ..... 84

Figure 6.5 XRD patterns of E) 40TaYSZ, F) 50TaYSZ, G) 60TaYSZ and H) 70TaYSZ after hot corrosion in $Na_2SO_4 + V_2O_5$ at 1100˚C for 40 hours 85

Figure 6.6 SEM surface images of A) 40TAYSZ, B) 50TaYSZ, C) 60TaYSZ, D) 70TaYSZ, after hot corrosion in $Na_2SO_4 + V_2O_5$ at 1100˚C for 40 hours 86

Figure 7.1 Cross-section SEM images of as received APS coatings A) YSZ, B) CSZ, C) TiSZ 96

Figure 7.2 XRD patterns of as-received A) YSZ, B) CSZ, C) TiSZ 97

Figure 7.3 XRD patterns of A) YSZ after 20 h, B) CSZ after 28 h, C) TiSZ after 40 h, hot corrosion in Na_2SO_4+V_2O_5 at 1050ºC 97

Figure 7.4 SEM surface images of A) YSZ after 5 cycles and B) CSZ after 7 cycles, hot corrosion in Na_2SO_4+V_2O_5 at 1050ºC 99

Figure 7.5 SEM surface images of TiSZ A) after 5 cycles, B) 10 cycles and C) 10 cycles (higher magnification), hot corrosion in $Na_2SO_4 + V_2O_5$ at 1050˚C 100

Figure 7.6 Cross-section SEM Images of APS coatings (A) YSZ, (B) CSZ, (C) TiSZ after hot corrosion in $Na_2SO_4 + V_2O_5$ at 1050˚C..... 103

Abstract

Thermal barrier coatings (TBCs) are used gas turbine engines. The current material of choice (YSZ) degrades when it contacts with impurities arise from low quality fuels such vanadium and sulfur. YSZ cannot be used in temperature higher than 900˚C. Higher efficiency and performance of gas turbine engines will require a new generation of thermal barrier coatings (TBCs).

In current work, hot corrosion behavior of new candidates including $Gd_2Zr_2O_7$, ZrO_2 stabilized with Ta_2O_5, zirconia stabilized with both Ta_2O_5 and Y_2O_3 and zirconia stabilized with CeO_2 and TiO_2 is investigated.

For YSZ case, the reaction between $NaVO_3$ and Y_2O_3 produces YVO_4 and leads to the transformation of tetragonal ZrO_2 to monoclinic ZrO_2. Comparing to YSZ, under a temperature of 1050 °C, $Gd_2Zr_2O_7$ is found to be more stable, both thermally and chemically, than YSZ, and exhibits a better hot corrosion resistance.

To examine the effect of stabilizing zirconia with tantalum oxide, different compositions of ZrO_2-Ta_2O_5 samples in the presence of molten mixture of Na_2SO_4 + V_2O_5 at 1100˚C were tested. Hot corrosion results show that orthorhombic zirconium-tantalum oxide is more stable, both thermally and chemically in Na_2SO_4+V_2O_5 media at 1100˚C, and shows a better hot corrosion resistance than the tetragonal phase.

When zirconia stabilized with yttria and tantalum oxide (TaYSZ sample), minor amounts of $NaTaO_3$, $TaVO_5$ and Ta_9VO_{25} are formed as the hot corrosion products with only traceable amounts of YVO_4. Due to the synergic effect of doping of zirconia with both Y_2O_3 and Ta_2O_5, the TaYSZ sample has a much better hot corrosion resistance than YSZ.

In zirconia stabilized with CeO_2 coating, the formation of $CeVO_4$ crystals possibly postponed the formation of YVO_4 and transformation of tetragonal zirconia to monoclinic. On surface of zirconia stabilized with TiO_2 coating, $TiVO_4$ crystals are significantly smaller (about 5µm in length) than the large plate shaped YVO_4 and $CeVO_4$ found on the YSZ and CSZ samples. TiSZ coating was found to have a better hot corrosion resistance at a temperature of 1050˚C than both YSZ and CSZ coatings.

1 Overview

Over the past 50 years the development of high temperature materials has been a primary method of increased operating temperatures for gas turbine engines. This has led to higher turbine power and efficiency. Future improvements are impeded by a slowing in the development of materials with even higher temperature capabilities. Nickel based superalloys are currently the material of choice for gas turbine blades. These alloys have the required combination of strength and toughness at high temperatures. Alloy development approaches have enabled significant advances in material performance but further improvements appear unlikely since they now operate in environments where the temperature approaches 80% of their melting point. This fact made researchers to search for other concepts to reduce the superalloy temperature during service and limit thermally induced failure of the gas turbine blades.

Nowadays, coatings are commonly used on the metallic parts of engines to protect against severe high temperatures environments. Ceramic thermal barrier coatings (TBCs) are widely used in hot sections of gas turbines as thermal insulation to promote their operating temperature and enhance the engine efficiency. Yttria Stabilized Zirconia (YSZ) is currently the material of choice for thermal barrier coatings application. The life of TBCs depends on several factors. Among them the resistance of TBCs to high temperature corrosion is very important. YSZ cannot be used at temperature more than 900-1000˚C because of phase transformation and hot corrosion issue. To achieve higher turbine efficiency and better thermal durability, next generation TBCs should be used instead of YSZ.

Many new TBCs materials have been proposed to achieve low thermal conductivity, high temperature capability and higher hot corrosion and oxidation resistivity of the coating systems.

Since TBCs are used in environment operated with low quality fuels, it should be noted that the hot corrosion resistance mechanism of the TBC material against different kinds of corrosive environments is one of the imperative factors that must be taken into account along with other factors such as thermal conductivity, phase stability and thermal expansion coefficient of the TBC material while exploring for new TBC materials.

1.1 Research Objective

The objective of this research is finding novel candidate for next generation thermal barrier coatings. The first step is studying potential ceramic materials characteristics with regard to their availability. Samples had been made with either with Air Plasma Spray method or conventional pressing and sintering method. Only sprayable powders can be fed in plasma spray chambers. These ceramic oxide powders should have specific morphology, particle size and microstructures. The second step is studying phase stability and the high temperature corrosion behavior of samples in turbine simulated environment. In this investigation, attempts were made to thoroughly understand the thermochemical degradation mechanisms of different TBCs by various possible corrosive molten deposits.

To start with, hot corrosion studies of YSZ coatings by sulfate and vanadate melts were performed. A clear understanding of hot corrosion reactions by which YSZ and MCrAlY coatings degrade by molten deposits would help as a basic theory for development of protective coatings for gas turbine applications. With a motivation to identify promising engineering materials that withstand severe high temperature environments, various ceramic oxides were reviewed.

The important issue is to understand chemical reactions and physical changes that occur at the molten salt/TBC and bondcoat/topcoat interfaces. The chemical properties of contaminant salts are important to gain a fundamental understanding of how these salts react with TBC top coats with engineered chemistry. This understanding is eventually going to be used to create and develop TBCs that are resistant to hot corrosion degradation.

According to the history of TBC development in literature, alternative coating materials other than the YSZ system has consisted of two main approaches: (I) alternative materials to ZrO_2-based systems, and (II) alternative stabilizers to Y_2O_3 for ZrO_2-based systems.

An alternate material to zirconia based top coats is $A_2B_2O_7$-type rare-earth zirconate ceramic, such as $La_2Zr_2O_7$, $Nd_2Zr_2O_7$, $Gd_2Zr_2O_7$ and $Sm_2Zr_2O_7$, have been shown recently to have lower thermal conductivity, higher melting points, relatively higher thermal expansion coefficients (TEC), higher stability, and better ability to accommodate defects than YSZ. Thus $Gd_2Zr_2O_7$ was selected and phase stability and high temperature reactivity of $Gd_2Zr_2O_7$ and composite $Gd_2Zr_2O_7$+YSZ have been studied.

There are several oxides which can be used as stabilizer of zirconia rather than yttria. Literature review reveals that previous researchers investigated various stabilizers including MgO, Y_2O_3, Sc_2O_3, In_2O_3, CeO_2, and SmO_2. An alternate approach to YSZ TBC improvement is using Ta_2O_5 as a co-doped stabilizer. Ta_2O_5 has a melting point over 1800˚C. On heating it undergoes a phase transformation at 1360˚C which is well above the typical turbine surface temperatures. Data in literature indicate defect association between the larger oxide of Y and the smaller oxide of Ta in YSZ. According to acid-base Lewis chemical reactions, by virtue of Ta's position in the periodic table, tantalum is more acidic than vanadium. Thus, the ZrO_2-Ta_2O_5 is expected to be substantially more resistant to corrosion by the acidic oxides than ZrO_2-Y_2O_3. So, first Ta_2O_5

was used as single stabilizer of zirconia and then Zirconia samples doped with both yttria and tantalum oxide have been made and phase stability and hot corrosion behavior of ZrO_2-Ta_2O_5 and ZrO_2-Ta_2O_5-Y_2O_3 were studied.

To achieve the overall objective, the following goals were identified, and the corresponding work was carried out.

- To understand the degradation mechanisms of the plasma sprayed YSZ TBCs by corrosive compounds that exist in low quality fuels such as V_2O_5, Na_2SO_4 and a Na_2SO_4+V_2O_5 mixture.
- To obtain a thorough understanding on degradation through hot corrosion of the plasma sprayed MCrAlY coatings by corrosive salts.
- To find promising engineering materials in order to protect the current generation gas turbine blade from such molten deposit-induced environmental damage.
- To Find and optimize spraying parameters for depositing $Gd_2Zr_2O_7$ on Inconel substrate
- To Investigate the phase stability and hot corrosion behavior of $Gd_2Zr_2O_7$ and composite $Gd_2Zr_2O_7$+YSZ TBCs at turbine simulated environment
- To make composite of ZrO_2-Ta_2O_5 and ZrO_2-Ta_2O_5-Y_2O_3 sample with different material ratio, using conventional pressing and sintering method and to find optimized pressing pressure and sintering time and temperature for different samples
- To study phase stability and hot corrosion behavior of ZrO_2-Ta_2O_5 and ZrO_2-Ta_2O_5-Y_2O_3 composite samples.
- To Find and optimize spraying parameters for depositing zirconia stabilized with CeO_2 and TiO_2 on Inconel substrate
- To study hot corrosion behavior of zirconia stabilized with CeO_2 and TiO_2

1.2 Framework of the Thesis

The findings of the present work are organized in eight chapters.

In chapter I, the review fir this research, goals and motivation of the present work and report outline were reviewed.

The introduction in chapter II addresses gas turbine environment, material aspects of thermal barrier systems for advanced gas turbines, hot corrosion definition and outlines for finding new candidates for TBCs.

Chapter III presents the background for choosing rare earth zirconate $Gd_2Zr_2O_7$ as one potential candidate for TBC application. Experimental procedure for depositing this material is explained and finally results and discussion about hot corrosion behavior of YSZ, $Gd_2Zr_2O_7$ and composite $Gd_2Zr_2O_7$+YSZ TBCs have been presented.

In chapter IV, Ta_2O_5 as new candidate for stabilizing of zirconia rather than Y_2O_3 was introduced. Then experimental procedure for fabricating samples in ZrO_2-Ta_2O_5 system was presented. Hot corrosion mechanism and phase stability of different ZrO_2-Ta_2O_5 samples identified and presented in this chapter.

Chapter V presents the effect of Ta_2O_5 as co-dopant of ZrO_2 on hot corrosion behavior of YSZ in turbine simulated environment. TaYSZ sample (50 Wt. % YSZ+ 50 Wt. %Ta_2O_5) was made and hot corrosion behavior of this sample in Na_2SO_4+V_2O_5 at 1100˚C temperature was studied.

In chapter VI, eight samples were made with different YSZ-Ta_2O_5 ratio and hot corrosion behavior of these samples in Na_2SO_4+V_2O_5 at 1100˚C temperature was studied and compared with the others.

Chapter VII presents the experimental procedure for depositing CSZ and TiSZ. The hot corrosion behavior of YSZ, CSZ and TiSZ in Na_2SO_4+V_2O_5 at 1100˚C temperature was compared.

All used references were presented in chapter VIII.

2 Introduction

2.1 High Temperature Environment

Many industrial processes operate in very aggressive environments characterized by high temperature, increased temperature gradients, high pressure, large stresses on individual components, and the presence of oxidizing and corroding atmosphere[1].

The generation of large amounts of heat and associated high component temperature lie at the heart of all of these processes. For example, in gas turbine engines, fuel is mixed with highly compressed air and the mixture ignited. As a result of the heat generated, the air expands and works on the turbine to rotate it. The turbine in turn forces the compressor to rotate, which compresses the incoming air. The exiting exhaust gas creates thrust for propulsion [1-3]. For best performance, the combustion temperature should be maximum obtainable from the complete combustion of the oxygen and the fuel. However, turbine inlet temperature currently cannot exceed 1100˚C because of materials limit[4].

All these processes require materials of construction with high-temperature capability under load to meet performance and durability requirements. During operation, the structural materials of individual components degrade. In addition to fatigue and creep damage of structurally loaded components, the materials undergoes oxidation, corrosion, and erosive wear[1, 2].

The most advanced metallic alloy which is used in high pressure and temperature environment such as hot sections of gas turbine is nickel super alloys. This is a unique class of complex alloys based on Ni and Co that not only exhibits extraordinarily high strength but also maintains strength across a wide elevated temperature range, hence the name super alloys. The range of

strengths of these classes of alloys as a function of temperature in comparison with the other alloys is presented in Figure 2.1[1].

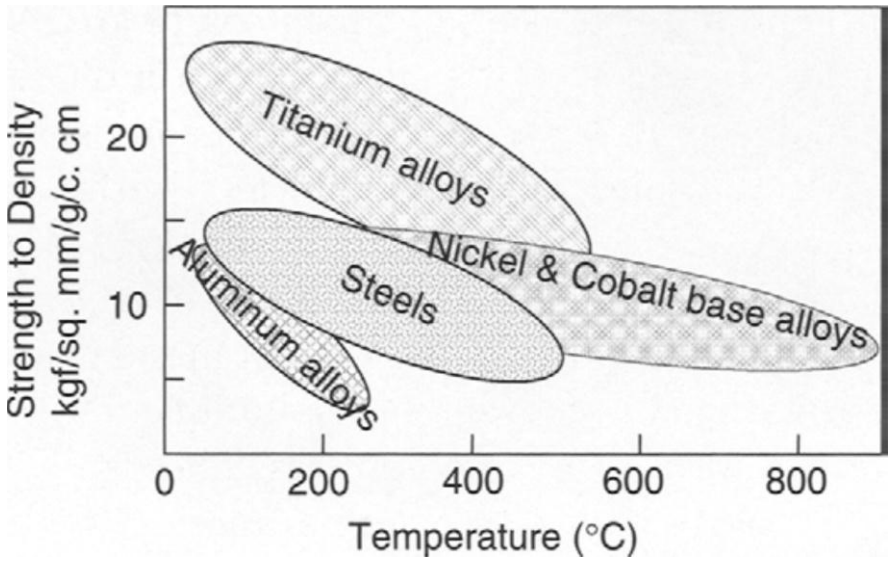

Figure 2.1Temperature capabilities of several classes of alloys[1].

Despite excellent fatigue and creep properties, if nickel super alloys are exposed to the high temperature turbine environment, they will degrade fast by oxidation and high temperature corrosion [1, 3, 5].

When a substrate material has to be chosen for its bulk design properties that are in contradiction with the requirements for its surface design properties, coating is applied to the substrate to meet its engineering requirement. The bulk material provides necessary mechanical strength for the component. Coating protects the component effectively from a variety of environmental degradation factors such as abrasion, erosion, wear, oxidation and corrosion[1, 2]. The only way to protect substrate metallic material against severe high temperature environments in gas turbine is using ceramic coatings. The coatings provide barriers between metallic alloys and environments.

2.2 Thermal Barrier Coatings System

Nowadays, coatings are commonly used on the metallic parts of engines to protect against severe high temperatures environments. Ceramic thermal barrier coatings (TBCs) are widely used in hot sections of gas turbines as thermal insulation to promote their operating temperature and enhance the engine efficiency [6, 7]. TBCs (100 μm to 1 mm thickness) have highly defective, porous microstructures, which impart them with the desirable properties of low thermal conductivity and high strain tolerance[8]. The main function of TBCs is to provide thermal insulation against hot gasses in engines and turbines and thus reduce the surface temperature of the underlying alloy components[9].

Figure 2.2 shows a TBC system applied on the turbine blade and temperature drop across the TBC thickness. In order for TBCs to be effective in reducing surface temperature, the coated component needs to be actively cooled to remove heat conducted through the TBC. The blade, coated with TBC, is actively cooled by cold air from the compressor of gas turbine engines. The cold air is routed through the internal cavity of the blade to remove the heat being conducted through the coatings and the blade walls [1].

2.3 Ceramic Top Coat

Typically, TBCs are multilayered thermal protection systems consisting of a ceramic topcoat for thermal insulation, a thermally grown oxide (TGO) scale, a MCrAlY metallic bond coat that provides oxidation/corrosion resistance and a superalloy substrate (Figure 2.2)[10, 11]. The ceramic top coat can be multilayer of the same or different ceramic materials. One multilayer system is introduced by the concept of functionally gradient material (FGM) into TBCs, which are referred to as FGM TBCs[3].

Functionally Graded Materials (FGM) TBCs are sprayed in the form of multi-layered coatings with a compositional gradient along the thickness direction and no obvious interface layers which provide a gradual transition in mechanical, physical and thermal properties such as thermal expansion coefficient, hardness, residual stress and young modules.

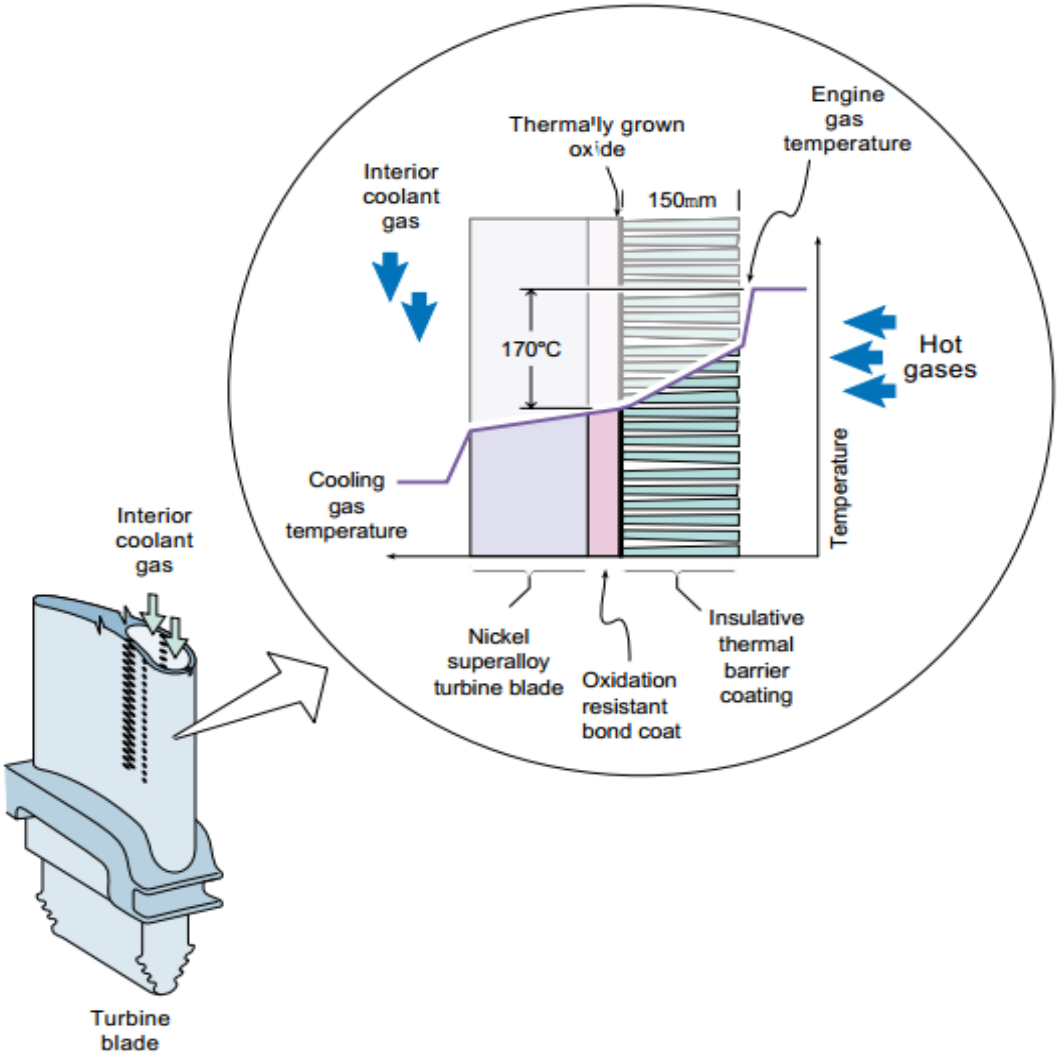

Figure 2.2 A schematic diagram of TBC components which is applied to turbine blade and the temperature drop across TBC[9].

2.4 Metallic Bond Coat

The term bond coat is used to call diffusion aluminide or MCrAlY coatings. The metallic bond coats are deposited between the metallic substrate and the ceramic top coat for increased adherence of the ceramic top coating to the substrate alloy[6]. The bonding between bond coat and substrate is physical. Usually bond coat is used to provide a gradual transition between the mismatch of metallic substrate and ceramic top coat coefficient of thermal expansion (CTE). Although these coatings enhance the bonding between alloy and TBC, their primary function is to increase the high-temperature oxidation and corrosion resistance of underlying structural alloy[3].

2.5 Thermally Grown Oxide (TGO)

The TBC system will have a Thermally Grown Oxide (TGO) that forms between the bond coat and the top coat. TGO is thin thermally grown oxide that slowly forms on the bond coat surface during high-temperature exposure to oxygen which forms a protective layer on the bond coat to prevent the inner surface of it from further oxidation[1, 3, 12]. The TGO is grown to 2–3 μm on the bond coat before the application of the ceramic top coat by a suitable heat treatment process to enhance the adhesion of the latter on the former. The TGO in some cases is grown during the ceramic coat deposition. The growth of the TGO to a thickness of 8–10 μm during the service condition leads to spallation of the TBC. The growth of TGO is controlled mainly by the inward ingression of oxygen anions, rather than the outward diffusion of cations[2].

2.6 Deposition Methods (APS and EB-PVD)

The ceramic top layer is typically applied either by air plasma spray (APS) or by electron beam physical vapor deposition (EBPVD)[13]. Plasma spray deposition is commonly utilized to deposit TBCs onto components such as combustor hardware, turbine outer air seal ring segments, and gas turbine blades [1, 3]. The capital cost in setting up a commercial EB-PVD plant is high, because of this plasma spraying technology is preferred method for TBC deposition up to now[14, 15].

In APS process a plasma jet melts the coating raw material in the form of powder. The plasma is created in a plasma gun. This process is conducted in air, so it is called the air plasma spray (APS) process[1]. In APS, particle size and morphology of powders define whether a certain powder can form a coating with APS method. The particle size of the powder should be around 40 µm. Larger particles tend not to melt completely. Particles finer than 10 µm, on the other hand, do not penetrate the plasma and do not flow in plasma velocity and reach to the surface of substrate. The morphology of the powders is also important because it determines the ability to flow and melt. Usually spherical shape particles have the best ability to flow [1].

The ceramic layer deposited with APS contains 10 to 15 vol. % porosity. Typically, finer powder particle size and closer spray distance result in lower porosity. Also, the interface between the top ceramic layer and the bond coat is rough [1, 3]. In APS, the ceramic top layer is built up of "splatted down" molten droplets and contains a certain amount of porosity. This porosity is highly critical in determining the thermal cycle life of APS TBCs. In contrast, the EB-PVD ceramic top layer consists of columnar particles that are "strain tolerant" and therefore thought to give increased thermal cycle life. Studies indicate that whereas APS coatings generally fail in the zirconia phase just at the bond coat/top coat layer interface, perhaps because

of strains introduced by oxidation of the bond coat, EB-PVD coatings fail within the bond coat oxide that is thermally grown on the bond coat during service life [17].

APS has relatively higher deposition efficiency than EBPVD[14]. MCrAlY bond coat can be deposited by APS or physical vapor deposition (PVD) processes[15]. Figure 2.3 represents the TBC structures deposited with different methods.

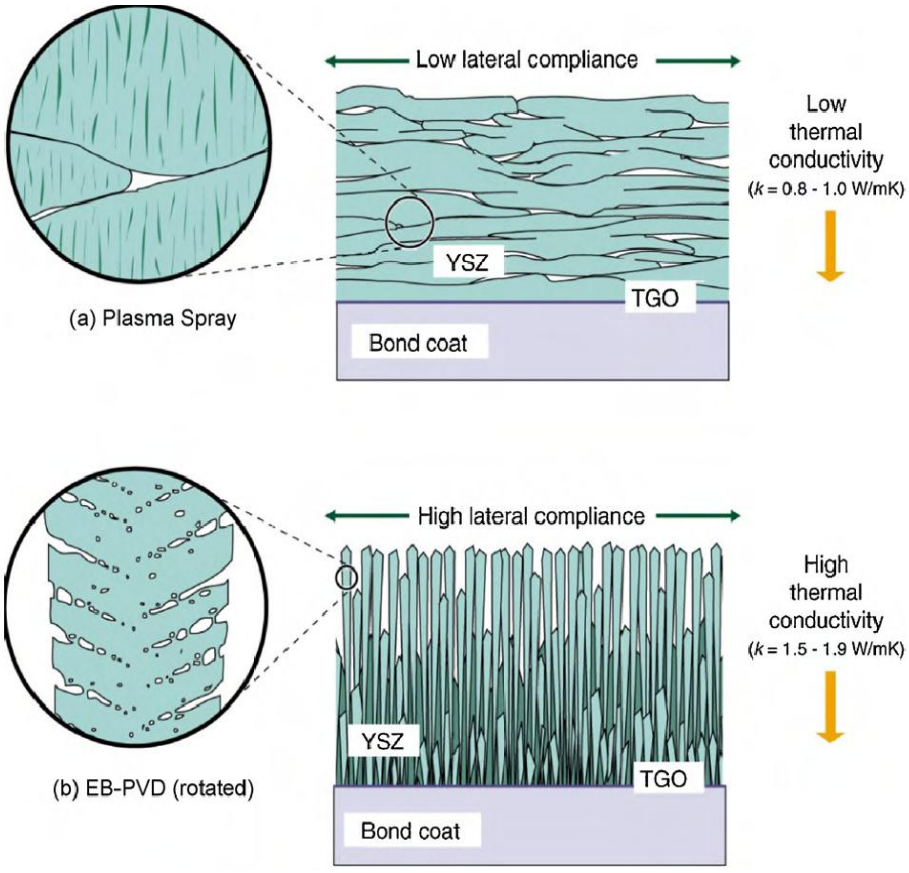

Figure 2.3Schematic cross-sections of TBCs produced by a)APS and b) EB-PVD[16].

2.7 Failure Mechanism of TBCs

There are several failure mechanisms for the TBCs. Four major failure mechanisms are: chemical decomposition of the coating due to penetration of molten salt and reacting with bulk

of coating at high temperatures (hot corrosion), physical damage as a result of an impact by foreign objects especially at lower temperatures, thermal mismatch stress induced at temperature cycles and spallation of the coating from the surface because oxidation of bond coat and metallic substrate. Erosion and hot corrosion are factors that contribute to the degradation of TBCs and become more important in the presence of high heat flux and a corrosive environment. One of these or a combination of many can cause a spallation by a sequence of crack nucleation, and its propagation [1, 3, 17].

2.8 Oxidation

Oxidation is an environmental phenomenon in which metals and alloys (and other materials) exposed to oxygen or oxygen-containing gases at elevated temperatures convert some or all of the metallic elements into their oxides. The oxide can form as a protective scale if it remains adherent, and reduces further oxidation, or may continually spall off, exposing fresh metal which results in progressive metal loss. Additionally, internal oxidation may occur. The technological implications of oxidation lie in the loss of load-bearing capability of the original metal or alloy component, eventually resulting in component failure [1-3].

2.9 Hot Corrosion- Definition

Hot corrosion of alloys and coatings take place in a gas turbine and may be defined as accelerated corrosion at elevated temperature, resulting from the presence of salt contaminants such as Na_2SO_4, V_2O_5 and NaCl that combine to form molten deposits, which damage the protective surface oxides [2, 4]. It is the result of accelerated oxidation at temperatures typically

between 700˚C and 1100˚C when metals, alloys and coatings become covered with contaminant molten salt[1].

There are two types of hot corrosion of alloys and coatings: Type I which is High Temperature Hot Corrosion and Type II which is Low temperature Hot Corrosion Type II hot corrosion is observed mainly within the temperature range of 650-850˚C. Type I hot corrosion is observed within the temperature range of 900-1100˚C [2, 4].

Among the various life-limiting factors, one key durability issue of TBCs is their resistivity to environmental degradation due to molten deposits arising from the aggressive combustion environment as well as from air-ingested foreign particles.

2.10 Hot Corrosion of Zirconia Based TBCs

The principal driving force for the degradation of TBCs by hot corrosion is chemical reaction between the stabilizing oxides (e.g., Y_2O_3, CeO_2, etc.) and the molten vanadate-sulfate engine deposits, or essentially vanadate-sulfate melts[18]. Attack by chemical reaction is characterized by the presence of an identifiable reaction product and usually by the ability to postulate a specific reaction. The laws of stoichiometry and thermodynamics apply; therefore, the conditions for chemical reaction should be predictable based on reactants, products and thermodynamic data[17]. Hot corrosion of ceramics happens with some successive chemical reactions. The reactions of ceramic oxides with vanadium compounds in low quality fuels are predominantly controlled by the Lux-Flood type of acid-base reactions and are explainable in terms of the relative acid-base character of the oxides. The most degradation-resistant stabilizing oxides are likely to be those that are sufficiently acidic to resist reaction with $NaVO_3$ and V_2O_5 but not so acidic as to react with the Na_2O component of $NaVO_3$ [19]. Figure 2.4 compares the acidity of

different oxides and their reaction with vanadium compounds and their products. This concept can be a good help for incorporation of new zirconia stabilizers to resist against hot corrosion chemical reactions.

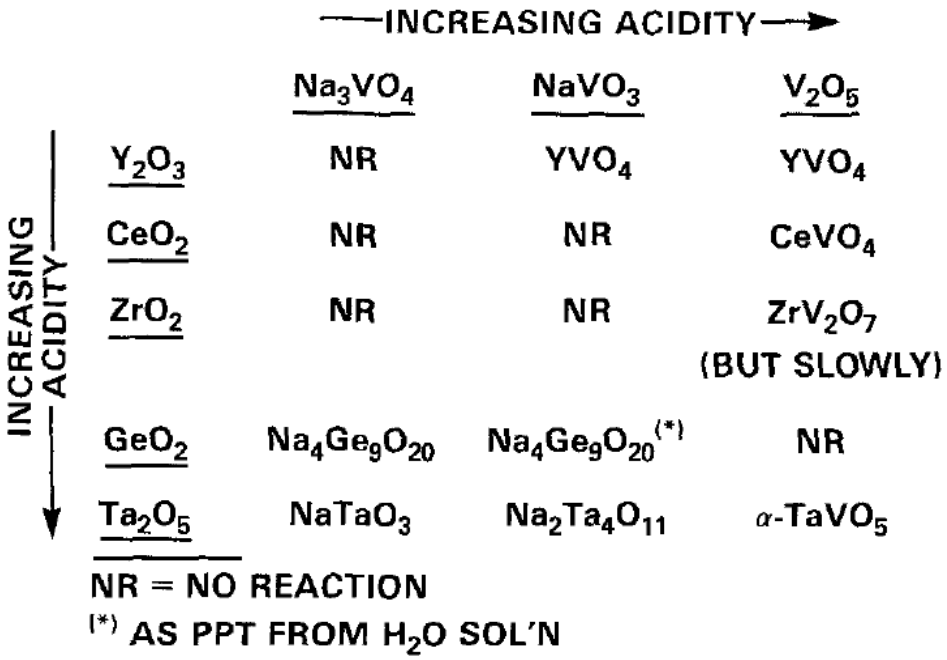

Figure 2.4 Acidity and reaction behavior and products for the various ceramic oxides with vanadium compound[19].

Hot corrosion mechanism of YSZ in media contains Na_2SO_4 and V_2O_5 can be classified as some successive chemical reactions. First Na_2SO_4 and V_2O_5 react with each other and $NaVO_3$ formed. The yttria stabilizer will leach out by the reaction with V_2O_5 or $NaVO_3$ and YVO_4 formed as hot corrosion reaction product, resulting in the transformation of tetragonal or cubic zirconia to monoclinic zirconia accompanied by a destructive volume expansion (3–5%), which finally leads to delamination and spallation of the ceramic top coat[20-22].

2.11 Yttria Stabilized Zirconia (YSZ)

Materials selection for TBC applications is restricted by some basic requirements such as high melting point, no phase transformation between room temperature and operating temperature, low thermal conductivity, chemical stability at high temperatures, thermal expansion match with metallic substrate, good adherence to metallic substrate and low sintering rate of porous microstructure[23].

Therefore, not too many available materials satisfy all the requirements of TBC and the number of materials that can be used as TBCs materials is very limited. Among different ceramic oxides, zirconia showed better compatibility with TBC requirements. Zirconia exhibits three well-defined polymorphs, monoclinic (to 1170˚C), tetragonal (to 2370˚C), and cubic (to the mp at 2680˚C) phase transformation during cyclic heating and cooling. The tetragonal to monoclinic phase transformation is associated with a large volume change (3-5%) which causes stresses and affect the integrity of coating [24].

Alloying zirconia with other oxides such as CaO, MgO, Y_2O_3, CeO_2, Sc_2O_3, and In_2O_3 inhibits the phase transformation, stabilizes the high temperature phase, and eliminates the volume change[24, 25]. Of the various stabilizers available, the yttria stabilized zirconia is preferred based on its adherence to the bonding coat, thermal stress resistance, erosion resistance, and stability[24]. The optimum yttria stabilizer content is approximately 6-8 wt. %. This has been determined by high-temperature durability rig testing at NASA of TBC coating as a function of yttria level. Significantly lower yttria contents do not inhibit the transformation to monoclinic phase, while higher levels stabilize a cubic phase which lacks adequate strength and toughness (Figure 2.5) [1]. The substitution of Y^{3+} for Zr^{4+} in the formation of the solid solutions results in a creation of oxygen-ion vacancies to balance the change in valence[26]. If ZrO_2 containing

about 8 wt.% Y_2O_3 is heated into the cubic or molten phase regions of the Y_2O_3-ZrO_2 phase diagram and then quenched rapidly (as in APS or EB-PVD processing), the non-transformable meta-stable tetragonal phase is produced (Figure 2.6) [17].

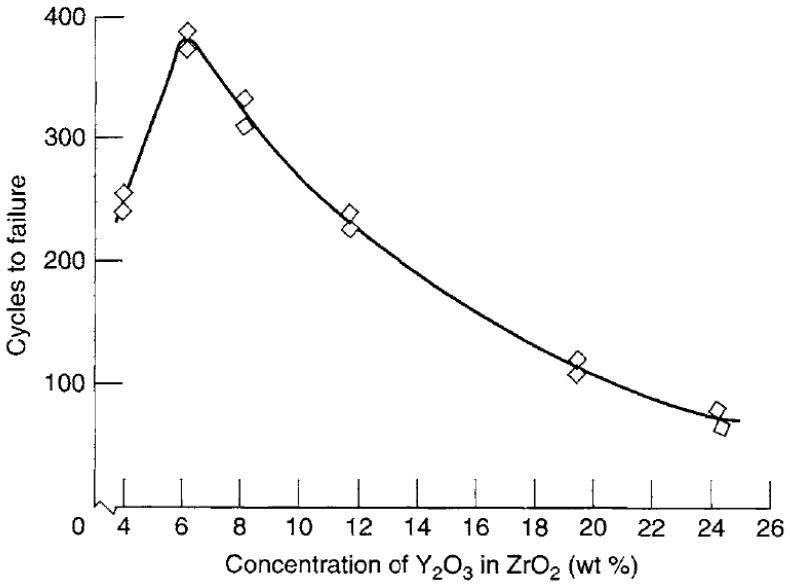

Figure 2.5 TBC composition selection is based on durability[1].

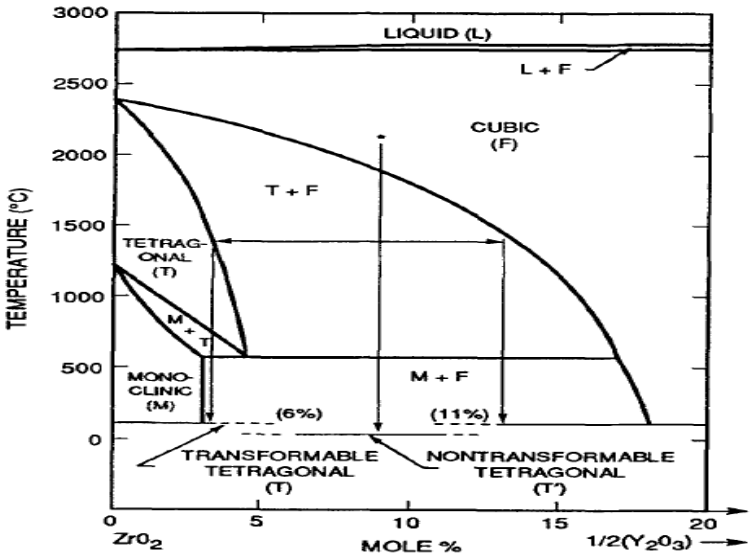

Figure 2.6 Phase diagram of the Y_2O_3-ZrO_2 system [17].

The distorted fluorite structure of tetragonal zirconia, alloyed with about 2 to 3 mol %(about 7-8 Wt. %) Y_2O_3, is a metastable phase at room temperature and has been considered as a structural ceramic because of its excellent mechanical properties, such as fracture toughness, strength, and hardness[26].

2.12 Disadvantages of Currently Used YSZ

The need for enhancing turbine efficiency leads to increasing turbine operating temperature. At high temperatures, YSZ usage become limited due to its phase transformation induced by hot corrosion, transparency and higher thermal conductivity and sintering or densification behavior at higher operating temperatures and corrosive environments. Hence, the reliability of the most widely used TBC top coat composition, i.e. yttria stabilized zirconia (YSZ) coatings, has been weakened [27].

The life of YSZ TBCs depends on several factors. Among them the resistance of YSZ and MCrAlY high temperature corrosion is very important. Thermal barrier coatings are usually operated with low-quality fuel and corrosive environments[28]. The low-quality fuels usually contain impurities, such as sodium, sulfur and vanadium, which can form Na_2SO_4 and V_2O_5 salts and condense on the surface of TBCs[29]. During high temperature exposure of YSZ Based TBCs to molten salt, such salts which penetrate through the micro cracks and open pores of YSZ, react with stabilizer of zirconia and tetragonal to monoclinic phase transformation happens[30]. Also molten salt penetrated through the thickness of YSZ attack bond coat, and then lead to the delamination and spallation of the YSZ top coat from bond coat. In addition, a coefficient of thermal expansion mismatch between bond coat and ceramic topcoat can exasperate the coating

failure during thermal cycles[1]. These happenings cause compressive residual stress leading to TBC failure either in bondcoat/topcoat substrate or entire thickness of topcoat.

2.13 New Candidates for TBCs

Higher performance and durability requirements of gas-turbine engines will require a new generation of thermal barrier coatings (TBCs). Many new TBCs materials have been proposed to achieve low thermal conductivity, high temperature capability and higher hot corrosion and oxidation resistivity of the coating systems. Since TBCs are used in environment operated with low quality fuels, it should be noted that the hot corrosion resistance mechanism of the TBC material against different kinds of corrosive environments is one of the imperative factors that must be taken into account along with other factors such as thermal conductivity, phase stability and thermal expansion coefficient of the TBC material while exploring for new TBC materials. The rising needs of the industrial sector have resulted in the emergence of the concept of developing advanced TBC system against hot corrosive environments.

The search for alternative coating materials other than the well-established YSZ system has consisted of two main approaches: (I) alternative materials to ZrO_2-based systems, and (II) alternative stabilizers to Y_2O_3 for ZrO_2-based systems[31].

In recent years, rare-earth zirconate ceramics working as TBCs materials have drawn more attention due to their higher phase transformation temperature, higher melting points and lower thermal conductivity than that of YSZ [32, 33]. Rare earth zirconate general composition is $A_2B_2O_7$, where A is a $^{3+}$ cation (La to Lu) and B is a $^{4+}$ cation (Zr, Ce, Hf, etc.)[34]. It is well known that the partial or complete substitution of the anions in ion crystal by other elements can enhance the phonon scattering which indicates that the thermal conductivity of $Ln_2Zr_2O_7$

(Ln represents rare earth element) may be reduced further by substitution of Ln or Zr by other elements[33]. Therefore, rare-earth zirconate ceramics such as $La_2Zr_2O_7$, $Nd_2Zr_2O_7$, $Gd_2Zr_2O_7$ and $Sm_2Zr_2O_7$ with pyrochlore structure or defect fluorite-type structure have been considered as potential ceramic materials for thermal barrier coatings for industrial applications[31, 35].

For this research, $Gd_2Zr_2O_7$ was selected and phase stability and high temperature reactivity of $Gd_2Zr_2O_7$ and composite $Gd_2Zr_2O_7$+YSZ have been studied.

Recent studies have been published focusing new methods to reduce thermal conductivity and improve the oxidation resistance, like doping of and co-doping ZrO_2 with trivalent and pentavalent oxides[36]. A comparative analysis of various stabilizers including MgO, Y_2O_3, Sc_2O_3, In_2O_3, CeO_2, SmO_2 appeared in [37]. Scandia- and india-stabilized zirconia have proven more resistant than yttria-stabilized zirconias to corrosion by vanadia [21, 38]. This behavior shows that an oxide whose cation is more acidic than yttrium, such as scandium and indium, would be thermodynamically less prone to react with acidic oxides. Thus, when stabilized with such oxides the zirconia would be more resistant to hot corrosion by acidic oxides [37, 39, 40]. A review of the literatures on the ZrO_2–CeO_2 system reveals that this system is resistant to hot corrosion but can be subject to phase transformation at high temperatures and may exhibit formation of $CeVO_4$ in media with fuels contaminated with high levels of S and V [37, 41] Interestingly, ceria stabilized zirconia (CSZ) is generally acknowledged to have a lower erosion resistance than YSZ [41].

An alternative approach to improve YSZ is the co-doping of yttria with pentavalent oxides such as Ta_2O_5. Ta_2O_5 has a melting point over 1800˚C. On heating it undergoes a phase transformation at 1360˚C which is well above the typical turbine surface temperatures[42]. According to ionic conductivity measurements [43], tantalum ions reside as substitutional defects

in the zirconium lattice, annihilating oxygen vacancies generated by yttria. Data in literature indicate defect association between the larger oxide of Y and the smaller oxide of Ta in YSZ. Such defect association should lower the activity and diffusivity in zirconia solid solution thus make this composition more resistant to hot corrosion [40]. Also, according to acid-base Lewis chemical reactions, by virtue of Ta's position in the periodic table, tantalum is more acidic than vanadium. Thus, the ZrO_2-Ta_2O_5 is expected to be substantially more resistant to corrosion by the acidic oxides than ZrO_2-Y_2O_3 [36, 44, 45].

On the Y_2O_3-Ta_2O_5-ZrO_2 phase diagram at 1500˚C, [45], apart from the tetragonal zirconia phase, formed by equal co-doping of Y_2O_3-Ta_2O_5 into ZrO_2, a stable orthorhombic zirconia phase ($TaZr_{2.75}O_8$) also exists, when ZrO_2 is doped with low level of Y_2O_3 and high level of Ta_2O_5. For this research, Ta_2O_5 was used both as single stabilizer of zirconia and co-dopant stabilizer of zirconia with yttria. Phase stability and hot corrosion behavior of different samples made in ZrO_2-Ta_2O_5 and ZrO_2-Ta_2O_5-Y_2O_3 systems were studied.

3 Evolution of Hot Corrosion Resistance of YSZ, $Gd_2Zr_2O_7$, and $Gd_2Zr_2O_7$+YSZ Composite Thermal Barrier Coatings in Na_2SO_4+V_2O_5 at 1050°C[1]

3.1 Abstract

Thermal barrier coatings (TBCs) are frequently used on hot section components in gas turbines. Corrosive gases coming from the combustion of low grade fuels may penetrate deeply into the coating and lead to the hot corrosion degradation of the coating. This paper compares the hot corrosion performance of yttria stabilized zirconia (YSZ), $Gd_2Zr_2O_7$ and YSZ+$Gd_2Zr_2O_7$ composite coatings in the presence of molten mixture of Na_2SO_4+V_2O_5 at 1050°C. These YSZ and rare earth zirconate coatings were prepared by air plasma spray (APS). Chemical interaction is found to be the major corrosive mechanism for the deterioration of these coatings. Characterizations using X-ray diffraction (XRD) and scanning electron microscope (SEM) indicate that in the case of YSZ, the reaction between $NaVO_3$ and Y_2O_3 produces YVO_4 and leads to the transformation of tetragonal ZrO_2 to monoclinic ZrO_2. For the $Gd_2Zr_2O_7$+YSZ composite coating, by the formation of $GdVO_4$, the amount of YVO_4 formed on the YSZ+$Gd_2Zr_2O_7$ composite coating is significantly reduced, thus the amount of monoclinic phase in the TBC coating is substantially reduced, which renders YSZ+$Gd_2Zr_2O_7$ composite coating a better hot corrosion resistance than that of YSZ. Molten salt is also found to react with $Gd_2Zr_2O_7$ to form $GdVO_4$. Comparing to YSZ, under a temperature of 1050 °C, $Gd_2Zr_2O_7$ is found to be more stable, both thermally and chemically, than YSZ, and exhibits a better hot corrosion resistance.

[1] Chapter 3 previously appeared as [M.H. Habibi, Li Wang and S.M. Guo, Evolution of Hot Corrosion Resistance of YSZ, $Gd_2Zr_2O_7$, and $Gd_2Zr_2O_7$ + YSZ Composite Thermal Barrier Coatings in Na_2SO_4 + V_2O_5 at 1050°C, *Journal of the European Ceramic Society* 32 (2012) 1635–1642]. It is reprinted by permission of *Journal of The European Ceramic Society* (See Appendix A)

3.2 Introduction

Thermal barrier coatings (TBCs) are frequently used on the blades and vanes of gas turbines to provide thermal insulation. By lowering the metal temperature in conjunction with the use of internal cooling and film cooling technology, TBC improves both component durability and engine efficiency [46, 47]. TBC is comprised of a ceramic top layer and a metallic bond coat [17, 48]. The most common top layer is made of yttria partially stabilized zirconia (YSZ) for reducing the temperature of the substrate, and a typical bond coat is the MCrAlY alloy, for efficiently preventing the substrate from oxidation and hot corrosion. Thermal barrier coatings can be fabricated by various processing techniques such as air plasma spray (APS), vacuum plasma spray, HVOF (High Velocity Oxygen Fuel) thermal spray, and electron beam physical vapor deposition (EB-PVD)[49]. Although YSZ based TBC systems have been used widely in gas turbine industry, YSZ is prone to hot corrosion caused by molten salts, such as Na, S and V, contained in low-quality fuels at high working temperatures [41, 50]. The search for alternative coating materials other than the well established YSZ system has consisted of two main approaches: (i) alternative materials to ZrO_2-based systems, and (ii) alternative stabilizers to $Y_2O_3$for ZrO_2-based systems. Significantly, the $A_2B_2O_7$-type rare-earth zirconate ceramics, such as $La_2Zr_2O_7$, $Nd_2Zr_2O_7$, and $Gd_2Zr_2O_7$ and $Sm_2Zr_2O_7$, have been shown recently to have lower thermal conductivity, higher melting points, relatively higher thermal expansion coefficients (TEC), higher stability, and better ability to accommodate defects than YSZ [51-53]. However, for the hot corrosion behavior of $Gd_2Zr_2O_7$ and other rare earth zirconates, most of early studies reported a testing temperature range between 650 to 900ºC. Up to date, no data on hot corrosion behavior of $Gd_2Zr_2O_7$ based coatings in molten salts at temperatures higher than 900ºC can be found in open literatures. In this paper, the hot corrosion behavior of $Gd_2Zr_2O_7$, YSZ, and

$Gd_2Zr_2O_7$+YSZ composite coatings by Na_2SO_4+V_2O_5 mixture is examined at an engine representative temperature of 1050ºC.

3.3 Experimental

Nickel-based superalloy (Inconel 738) disks of Φ25×1.5mm were employed as the substrates. TBCs composed of a ceramic top coating and a NiCrAlY bond coat (Amdry 9625, Sulzer Metco, with particle size 45~75 μm) were deposited onto the superalloy substrates by the atmospheric plasma spray (APS) process. Three types of top coats, YSZ, 50 wt% YSZ+50 wt% $Gd_2Zr_2O_7$and $Gd_2Zr_2O_7$, were made using agglomerated powders. The plasma spraying was carried out using a Sulzer-Metco 9M plasma spray system using an Ar/H_2 gas mixture. The spraying parameters are given in Table 3.1.

To perform an accelerated high-temperature hot corrosion test on TBCs, a mixture of Na_2SO_4+V_2O_5 deposit was spread onto the surfaces of the TBC specimens with a salt amount of 20 mg/cm^2. The specimens were then set in an electric furnace with an air atmosphere under a maximum temperature of 1050°C for 4 hours, Figure 3.1. After each 4 hours of testing at 1050°C, the samples were allowed to cool down inside the furnace, and then the coatings were inspected using optical microscope for possible crack initiations. The samples were then recoated with the Na_2SO_4+V_2O_5 salt mixture and the heating profile was repeated for nine times. The morphology and microstructure of the as-sprayed TBC coatings and the coatings after the hot corrosion tests were examined using field emission scanning electron microscopy (Quanta 3D FEG, FEI Company, USA). For surface morphology studies, a thin Pt coating was evaporated onto the coating samples for electrical conductivity before they were examined by SEM. To obtain a cross-section, the specimens were first mounted in an epoxy resin. The mounted

specimens were then sectioned with a slow speed diamond cutter and subjected to polishing using a diamond paste (1 μm). X-ray diffraction (MiniFlex XRD, Rigaku Corporation, Japan)

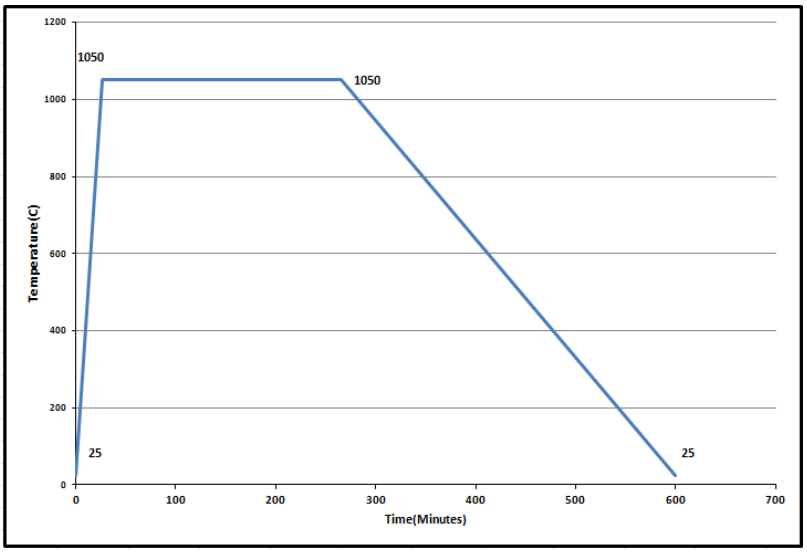

Figure 3.1 Temperature profile of hot corrosion test

with Cu K_α radiation λ=1.54178Å at a scan speed of 1°/min was used to establish the phase composition of the coatings.

Table 3.1. Plasma spraying parameters.

Layer	Arc current (A)	Coating distance (mm)	Plasma gas Ar/H_2(SCFH)	Carrier gas Ar (SCFH)	Powder feed rate (g/min)
Bond coat	500	130	96/15	8	40
Ceramic layer	660	80	64/32	8.4	40

3.4 Results and Discussion

Figure 3.2 reveals the X-ray diffraction patterns for the as-received conventional YSZ, $Gd_2Zr_2O_7$+YSZ, and $Gd_2Zr_2O_7$ coatings. It can be seen that the major phase of the APS coated YSZ is tetragonal zirconia, $Gd_2Zr_2O_7$+YSZ coating includes both tetragonal ZrO_2 and $Gd_2Zr_2O_7$

phases, and $Gd_2Zr_2O_7$ has a single phase as expected. The cross-sectional microstructure of APS YSZ, $Gd_2Zr_2O_7$+YSZ and $Gd_2Z_2O_7$ TBC specimens are shown in Figure 3.3. All layers of the as-sprayed specimens have similar microstructures with a noticeable level of porosity without any visible cracks. For the as-sprayed TBC samples, no delamination can be found along the YSZ / $Gd_2Zr_2O_7$+YSZ / $Gd_2Zr_2O_7$ top layer and the NiCrAlY bond coat interface. Figure 3.4 shows the XRD patterns obtained from the YSZ, $Gd_2Zr_2O_7$+YSZ, and $Gd_2Z_2O_7$ coatings after the hot corrosion test with the Na_2SO_4+V_2O_5 salt mixture at 1050ºC. Comparing the patterns of the as-sprayed TBC samples, most of the tetragonal zirconia in the YSZ sample has changed to the monoclinic phase and YVO_4 is formed as a hot corrosion product, while for the other two specimens, besides monoclinic ZrO_2 the newly evolved peak is related to $GdVO_4$.

Typical surface morphologies of YSZ, $Gd_2Zr_2O_7$+YSZ and $Gd_2Zr_2O_7$ specimens after hot corrosion tests are presented in Figure 3.5, with the apparent formation of new crystals. Apart from XRD analysis, Figure 3.4, Energy Dispersive Spectroscopy (EDS) analysis, Figure 3.6, was performed at different regions of the TBC surfaces to confirm the chemical compositions of the hot corrosion products.

EDS analysis from region A on Figure 3.5A demonstrated that the crystals were composed of yttrium, vanadium and oxygen, then they were identified by XRD analysis to be YVO_4. The EDS spectra obtained at different regions of A and B in Figure 3.5C confirmed the presence of elements consistent with the formation of $GdVO_4$ (region A) and existence of $Gd_2Zr_2O_7$ (region B). For Gd_2VO_4 specimen, small amount of zirconium coming from the background was also detected (Figure 3.6C). For the conventional YSZ TBC coating, after hot corrosion tests for 20 hours at peak temperature of 1050°C (five 4-hours cycles), serious degradation and spallation

started to occur, Figure 3.5A. Due to the damage by the Na_2SO_4+V_2O_5 corrodents, a porous layer was formed on the YSZ coating.

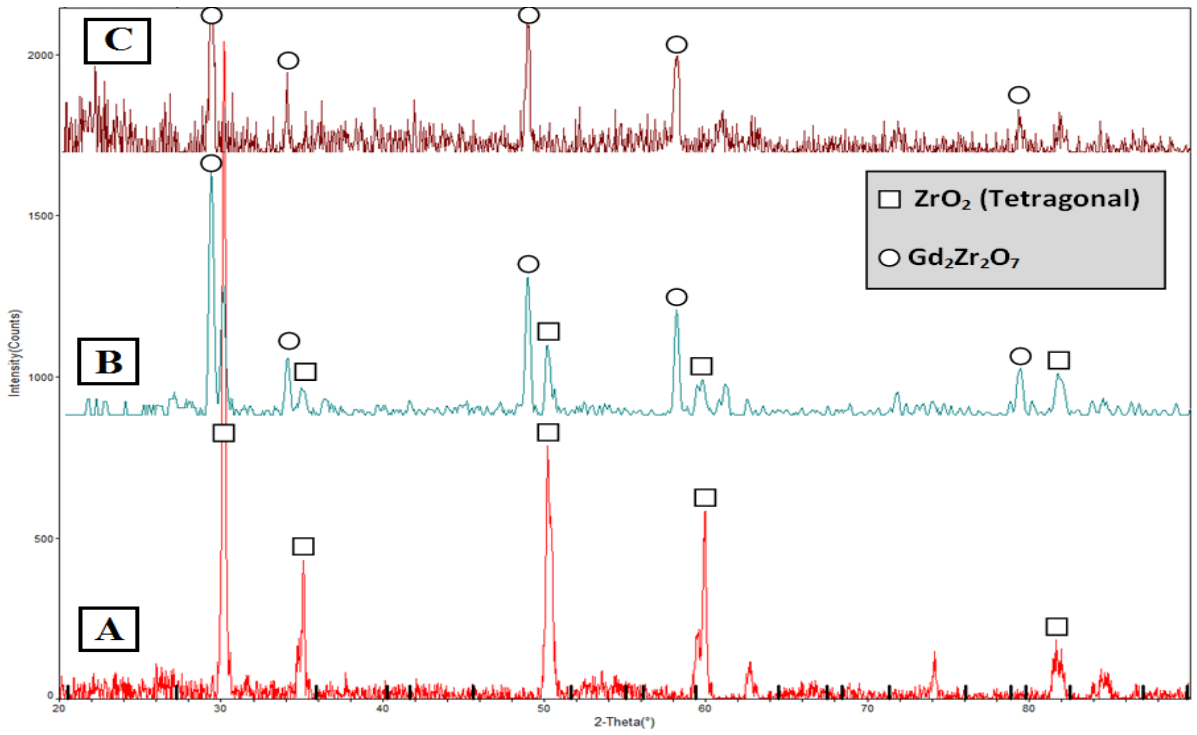

Figure 3.2 XRD patterns of as-received A) conventional YSZ, B) $Gd_2Zr_2O_7$+YSZ, C) $Gd_2Zr_2O_7$

Phase analysis results on these porous areas showed that a large amount of tetragonal zirconia on the surfaces of the conventional YSZ top layer had transformed to monoclinic phase due to the depletion of yttria. In addition, large quantity of rod shaped hot corrosion reaction product, YVO_4, was detected on the surface of the conventional YSZ coating. Similar findings have been reported by other researchers [21, 22, 41]. For the $Gd_2Zr_2O_7$+YSZ and $Gd_2Zr_2O_7$ coating, the corrosion products are $GdVO_4$ and YVO_4 as well as monoclinic ZrO_2. In Figure 3.5B, it is obvious that some regions are perfectly intact and the major phase in these areas is $Gd_2Zr_2O_7$.

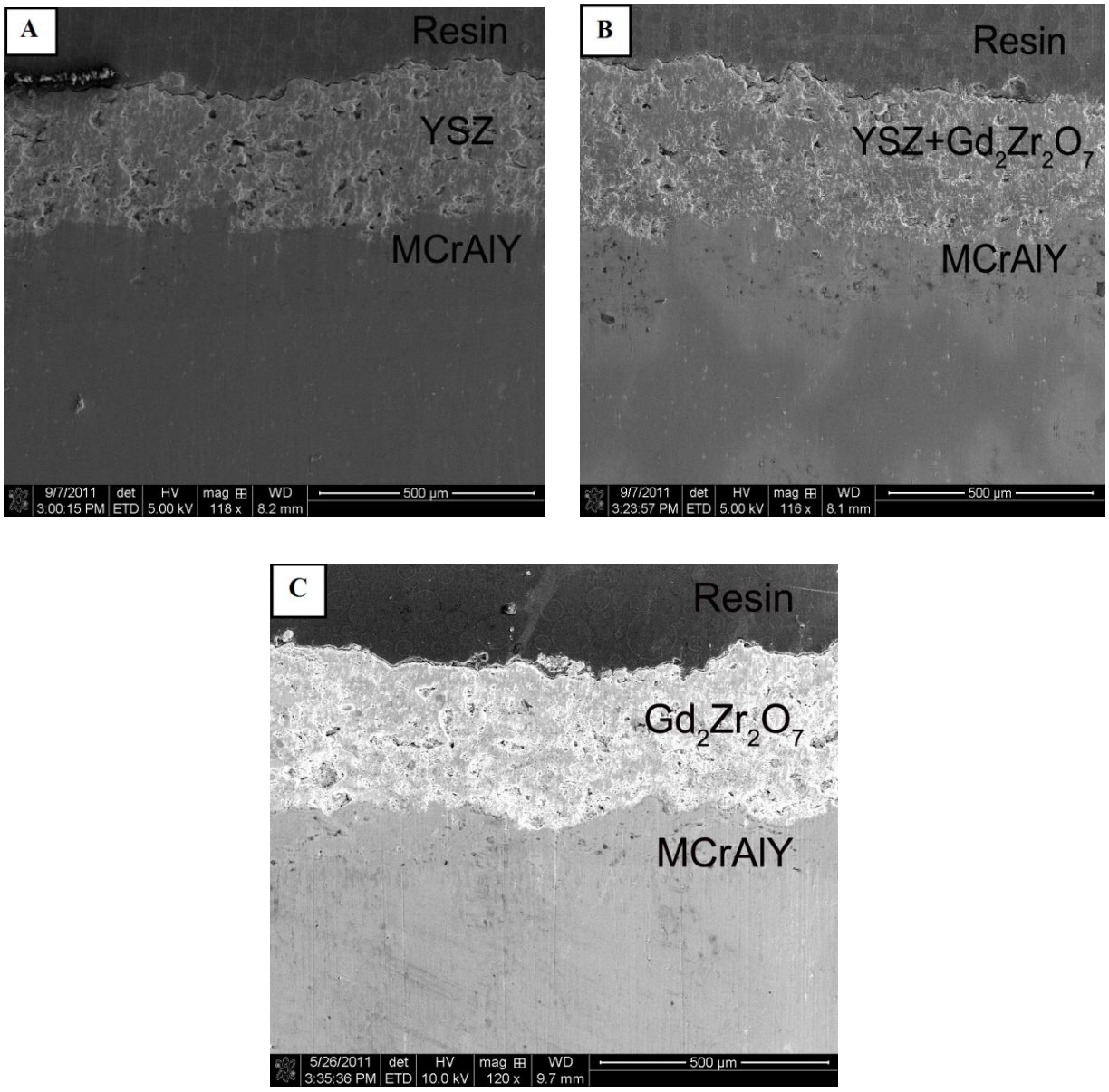

Figure 3.3 Cross-section of APS coatings A) conventional YSZ, B) $Gd_2Zr_2O_7$+YSZ, C) $Gd_2Zr_2O_7$

. Compare to YVO_4, the $GdVO_4$ crystals are much smaller in size and quantity and they have a unique dendrite shape. For the YSZ sample, after hot corrosion tests, large quantity of rod shaped YVO_4 crystals are visible on the coating surfaces. After exposure to molten salt at 1050ºC for 20 hours (five 4-hours cycle), spallation and delamination started to occur in conventional YSZ coating.

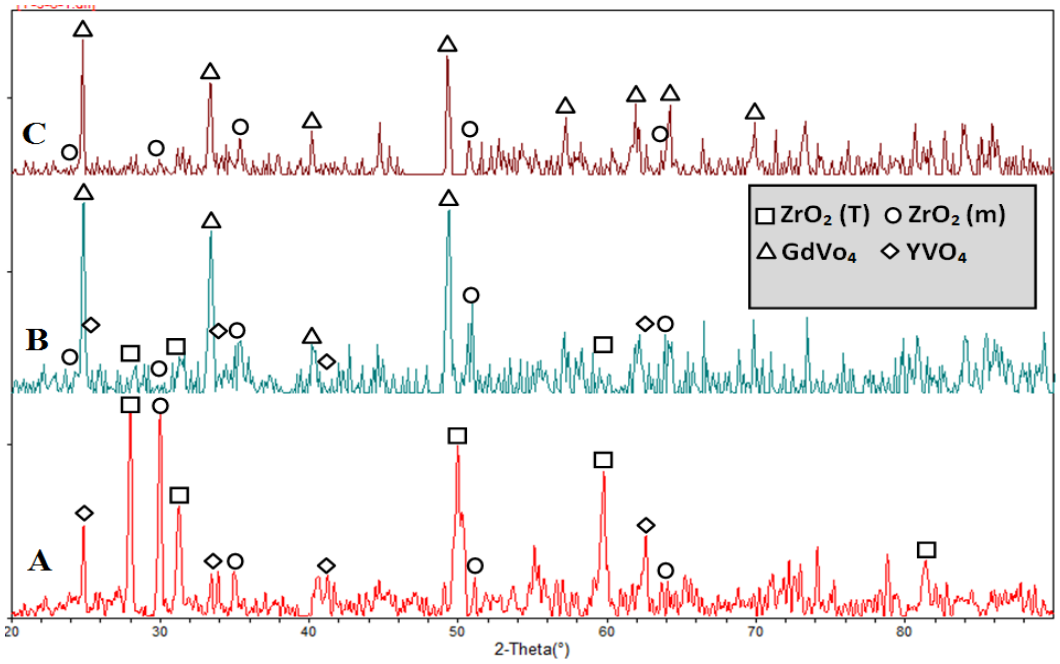

Figure 3.4 XRD patterns of A) conventional YSZ, B) $Gd_2Zr_2O_7$+YSZ, C) $Gd_2Zr_2O_7$ after hot corrosion in Na_2SO_4+V_2O_5 at 1050ºC

Chemical degradation of conventional YSZ coatings can be classified as successive occurrence of related chemical reactions during the hot corrosion tests.

During the exposure of V_2O_5 and Na_2SO_4 salt mixture at a high temperature (1050°C), a new compound of $NaVO_3$ will be formed.

$$V_2O_5 + Na_2SO_4 \rightarrow 2\ (NaVO_3) + SO_3 \quad (1)$$

Then, $NaVO_3$, having a melting point of 610 °C, reacts with yttria from the YSZ solid solution to form YVO_4:

$$ZrO_2\ (Y_2O_3) + 2(NaVO_3) \rightarrow ZrO_2 + 2(YVO_4) + Na_2O \quad (2)$$

Also Na_2O can react with V_2O_5 directly to form $NaVO_3$:

$$Na_2O\ (base) + V_2O_5\ (acid) = 2NaVO_3\ (salt) \quad (3)$$

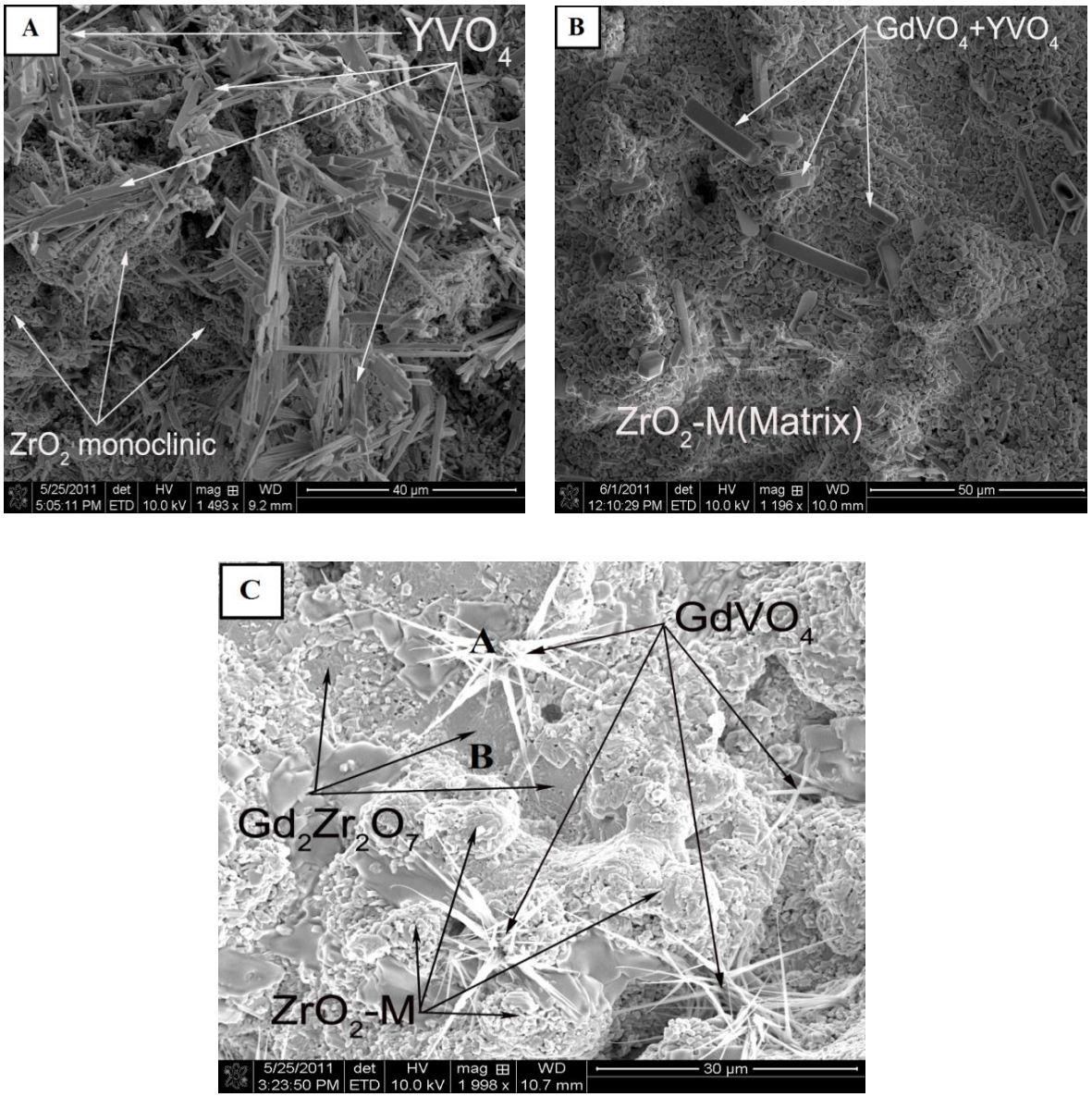

Figure 3.5 SEM surface images of A) conventional YSZ, B) $Gd_2Zr_2O_7$+YSZ, C) $Gd_2Zr_2O_7$ after hot corrosion in Na_2SO_4+V_2O_5 at 1050ºC

The molten $NaVO_3$ is also reported to increase the atom mobility, hence further promote the depletion of yttria from YSZ and the growth of YVO_4 crystals [17, 24, 54]. The Kinetic of reaction (2) is controlled by the mobility the Y^{3+} in the lattice which migrate preferentially toward the reaction interface due to the high V concentration present on the coating surface[55].

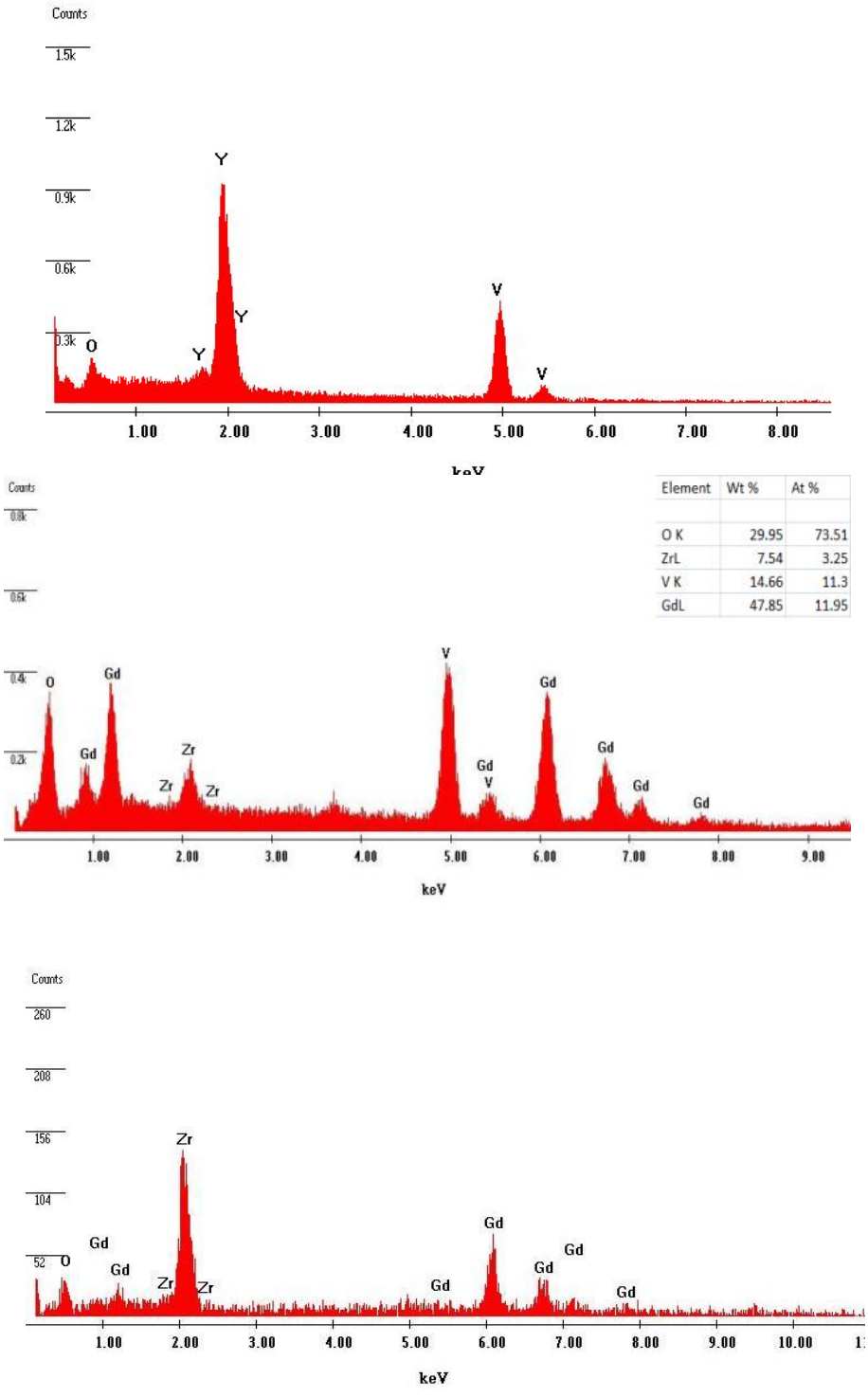

Figure 3.6 EDS spectra from the surface of the coatings A) crystal at region A in Figure 3.5A, B) crystal at region A in Figure 3.5C, C) region B in Figure 3.5C

After losing Y_2O_3, the transformation of tetragonal zirconia to monoclinic zirconia during the cooling stage of thermal cycling is accompanied by 3-5% volume expansion, leading to cracking and spallation of TBCs [41, 54-57].

The $Gd_2Zr_2O_7$+YSZ and $Gd_2Zr_2O_7$ coatings started to degrade after 36 hours (nine 4-hours cycles) of hot corrosion testing. For comparison, microscopic observations and phase analysis has been done after the same duration of hot corrosion testing as for YSZ (five 4-hours cycles). Exposure of the $Gd_2Zr_2O_7$+YSZ and $Gd_2Zr_2O_7$ coatings to the molten mixture of Na_2SO_4+V_2O_5 at 1050ºC, after hot corrosion tests for five 4-hours cycles at peak temperature of 1050°C, results in additional peaks on XRD measurements attributed to $GdVO_4$ and monoclinic ZrO_2. As described earlier, if Na_2SO_4 and V_2O_5 react and $NaVO_3$ forms then, the possible reactions that would have produced these phases can be written as: [58-61].

$$Gd_2Zr_2O_7(s) + 2NaVO_3\,(l) \rightarrow 2GdVO_4(s) + 2ZrO_2\ (\text{monoclinic}) + Na_2O \quad (4)$$

$$Gd_2O_3(s) + 2NaVO_3\,(l) \rightarrow GdVO_4(s) + Na_2O \quad (5)$$

No evidences from the XRD patterns indicate direct chemical interactions between Na_2SO_4 with YSZ and $Gd_2Zr_2O_7$, thus the chemical reactions between Na_2SO_4 and YSZ and $Gd_2Zr_2O_7$ are believed to be minimum at the elevated temperature of 1050ºC, which has also been reported by other researchers [58-61].

V_2O_5 may also react with $Gd_2Zr_2O_7$ directly at elevated temperature to form $GdVO_4$, monoclinic ZrO_2 or ZrV_2O_7 [60-63].

$$3V_2O_5\,(l) + Gd_2Zr_2O_7(s) \rightarrow 2ZrV_2O_7(s) + 2GdVO_4(s) \quad (6)$$

$$V_2O_5\,(l) + Gd_2Zr_2O_7(s) \rightarrow 2GdVO_4(s) + 2ZrO_2\ (\text{monoclinic}) \quad (7)$$

Based on XRD analysis, both $GdVO_4$ and monoclinic ZrO_2 are found in the hot corrosion products of the $Gd_2Zr_2O_7$ coatings; thus reactions (4) and (7) are believed to be the main mechanisms for the degradation of $Gd_2Zr_2O_7$ coatings.

It has been reported that $GdVO_4$ crystals can be produced by the reaction of $Gd_2Zr_2O_7$ and $NaVO_3$ at a temperature as low as 600°C [58, 59]. The production of $GdVO_4$ consumes V_2O_5 and thus postpones the formation of YVO_4 crystals and consequently less monoclinic ZrO_2 and less YVO_4 crystals are formed. This is believed to be the main mechanism for the improved hot corrosion resistance for the $Gd_2Zr_2O_7$+YSZ composite coating.

On the surface of the YSZ+$Gd_2Zr_2O_7$ composite coating, YVO_4 crystals have a small rod shape (about 20 μm in length), which is significantly smaller than the large rod shaped YVO_4 found in the conventional YSZ coatings (about 50 μm in length). The presence of fine-grained $Gd_2Zr_2O_7$ around YSZ particles also reduces the direct contact of conventional YSZ with molten salt, thus a better corrosion resistance.

For pure YSZ coatings, YVO_4 forms throughout the entire thickness of the coating, apart from the stresses induced by the ZrO_2 phase transfer due to the reduction of Y_2O_3, as foreign objects, the corrosion product (YVO_4) could impose extra stresses, which can easily initiate cracks and damage the coating [58-62]. The smaller the YVO_4 size, the lower the stresses and thus a better durability.

For the YSZ+$Gd_2Zr_2O_7$ composite coating, after 36 hours of accelerated hot corrosion test, many regions in the YSZ+$Gd_2Zr_2O_7$ composite coatings are still intact and the original tetragonal ZrO_2 phases exist. Clearly, YSZ+$Gd_2Zr_2O_7$ composite coating provides better resistance against hot corrosion than the conventional YSZ.

In the $Gd_2Zr_2O_7$ case, the corrosive area is small with isolated dendritic shaped $GdVO_4$ crystals. Also many surface regions are still intact with the original $Gd_2Zr_2O_7$ phase. Unlike the YSZ case, where the hot corrosion attacks the stabilizer Y_2O_3, which has a small quantity in nature, the hot corrosion attacks the bulk $Gd_2Zr_2O_7$ layer, thus the $Gd_2Zr_2O_7$ coating provides a better resistance against hot corrosion than the conventional YSZ.

Hot corrosion of ceramic oxides against molten salt such as V_2O_5 and $NaVO_3$ is mostly controlled by Lux-Flood type of acid-base reactions and are explainable in terms of the relative acid-base character of the oxide. The severity of the reactions increases as the relative acidity to basicity between the reactants increases [17, 24].

There is no direct information about the relative basicity of rare-earth zirconates in the open literature; however, we could estimate the basicity from the respective metal oxides. According to the model proposed by [64], rare earth oxides such as Sm_2O_3, Yb_2O_3, Gd_2O_3 are more basic than Y_2O_3 therefore, it will react at lower vanadium (or vanadium oxide) activities. On the other hand, as reflected from the thermodynamic data, $GdVO_4$ is more stable than YVO_4, which indicates that a higher V_2O_5 or $NaVO_3$ activity is required for $GdVO_4$ formation than for YVO_4 formation.

Lewis basicity reflects the thermodynamic tendency of a substance to act as a Lewis base. Therefore, the basicity difference is the indicative information of corrosion resistance from the viewpoint of thermodynamic factor [65, 66]. In this experiment, $Gd_2Zr_2O_7$ is less basic than YSZ which means that the driving force of reaction (2) is larger than that of reaction (4) thermodynamically. Besides, the better hot corrosion immunity of $Gd_2Zr_2O_7$ might be favored by kinetic factors, such as dissolution kinetics. Because the dissolution process usually involves two steps: dissociation of the compound into ions or atoms and the subsequent diffusion of these ions

or atoms into the melt. Consequently, the dissolution kinetics may be affected by the interface dissociation, the diffusion in the melt, or both of them [65-67].

The representative cross section SEM images of the conventional YSZ, $Gd_2Zr_2O_7$+YSZ and $Gd_2Zr_2O_7$ coatings after the hot corrosion tests are presented in Figure 3.7. As shown in Figure 3.7A, the corroded areas near the YSZ/bond coat interface implies a weak coating which can be easily torn off; large harmful horizontal cracks have formed inside the conventional YSZ layer throughout the thickness of coating. Transverse cracks are clearly visible in the YSZ coating, Figure 3.7A.

In certain regions, the cracks divided the YSZ layer into several sub-layers, implying the initiation of delamination and spallation of the YSZ coating. Some large cracks have propagated and extended deep into the ceramic coat and even reached the top-coat/bond-coat interface, which would be susceptible to cause the debonding of the ceramic coat from the bond coat. Moreover, comparing Figure 3.3A and Figure 3.7A, the thickness of YSZ layer has been reduced after hot corrosion test. YSZ tetragonal to monoclinic phase transformation initiated from the beginning of hot corrosion test. As it accompanied by volume expansion, it can be tore off easily by small thermal and mechanical shocks during the hot corrosion cycles. So the failure of YSZ coating may occur by gradual loss of YSZ coating from the surface toward bond coat. This means, the thickness of YSZ layer should be reduced after hot corrosion test. The micro cracks and pores were observed in both conventional YSZ and YSZ+$Gd_2Zr_2O_7$ coatings. In comparison, the YSZ+$Gd_2Zr_2O_7$ coating has finer and fewer micro cracks than the conventional YSZ coating.

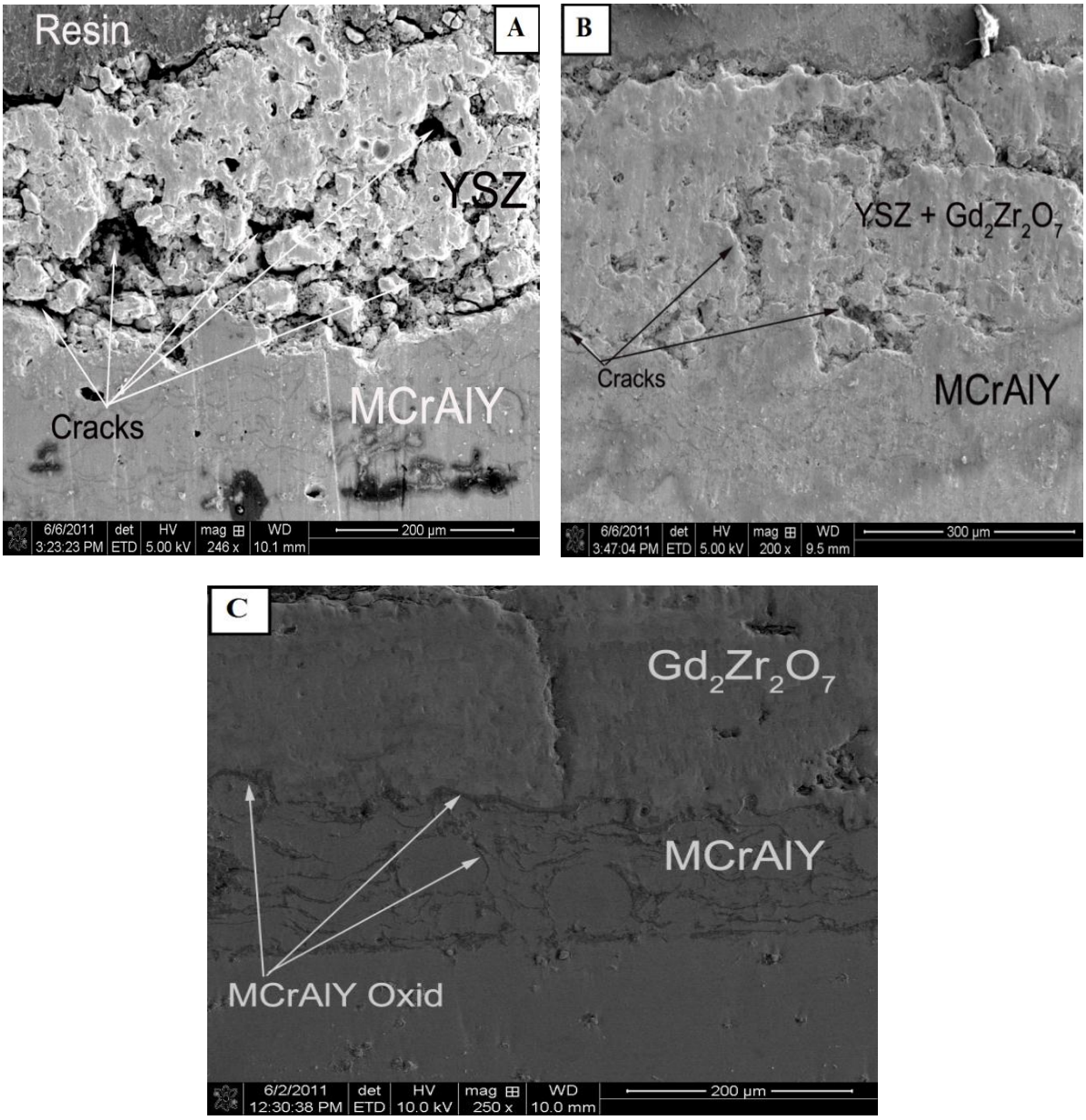

Figure 3.7 Cross-section of A) conventional YSZ, B) $Gd_2Zr_2O_7$+YSZ, C) $Gd_2Zr_2O_7$ after hot corrosion in Na_2SO_4+V_2O_5 at 1050ºC

In the case of YSZ+$Gd_2Zr_2O_7$ composite coatings, only a few visible cracks were observed inside the zirconia layer after the hot corrosion test but without spallation. It can be concluded that molten salts and oxygen penetration were retarded in this specimen thus a better hot corrosion resistance. Figure 3.7C shows a $Gd_2Zr_2O_7$ coating cross-section, which has no significant degradation and spallation after hot corrosion test. Although one vertical-crack

appears from the surface to bond coat, no visible degradation around the tip of the crack is observed. The cross-section image of the $Gd_2Zr_2O_7$ coating shows less porosity than the conventional YSZ which means it's harder for the molten salts and the oxygen to penetrate through the $Gd_2Zr_2O_7$ layer. This further confirms that the $Gd_2Zr_2O_7$ coating exhibits a good hot corrosion resistance and good durability. Figure 3.8 shows the crack of a delaminated YSZ coating. The infiltration of molten salt through the entire YSZ coating leads to the formation of dendritic YVO_4 crystals throughout the entire thickness of the crack. The formation of YVO_4 crystals implies the depletion of Y_2O_3 in this region, which leads to the subsequent tetragonal to monoclinic ZrO_2 transformation and thus a large destructive volume changes/stresses within the ceramic coat.

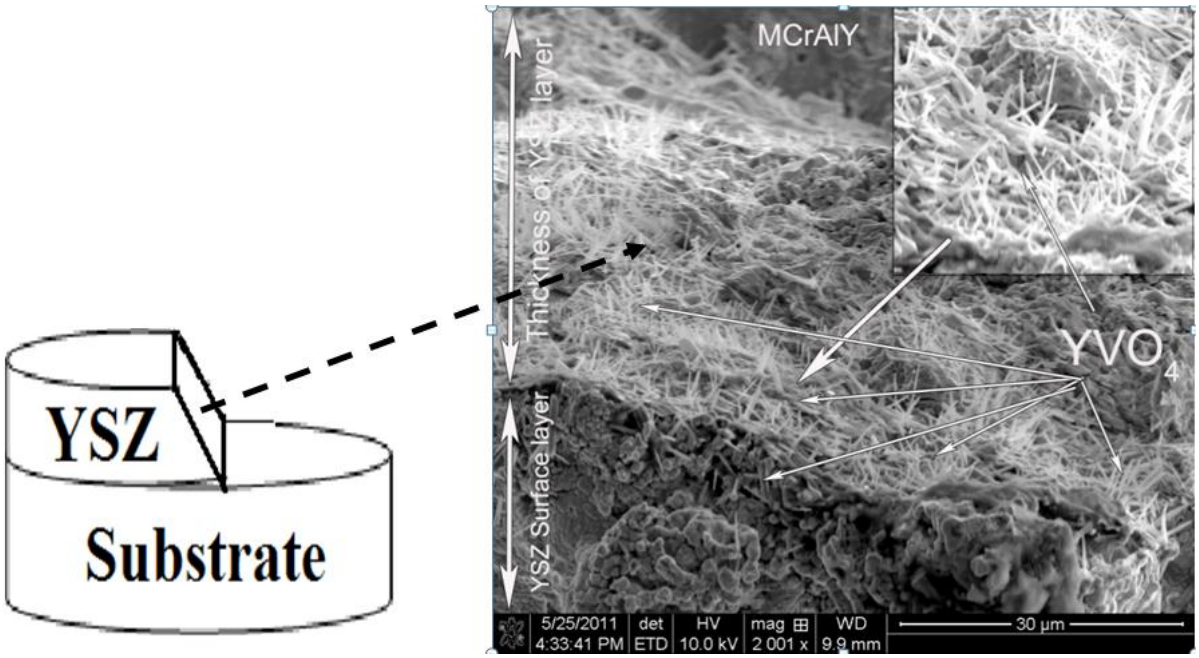

Figure 3.8 Cross section along the crack of a delaminated YSZ coating after hot corrosion in $Na_2SO_4+V_2O_5$ at 1050ºC

3.5 Conclusion

Under a typical gas turbine working temperature of 1050°C, the reactions between yttria (Y_2O_3) and V_2O_5 / $NaVO_3$ produce YVO_4, leaching Y_2O_3 from the YSZ and causing progressive tetragonal to monoclinic destabilization transformation. Based on hot corrosion chemical reactions formulas, the amount of corrosive salt charged in the tests was enough to react with the entire YSZ and $Gd_2Zr_2O_7$ layers (20 mg/cm^2 per cycle). After 20 hours (5 cycles) of hot corrosion test at 1050°C, the failure of the YSZ TBCs has initiated and propagated throughout the entire top coat, and led to the top coat delamination and spallation near the top coat–bond coat interface.

The YSZ cross section shows severe macro-cracks and enhanced porosity due to the hot corrosion from the Na_2SO_4+V_2O_5 molten salts. For YSZ+$Gd_2Zr_2O_7$ coating, molten Na_2SO_4+V_2O_5 mixture reacts with $Gd_2Zr_2O_7$ to form $GdVO_4$ and monoclinic ZrO_2. The production of $GdVO_4$ predominately consumes V_2O_5 and thus postpones the formation of YVO_4 crystals and consequently less monoclinic ZrO_2 and less YVO_4 crystals are formed. On the surface of the YSZ+$Gd_2Zr_2O_7$ composite coating, YVO_4 crystals, are significantly smaller (about 20 μm in length) than the large rod shaped YVO_4 found in the conventional YSZ coatings (about 50 μm in length). The presence of fine-grained $Gd_2Zr_2O_7$ around YSZ particles also reduces the direct contact of conventional YSZ with molten salt, thus a better corrosion resistance.

Molten Na_2SO_4+V_2O_5 mixture may also react with $Gd_2Zr_2O_7$ coating. However, unlike the YSZ case, where the molten salts attack the stabilizer Y_2O_3, molten Na_2SO_4+V_2O_5 mixture reacts with the bulk $Gd_2Zr_2O_7$ layer to form $GdVO_4$ and monoclinic ZrO_2. Under this accelerated hot corrosion test, bulk $Gd_2Zr_2O_7$ layer started to degrade after 36 hours of hot corrosion testing (9 cycles), which is much better than the YSZ case, which started to fail after 5 cycles. Also based

on the results, $Gd_2Zr_2O_7$ layer provides a slightly better hot corrosion resistance than YSZ+$Gd_2Zr_2O_7$ coating. The chemical interactions, and the induced phase transformation, are the primary factors for degradation and spallation of the conventional YSZ and $Gd_2Zr_2O_7$ coatings. Based on the degradation rate, the corrosive layer thickness, and the general status of the coating after hot corrosion, $Gd_2Zr_2O_7$ containing coatings have a better hot corrosion resistance at a temperature of 1050°C than that of YSZ coatings.

3.6 Acknowledgments

This material is based upon work supported by the Department of Energy National Energy Technology Laboratory under Award Number DE-FE0004734.

3.7 Disclaimer

4 Phase Stability and Hot Corrosion Behavior of ZrO_2-Ta_2O_5 Compound in Na_2SO_4-V_2O_5 Mixtures at Elevated Temperatures[2]

4.1 Abstract

For thermal barrier coating (TBC) applications, yttria stabilized zirconia (YSZ) is susceptible to hot corrosion. This paper examines the hot corrosion performance of ZrO_2/Ta_2O_5 compounds. Different compositions of ZrO_2-Ta_2O_5 samples in the presence of molten mixture of Na_2SO_4 + V_2O_5 at 1100˚C were tested. The compositions were selected to form tetragonal and orthorhombic phases of zirconium-tantalum oxides. Results show that orthorhombic zirconium-tantalum oxide is more stable, both thermally and chemically in Na_2SO_4+V_2O_5 media at 1100˚C, and shows a better hot corrosion resistance than the tetragonal phase.

4.2 Introduction

Ceramic thermal barrier coatings (TBCs) are widely used as insulation materials in turbine engines to protect hot-section metallic components. The most commonly used TBC top coat material is yttria-stabilized zirconia (YSZ) with a composition of 6–8 wt% (3.5–4.5 mol%) of Y_2O_3 in ZrO_2 [11, 15, 68-71].

Vanadium and sodium are common impurities found in low grade petroleum fuels. Molten sulfate–vanadate deposits resulting from the using of such fuels are extremely corrosive. Hot corrosion degradation due to molten deposits arising from the aggressive combustion environment is one of the major failure mechanisms for TBCs [17, 34, 37].

[2] Chapter 4 previously appeared as [M.H. Habibi, Shizhong Yang and S.M. Guo, Phase Stability and Hot Corrosion Behavior of ZrO_2–Ta_2O_5 Compound in Na_2SO_4–V_2O_5 Mixtures at Elevated Temperatures, *Ceramics International,* 40(2014)4077–4083]. It is reprinted by permission of *Ceramics International Journal* (See Appendix A)

Much efforts have been devoted to improve the phase stability and hot corrosion resistance of YSZ by doping extra metal oxides, for example, different sizes of rare-earth cations [36, 72, 73]. A comparative analysis of various stabilizers including MgO, Y_2O_3, Sc_2O_3, In_2O_3, CeO_2, SmO_2, Gd_2O_3 and TiO_2 appeared in [37]. Scandia- and india-stabilized zirconia was found to be more resistant than YSZ to corrosion by vanadia [21, 38-41, 74]. It's understandable that for an oxide whose cation is more acidic than yttrium, such as scandium, it would be thermodynamically less prone to react with acidic oxides. Thus, zirconia stabilized with such oxides would be more resistant to hot corrosion by acidic oxides [37, 39, 40]. However, the addition of extra trivalent oxides to YSZ generally decreases the cyclic life and erosion resistance due to the decrease in tetragonality and the high affinity for V_2O_5 [37, 44, 75].

An alternative approach to improve YSZ is the co-doping of yttria with pentavalent oxides such as Ta_2O_5. Ta_2O_5 has a melting point over 1800˚C. On heating it undergoes a phase transformation at 1360˚C which is well above the typical turbine surface temperatures[42]. According to ionic conductivity measurements [43], tantalum ions reside as substitutional defects in the zirconium lattice, annihilating oxygen vacancies generated by yttria. Data in literature indicate defect association between the larger oxide of Y and the smaller oxide of Ta in YSZ. Such defect association should lower the activity and diffusivity in zirconia solid solution thus make this composition more resistant to hot corrosion [40].

Also, according to acid-base Lewis chemical reactions, by virtue of Ta's position in the periodic table, tantalum is more acidic than vanadium. Thus, the ZrO_2-Ta_2O_5 is expected to be substantially more resistant to corrosion by the acidic oxides than ZrO_2-Y_2O_3. According to S. Raghavan et. al. [76] the Y_2O_3-Ta_2O_5 co-doped zirconia is more resilient to the $NaVO_3$ attack. Ta-doped YSZ, which is stable up to 1500˚C and has a low thermal conductivity, has been

reported as one prospective TBC [36, 44, 45]. On the Y_2O_3-Ta_2O_5-ZrO_2 phase diagram at 1500˚C, [45], apart from the tetragonal zirconia phase, formed by equal co-doping of Y_2O_3-Ta_2O_5 into ZrO_2, a stable orthorhombic zirconia phase ($TaZr_{2.75}O_8$) also exists, when ZrO_2 is doped with low level of Y_2O_3 and high level of Ta_2O_5. Previous reports on Y_2O_3-Ta_2O_5 co-doped zirconia systems mainly have a focus on the system stability with equal co-dopants and on the study of associated thermal properties.

The investigated compositions generally have a low Ta_2O_5 content of less than 20 wt. % [36, 40, 45, 77]. In this paper, we report the hot corrosion behavior of both tetragonal and orthorhombic phase zirconia samples. ZrO_2-Ta_2O_5 composite mixtures (30 to 70 wt%Ta_2O_5) and YSZ- Ta_2O_5 composite mixtures (70 wt% YSZ + 30 wt% Ta_2O_5, 30TaYSZ) were made. The hot corrosion behavior of the samples with two different phases in Na_2SO_4+V_2O_5 at 1100˚C is presented.

4.3 Experimental Procedure

Hot corrosion studies using Na_2SO_4 and V_2O_5 mixtures were conducted on samples at 1100˚C in air. For the above mixtures, 95% Na_2SO_4 and 99.9% V_2O_5 from Sigma Aldrich were used. Five types of ceramic samples, YSZ, 70 wt%ZrO_2 + 30 wt% Ta_2O_5 (30TaSZ), 70 wt% YSZ + 30 wt% Ta_2O_5 (30TaYSZ), 50 wt%ZrO_2 + 50 wt% Ta_2O_5 (50TaSZ), and 30 wt%ZrO_2 + 70 wt% Ta_2O_5 (70TaSZ) were made using agglomerated powders from Sigma Aldrich. To obtain the samples, powders were first pressed with binders in a uniaxial die (2.5 cm inner diameter) at 350 MPa pressure to obtain the compressed green bodies, which were then sintered at 1450˚C for 5 hours and 30 minutes to obtain the dense bodies. To perform an accelerated high-temperature hot corrosion test on samples, a mixture of 50wt% Na_2SO_4 + 50wt% V_2O_5 deposit was spread evenly

onto the surfaces of the specimens with a mixed salt amount of 20 mg/cm^2. The specimens were then set in an electric furnace with an ambient atmosphere under a maximum temperature of 1100˚C for 4 h. The furnace has two small holes for air to flow naturally. After each 4 h of testing at 1100˚C, the samples were allowed to cool down inside the furnace, and then the samples were inspected both visually and with an optical microscope for possible crack initiation. To repeat the test, the samples were recoated with the $Na_2SO_4 + V_2O_5$ salt mixture and the heating profile was repeated. The morphology and microstructure of the as received samples and the samples after the hot corrosion tests were examined using field emission scanning electron microscopy (Quanta3D FEG, FEI Company, USA). For surface morphology studies using SEM, a thin Pt layer was sputtered onto the samples to improve the electrical conductivity. X-ray diffraction (MiniFlex XRD, Rigaku Corporation, Japan) with Cu Kα radiation λ = 1.54178 Å at a scan speed of 1˚/min was used to establish the phase composition of the specimen.

4.4 Results

Figure 4.1 depicts the X-ray diffraction patterns for the as-received YSZ, 30TaSZ, 50TaSZ and 70TaSZ specimens. In Figure 4.1A, for sintered YSZ, only diffraction peaks corresponding to tetragonal ZrO_2 can be distinguished. In the 30TaSZ, a mixed tetragonal and orthorhombic phases form, and 50TaSZ sample shows a near pure orthorhombic phase of zirconium tantalum oxide. The zirconium tantalum compound in orthorhombic phase is found to be $TaZr_{2.75}O_8$, based on the XRD patterns of 30TaSZ and 50TaSZ. For 70TaSZ sample, besides $TaZr_{2.75}O_8$, well-defined peaks corresponding to Ta_2O_5 are also observed. Note in Figure 4.1, the more intense peaks of Ta_2O_5 are at 2θ =22.8° and 28.3°.

Figure 4.2 shows the as-received SEM image of YSZ, 30TaSZ, 50TaSZ and 70TaSZ. These SEM images show a typical microstructure of pressed and sintered samples with certain amount of porosity, visible on the surface of samples. In Figure 4.2D, for 70TaSZ sample, there are two distinct microstructures, a matrix of orthorhombic $TaZr_{2.75}O_8$ and some isolated Ta_2O_5 regions. This sample is made of 30 wt. % of ZrO_2 mixed with 70 wt. % of Ta_2O_5.

Figure 4.3 illustrates XRD patterns of YSZ, 30TaSZ, 50TaSZ and 70TaSZ specimens after hot corrosion at 1100˚C in Na_2SO_4+V_2O_5 salt for 40 hours (10 cycles). In Figure 4.3A, starting from tetragonal phase, after 40 hours of tests, a large portion of the YSZ sample changed to the monoclinic phase by the Na_2SO_4+V_2O_5 salt. YVO_4 is formed as the major hot corrosion product. An examination of XRD pattern of the 30TaSZ sample, besides $TaZr_{2.75}O_8$ and tetragonal zirconia peaks which are present in the original as-received sample, after hot corrosion, some new peaks are identified which can be contributed to monoclinic zirconia, $TaVO_5$ and Ta_9VO_{25}.

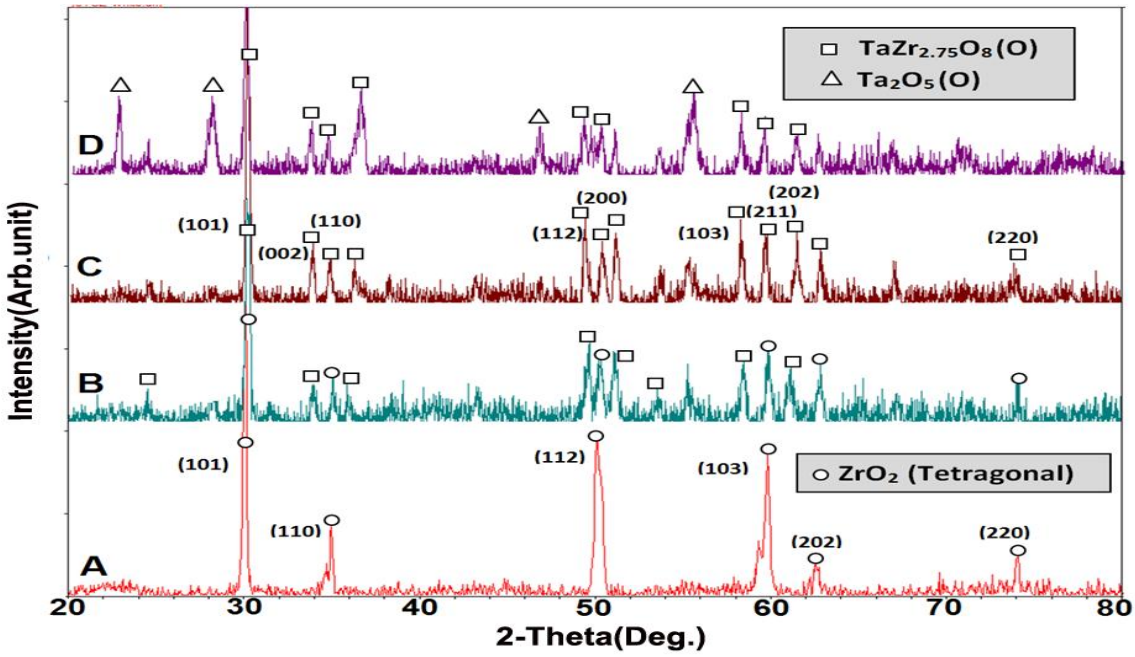

Figure 4.1 XRD patterns of as-received A) YSZ, B) 30TaSZ, C) 50TaSZ and D) 70TaSZ

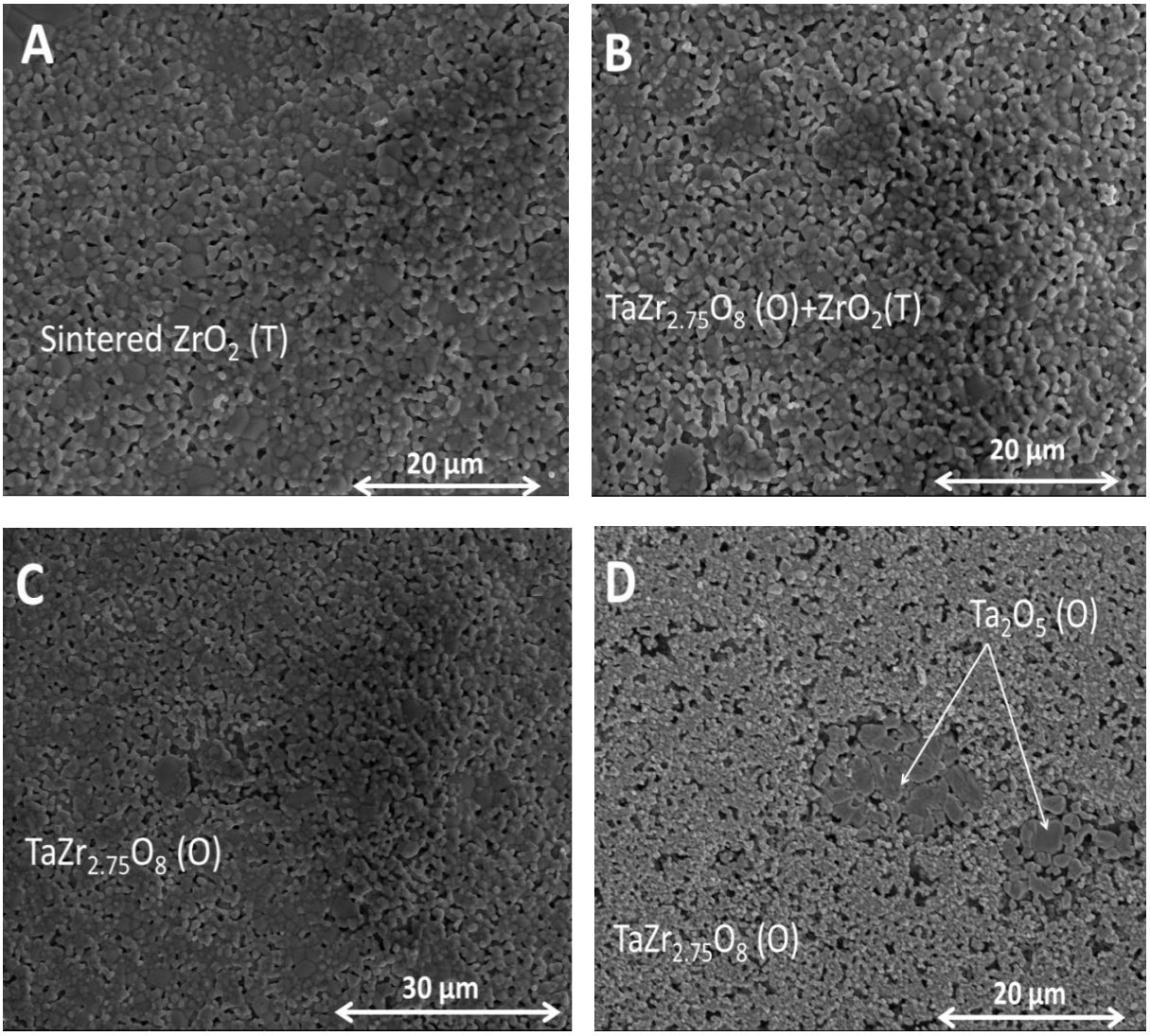

Figure 4.2 SEM images of as-received sintered A) YSZ, B) 30TaSZ, C) 50TaSZ and D) 70TaSZ

SEM images of the YSZ, 30TaSZ, 50TaSZ and 70TaSZ specimen after hot corrosion tests are presented in Figure 3.4. Apart from XRD analysis (Figure 4.3), Energy Dispersive Spectroscopy (EDS) analysis was performed at different regions of the samples to confirm the chemical compositions of the hot corrosion products. For crystals in Figure 4.4A, EDS analysis demonstrated that these crystals were composed of yttrium, vanadium, and oxygen. Further analysis confirmed these crystals were YVO_4. Hot corrosion products of 30TaSZ sample are rod-shape. The extent of the attack is, however, much smaller in comparison to the YSZ sample.

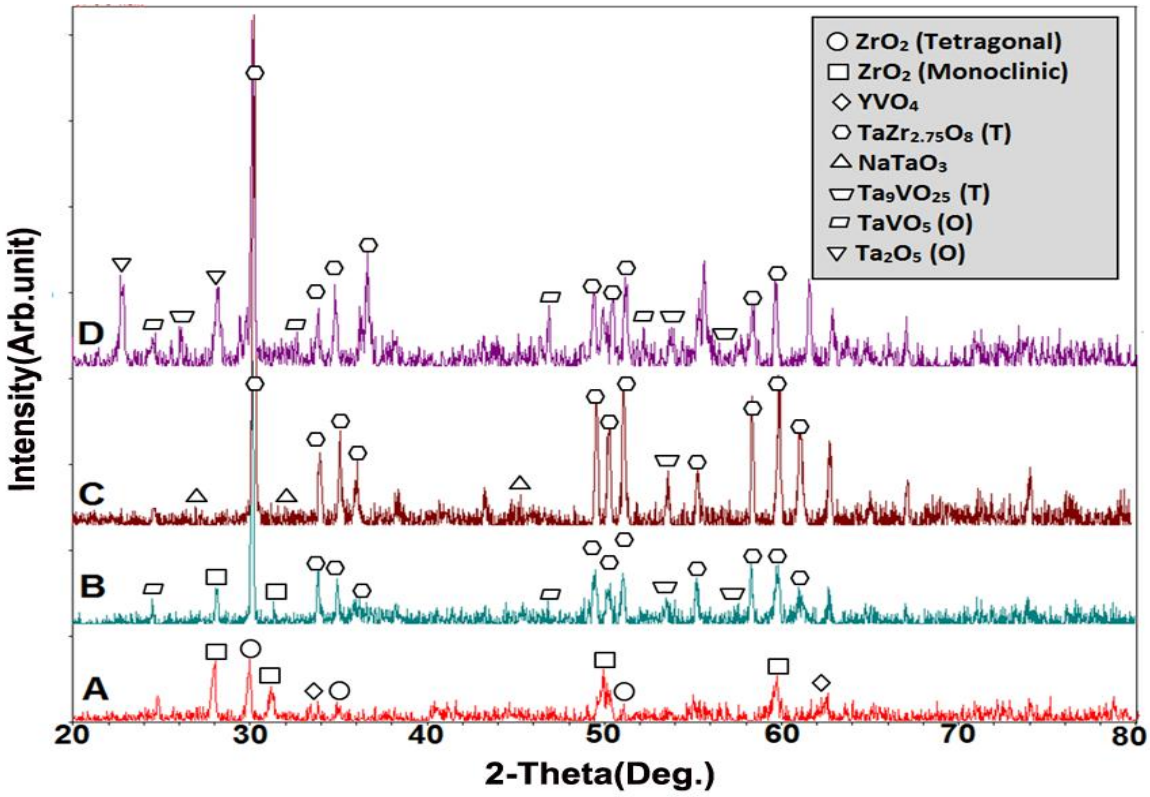

Figure 4.3 XRD patterns of A) YSZ, B) 30TaSZ, C) 50TaSZ and D) 70TaSZ after hot corrosion in Na_2SO_4 + V_2O_5 at 1100˚C for 40 hours

In the 50TaSZ case, after hot corrosion, only a small quantity of rod-shaped crystals was formed. According to EDS result, crystals in Figure 4.4C contain sodium, tantalum and oxygen and with considering the XRD pattern, they are found to be $NaTaO_3$. Most of the $TaZr_{2.75}O_8$ surface didn't react with molten salt and it is almost perfectly intact. XRD shows strong peaks of orthorhombic phase of zirconium tantalum oxide. In 70TaSZ sample, besides TaV_9O_{25}, strong peaks contributed to pure Ta_2O_5 and $TaVO_5$ were also detected, Figure 4.3D. The formation of considerable amount of $TaVO_5$ and Ta_9VO_{25} crystals in this sample is due to the large amount of excess Ta_2O_5, which reacts with the molten salt. Considering the intensity of the XRD peaks and the amount of hot corrosion products, reaction rate of 70TaSZ is higher than the 50TaSZ case.

However, exposure to Na_2SO_4+V_2O_5 salt does not cause destabilization of zirconium tantalum oxide to monoclinic phase seen for the YSZ sample.

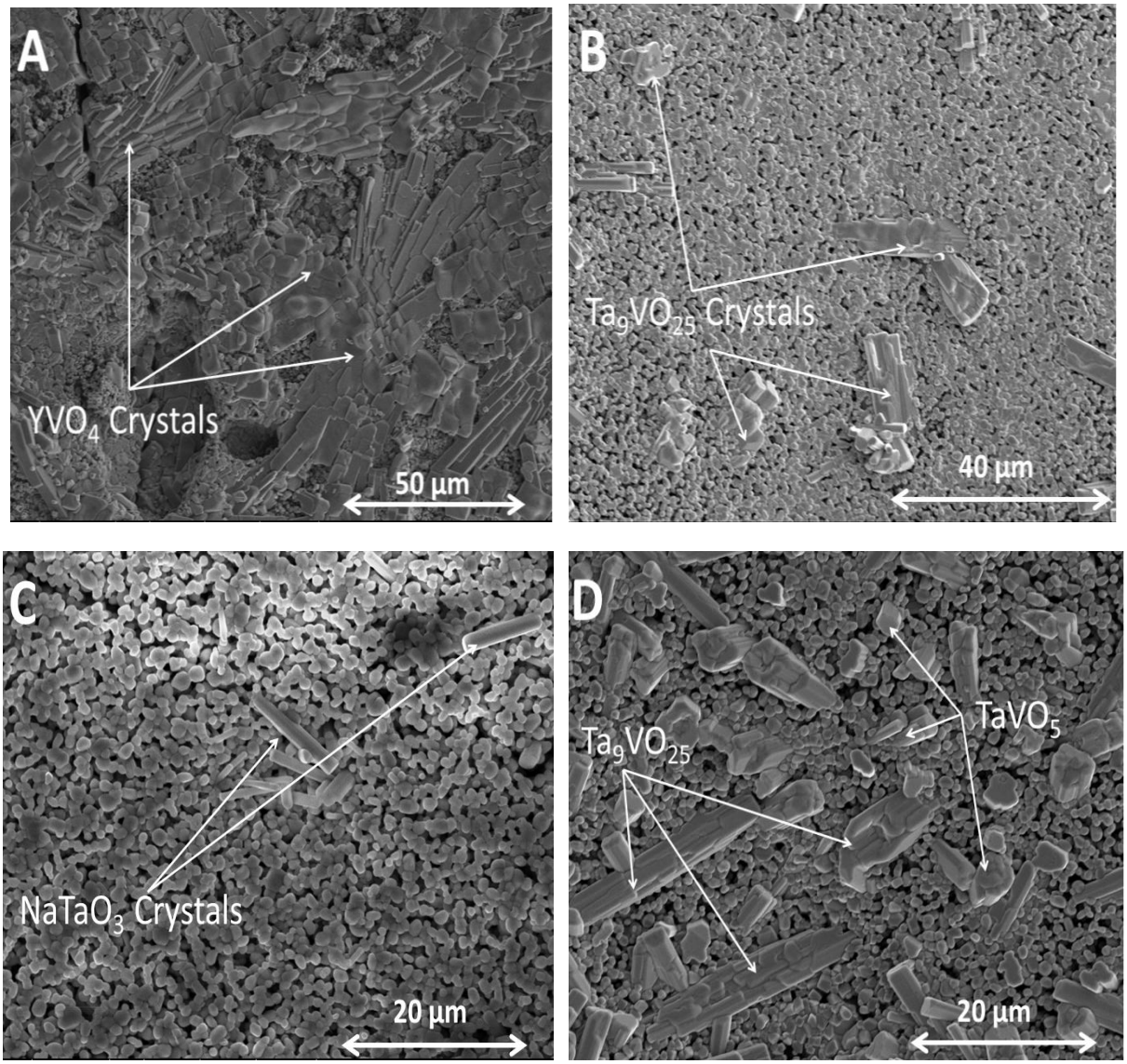

Figure 4.4 SEM surface images of A) YSZ, B) 30TaSZ, C) 50TaSZ, D) 70TaSZ after hot corrosion in Na_2SO_4 + V_2O_5 at 1100˚C for 40 hours.

It is noteworthy to compare the hot corrosion behavior of 30TaYSZ (30 wt. % Ta_2O_5+70 wt. % YSZ) with 30TaSZ (30 wt. % Ta_2O_5+70 wt. % ZrO_2). Figure 4.5 shows the XRD patterns of the as-received 30TaYSZ and 30TaSZ. As indicated by the XRD patterns, 30TaYSZ is a pure

tetragonal zirconia phase while 30TaSZ is a mixture of tetragonal zirconia and orthorhombic tantalum zirconium oxide ($TaZr_{2.75}O_8$). For 30TaYSZ, the amount of Ta_2O_5 added into YSZ is not high enough to form complex tantalum zirconium oxide. Instead, tetragonal zirconia is found to be the only phase formed, with Ta_2O_5–Y_2O_3 dopants in the ZrO_2 matrix. Similar findings are reported in previous studies [26, 77, 78].

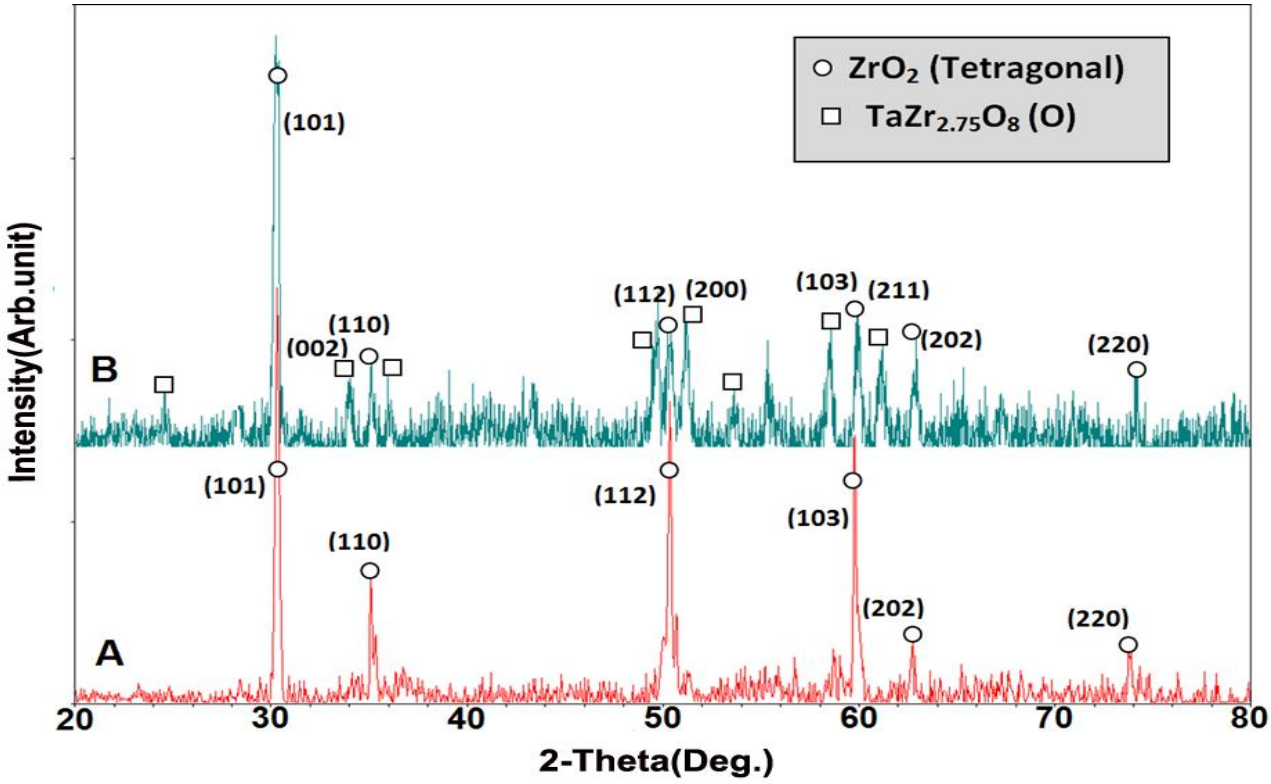

Figure 4.5 XRD patterns of as-received A) 30TaYSZ, B) 30TaSZ

Figure 4.6 shows XRD patterns of 30TaYSZ and 30TaSZ specimens after hot corrosion at 1100˚C in Na_2SO_4+V_2O_5 salt for 40 hours. In Figure 4.6A, it is seen that the 30TaYSZ sample, which is pure tetragonal to begin with, has high level of monoclinic phase, in conjunction with the formation of YVO_4, due to Na_2SO_4+V_2O_5 salt corrosion. Besides orthorhombic $TaZr_{2.75}O_8$ and tetragonal zirconia, some new peaks are identified on 30TaSZ sample after hot corrosion, which are monoclinic zirconia, $TaVO_5$ and Ta_9VO_{25}. Figure 4.7 shows SEM images of 30TaYSZ

and 30TaSZ after hot corrosion at 1100˚C in Na_2SO_4+V_2O_5 salt for 40 hours. Based on the quantity of corrosion products, 30TaSZ is found to have a better hot corrosion resistance than 30TaYSZ, due to the formation of the highly stable orthorhombic $TaZr_{2.75}O_8$ phase.

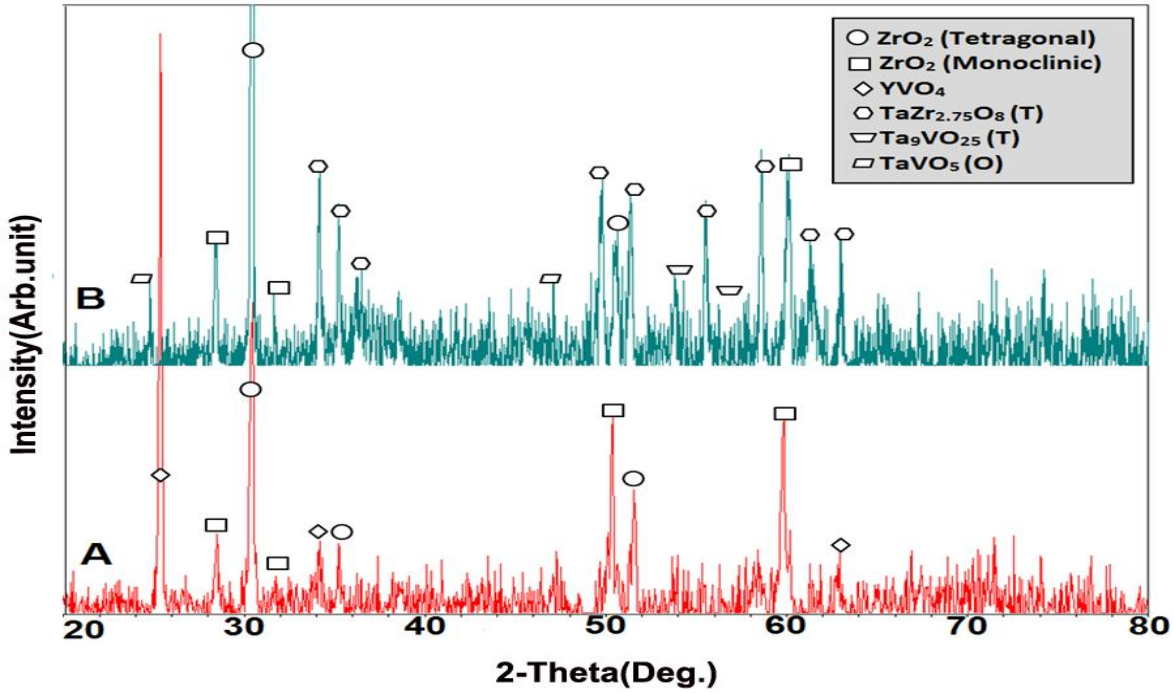

Figure 4.6 XRD patterns of A) 30TaYSZ, B) 30TaSZ after hot corrosion in Na_2SO_4 + V_2O_5 at 1100˚C for 40 hours

4.5 Discussion

For a conventional Y_2O_3-stabilized ZrO_2, a Na_2SO_4-V_2O_5 mixture can leach out the Y_2O_3 as follows [15, 24, 31, 38]. $NaVO_3$ forms due to the presence of both V_2O_5 and Na_2SO_4:

$$V_2O_5 + Na_2SO_4 \rightarrow 2(NaVO_3) + SO_3 \quad (1)$$

The Gibbs free energy of formation for this reaction is [79, 80]:

$\Delta G^0_{298K} = \Sigma \Delta G^0_{products} - \Sigma \Delta G^0_{reactants} = -2087.845$ kJ⁄mol

$\Delta G^0_{1400K} = -1686.066$ kJ⁄mol

Then, $NaVO_3$, having a melting point of 610˚C, reacts with yttria from the YSZ solid solution to form YVO_4:

$$ZrO_2\ (Y_2O_3) + 2(NaVO_3) \rightarrow ZrO_2 + 2(YVO_4) + Na_2O \quad (2)$$

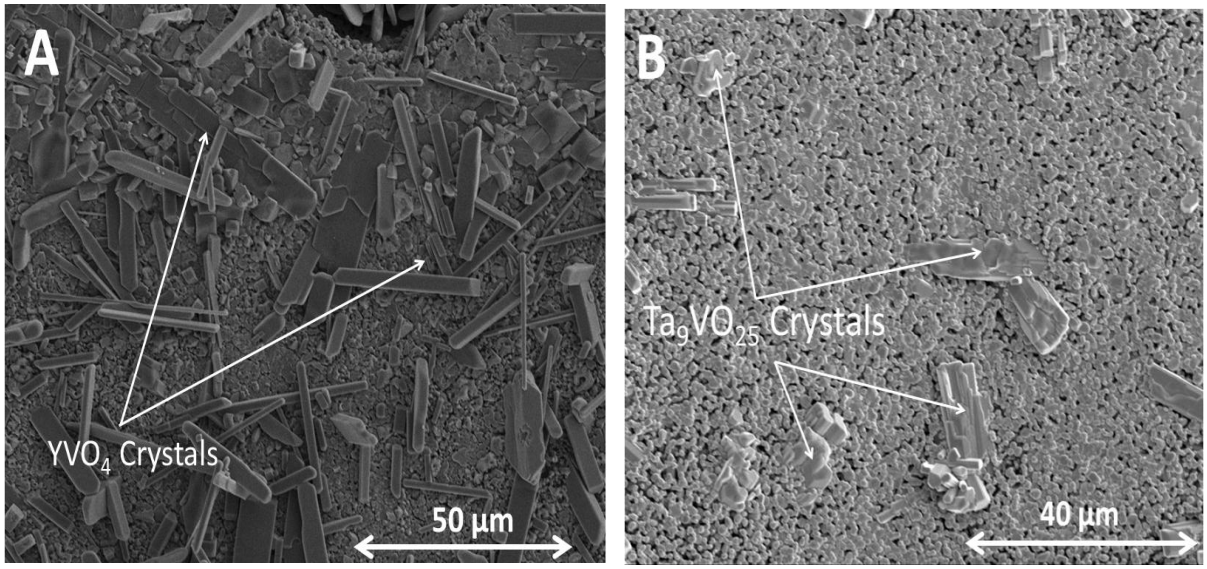

Figure 4.7 SEM surface images of A) 30TaYSZ, B) 30TaSZ, after hot corrosion in $Na_2SO_4 + V_2O_5$ at 1100˚C for 40 hours.

Na_2O released by above reaction can form more $NaVO_3$. Na_2O can react with V_2O_5 directly to form $NaVO_3$:

$$Na_2O\ (base) + V_2O_5\ (acid) \rightarrow 2NaVO_3\ (salt) \quad (3)$$

The molten $NaVO_3$ is also reported to increase mobility of Y^{3+}, hence further promote the depletion of yttria from YSZ and the growth of YVO_4 crystals. After losing Y_2O_3, the transformation of tetragonal zirconia to monoclinic zirconia during the cooling stage of thermal cycling is accompanied by a 3–5% volume expansion, leading to cracking and spallation of the YSZ coating. For 30TaSZ, 50TaSZ and 70TaSZ, as described earlier, Na_2SO_4 and V_2O_5 would

first react and form $NaVO_3$, then, the possible reactions that would have produced those identified reaction products include [37, 40, 44]:

$$TaSZ\ (Ta_2O_5)\ (s) + NaVO_3\ (l) \rightarrow NaTaO_3(s) + TaVO_5(s) \quad (4)$$

$$TaSZ\ (5Ta_2O_5)\ (s) + NaVO_3\ (l) \rightarrow NaTaO_3(s) + Ta_9VO_{25}(s) \quad (5)$$

In this study, there are many unusual substances, such as $TaVO_5$, Ta_9VO_{25}, whose thermodynamic data cannot be found easily. The authors checked several common handbooks, databases and software packages, such as the CRC Handbook of Chemistry and Physics, the Bureau of Mines and USGS database, the NIST-JANAF Thermochemical Tables, the MatNavi NIMS Materials Database, the HSC Chemistry package etc and failed to obtain useful information. A literature search also failed to generate the required complete thermodynamic data set [37, 79-85].

To further assist the understanding of the corrosive reactions, the authors performed *ab initio* density functional theory (DFT) based electronic structure simulations to obtain the relevant thermodynamic data. The Gibbs free energy of formation was calculated for each reactant and product by summation the energy of formation at 0K, zero point energy, vibrational internal energy and free energy at 1227 ˚C, and PV term. The phonon module in the software MedeA [86] was used to calculate the thermodynamic vibration parameters. The (VASP) [86-89] was used to perform DFT calculations where plane wave basis set was implemented. The *ab initio* projector augmented wave (PAW)[90, 91] general gradient approximation (GGA) calculation method with plane wave basis sets was used and 400 eV plane wave cut-off energy was set in the simulation. Each lattice in all of the supercells was selected to be larger than ~ 7 Å. Only harmonic vibration approximation was considered in the phonon calculations. The calculated Gibbs free energy of formation results are shown in Table 4.1. For $NaTaO_3$, the Gibbs free

energy of formation at 1500K is -1304.14 kJ/mol, while the Gibbs free energy of formation for $TaVO_5$ at 1500K is -2048.53 kJ/mol. To make a comparison, the Gibbs free energy of formation of YVO_4 at 1500K is -3960.34 kJ/mol. So, YVO_4 (Equation 2) is much more stable than both $NaTaO_3$ and $TaVO_5$ (Equations 4 and 5). Based on the calculated Gibbs free energy results, equation 2 is found to be endothermic while equations 4 and 5 are exothermic reactions.

Table 4.1: At 1500K, Gibbs free energy of formation in unit kJ/mol.

Substance	Y_2O_3	$NaVO_3$	YVO_4	Na_2O	Ta_2O_5	$NaTaO_3$	$TaVO_5$	Ta_9VO_{25}
Gibbs Energy	-2713.24	-1501.93	-3960.34	-494.51	-1719.71	-1304.14	-2048.53	-10693.86

However, in equation 2, since Na_2O has a low melting temperature of 1132 ˚C, the Y_2O_3 and YVO_4 can be easily dissolved in Na_2O. Also Na_2O can further feed the formation of $NaVO_3$ through equation 3. All these explain the experimentally observed fast reaction of equation 2 than equations 4 and 5.

V_2O_5 may also react with Ta_2O_5 directly at elevated temperature. According to Ta_2O_5-V_2O_5 phase diagram, in temperatures lower than 1200˚C, two possible components are $TaVO_5$ and Ta_9VO_{25}[37, 92].

$$V_2O_5\ (l) + TaSZ\ (Ta_2O_5)\ (s) \rightarrow 2TaVO_5\ (s) \quad (6)$$

$$V_2O_5\ (l) + 9\ TaSZ\ (Ta_2O_5)\ (s) \rightarrow 2Ta_9VO_{25}\ (s) \quad (7)$$

The detection of orthorhombic $TaZr_{2.75}O_8$ by XRD and EDS over a vast surface area of the 50TaSZ sample after hot corrosion suggests that this orthorhombic phase is stable to the molten salt attack. Molten salt is found to react with both Y_2O_3 and Ta_2O_5. The Y^{3+} in the lattice of ZrO_2

has the mobility to migrate preferentially toward the reaction interface due to the high V concentration presented on the sample surfaces [24].

The reactions between vanadium compounds and ceramic oxides follow a Lewis acid–base mechanism, where the acid vanadium compounds react more readily with the ceramic oxides that have stronger basicity. As reported in literature, the basicity of tantalum oxide, yttrium oxide, and zirconium dioxide follows the order: $Y_2O_3 > Ta_2O_5 > ZrO_2$, indicating that molten $NaVO_3$ has the tendency to react with Y_2O_3 more easily [17, 31, 37]. Following the nucleation and growth mechanism, at the beginning of the hot corrosion process, the hot corrosion products ($TaVO_5$, Ta_9VO_{25} and YVO_4) have dendritic like shapes; then as the hot corrosion proceeds, these hot corrosion products become larger and their morphologies change to rod/plate-like shapes. Based on thermodynamic data and basicity of Y_2O_3 and Ta_2O_5 and their tendency to react with molten salt, the growth rate of $TaVO_5$ and Ta_9VO_{25} is slower than that of YVO_4 in the prolonged hot corrosion tests which indicate better stability of zirconia, stabilized with Ta_2O_5 rather than with Y_2O_3.

Comparing all samples tested in this study, hot corrosion resistance of 50TaSZ is the best. This sample has a near single orthorhombic phase of $TaZr_{2.75}O_8$, which is highly stable in high temperatures and resistant to hot corrosion attack in molten salts.

4.6 Conclusions

The hot corrosion resistances of different compositions of YSZ, ZrO_2, and Ta_2O_5 samples to $Na_2SO_4 + V_2O_5$ mixture were studied, under a typical gas turbine component surface temperature of 1100˚C. The samples were selected to form both tetragonal and orthorhombic zirconium-tantalum oxides. Results show that orthorhombic zirconium-tantalum oxide is more stable, both

thermally and chemically in Na_2SO_4+V_2O_5 media at 1100˚C, and shows a better hot corrosion resistance than the tetragonal phase. Thus orthorhombic zirconium-tantalum oxides offers good opportunities for developing novel TBCs with improved resistance to corrosion by sulfate/vanadate melts.

4.7 Disclaimer

This report was prepared as an account of work sponsored by an agency of the United States Government. Neither the United States Government nor any agency thereof, nor any of their employees, makes any warranty, express or implied, or assumes any legal liability or responsibility for the accuracy, completeness, or usefulness of any information, apparatus, product, or process disclosed, or represents that its use would not infringe privately owned rights. Reference herein to any specific commercial product, process, or service by trade name, trademark, manufacturer, or otherwise does not necessarily constitute or imply its endorsement, recommendation, or favoring by the United States Government or any agency thereof. The views and opinions of authors expressed herein do not necessarily state or reflect those of the United States Government or any agency thereof.

4.8 Acknowledgments

This publication is based upon work supported by the US Department of Energy National Energy Technology Laboratory under Award Number DE-FE0004734 and NASA-EPSCoR program (Grant NNX09AP72A).

5 An Investigation on Hot Corrosion Behavior of YSZ-Ta_2O_5 in Na_2SO_4+V_2O_5 Salt at 1100˚C[3]

5.1 Abstract

This study compares the hot corrosion performance of yttria stabilized zirconia (YSZ), and YSZ-Ta_2O_5 (TaYSZ) composite samples in the presence of molten mixture of Na_2SO_4 + V_2O_5 at 1100˚C. For YSZ, the reaction between $NaVO_3$ and Y_2O_3 produces YVO_4 and leads to the transformation of tetragonal ZrO_2 to monoclinic ZrO_2. For TaYSZ, minor amounts of $NaTaO_3$, $TaVO_5$ and Ta_9VO_{25} are formed as the hot corrosion products with only traceable amounts of YVO_4. Due to the synergic effect of doping of zirconia with both Y_2O_3 and Ta_2O_5, the TaYSZ sample has a much better hot corrosion resistance than YSZ.

5.2 Introduction

Thermal barrier coating (TBC) systems are commonly used in the hot sections of gas turbines to protect them from thermal degradation and to increase the operational temperature for better efficiency. Much attention is being paid to zirconia-based TBCs owing to their inherent physical properties and the compatibility with the superalloys used in turbines [13, 20, 93-99].

Zirconia stabilized with 3.2–4.2 mol% (6–8 wt %) yttria (3–4YSZ) is the current material of choice for the TBC topcoat. However, the reliability and durability of plasma-sprayed YSZ TBCs are limited by the tendency of premature fracture and spallation during thermal cycling in hot corrosive environments [17, 75, 76, 94, 96, 100]. The maximum working temperature of YSZ is below 1200˚C, limited by the phase stability. The selection of TBC materials is restricted

[3] Chapter 5 previously appeared as [M.H. Habibi, Li Wang, Jiandong Liang and S.M. Guo, An Investigation on Hot Corrosion Behavior of YSZ-Ta_2O_5 in Na_2SO_4 + V_2O_5 Salt at 1100°C, *Corrosion Science*, 75 (2013) 409–414]. It is reprinted by permission of *corrosion Science Journal* (See Appendix A)

by a complex matrix of requirements such as: high melting point, no phase transformation between room temperature and the operational temperature, low thermal conductivity, chemical inertness, matching thermal expansion with the metallic substrate, good adherence to the metallic substrate, and low sintering rate of the porous microstructure[101]. Hot corrosion occurs in engines burning low quality fuels containing vanadium, sulfur and phosphorous. For example, molten sodium salts of vanadium and sulfur can condense on to the TBC in the 600–1300˚C temperature range.

The composition of the condensate depends on the levels of impurities in the fuel and the operating conditions. Providing the activity of the acidic salt is high enough, yttria can be easily leached out of YSZ, resulting in destabilization of the tetragonal phase and transformation to the monoclinic phase upon cooling. Stresses are also generated by the formation of solid corrosion products inside the coatings, which can dramatically reduce the coating's ability to accommodate thermal contraction upon cooling [30, 40, 60, 102].

There are numerous earlier studies on the hot corrosion behavior of the YSZ coatings against foremost corrosive materials such as vanadium pentoxide (V_2O_5), sodium sulfate (Na_2SO_4) etc. at elevated temperatures [15, 21, 22, 28, 31, 37, 38, 41, 54, 55, 74, 103]. There is a strong need in developing new TBC materials in order to address the challenges facing industry, demanding ever higher operating temperatures [104]. In order to enhance the stability of YSZ beyond 1200˚C, many researchers have tried further doping of the YSZ system, for example, with bigger or smaller cations of rare-earth elements [36].

A comparative analysis of various stabilizers including MgO,Y_2O_3, Sc_2O_3, In_2O_3, CeO_2, SmO_2 and TiO_2 appeared in [37, 41]. Scandia and indium oxide-stabilized zirconia were found to be more resistant than yttria-stabilized zirconia to corrosion by vanadia; however, the proposed

doping concentrations are likely to change the structure to cubic at high temperature, and thus a concomitantly lower toughness [36, 44].

A review of the literature on the ZrO_2–CeO_2 system reveals that this system is resistant to hot corrosion but can be subject to melt-mediated phase separation at high temperatures and may exhibit formation of $CeVO_4$ in media with fuels contaminated with high levels of S and V [37, 41, 74]. Interestingly, ceria stabilized zirconia (CSZ) is generally acknowledged to have lower erosion resistance than YSZ but some reports mention a higher toughness and lower thermal conductivity for the former which might be expected from the higher tetragonality of its unit cell [41, 43, 75, 105]. The addition of extra trivalent oxides to YSZ for further thermal conductivity reduction generally decreases the cyclic life and erosion resistance due to the decrease in tetragonality and the high affinity for V_2O_5 [37, 44, 75].

An alternate approach to YSZ TBC improvement is using Ta_2O_5 as a co-doped stabilizer. The solubility of Ta^{5+} in ZrO_2 is quite modest, but there is a strong synergism when co-doping with Y^{3+} so that the solubility of $YTaO_4$ in tetragonal ZrO_2 is much higher than that of Y^{3+} or Ta^{5+} alone [40, 43-45, 76, 77].

Due to the strong interaction between Y and Ta in solid solution and the formation of a highly stable phase, the tendency of Y to react with V in the melt could be substantially lower than in the YSZ case [44]. According to S. Raghavan et. al. [76] the Y_2O_3-Ta_2O_5 co-doped zirconia is more resilient to the $NaVO_3$ attack. Ta-doped YSZ, which is stable up to 1500˚C and has a low thermal conductivity, has been reported as one prospective TBC [36, 44, 45]. Along with the remarkable phase stability and mechanical properties, the Y_2O_3-Ta_2O_5 co-doped zirconia system was also found to be suitable for plasma spraying.

A strong interaction between the Y^{3+} and Ta^{5+} ions is beneficial for the TBC applications because it leads to remarkably low thermal conductivity even in absence of oxygen vacancies, better phase stability at elevated temperatures, comparable coefficient of thermal expansion and could reduce individual activities of cations and hence make the Y^{3+} cations less susceptible to react with foreign ions such as V^{5+}[36, 40, 44, 76].

It has been reported that the Y_2O_3-Ta_2O_5 co-doped zirconia system has a higher corrosion resistance against sulfate and vanadate melts as compared to YSZ [40, 44]. Air plasma spray (APS) coatings of the same material were also reported to show promising durability in burner rig testing[76]. However, previous reports on Y_2O_3-Ta_2O_5 co-doped zirconia systems mainly have a focus on the system stability with equal co-dopants and on the study of associated thermal properties. The investigated compositions generally have a low Ta_2O_5 content of less than 20 wt%. In all previous studies, the equal amount of Y_2O_3 and Ta_2O_5 have been used to stabilize ZrO_2. In the current study, we decided to choose the appropriate amount of Ta_2O_5 to get a single orthorhombic phase. 50 wt% YSZ+50 wt% Ta_2O_5 is equal to 4 mol% Y_2O_3 + 22 mol% Ta_2O_5+74 mol % ZrO_2. Hot corrosion behavior in Na_2SO_4 +V_2O_5 and with a temperature higher than 900˚C hasn't been reported. In this paper hot corrosion behavior of YSZ and 50wt%YSZ+50wt%Ta_2O_5 in Na_2SO_4+V_2O_5 at 1100˚C are presented. 50wt%YSZ+50wt%Ta_2O_5 was chosen to form complex zirconium tantalum oxides.

5.3 Material and Methods

Hot corrosion studies using Na_2SO_4 and V_2O_5 mixtures were conducted on samples at 1100˚C in air. For the above mixtures, 95% Na_2SO_4 and 99.9% V_2O_5 from Sigma Aldrich were used.

Two types of ceramic samples, YSZ and 50 wt%YSZ + 50 wt% Ta_2O_5 (TaYSZ), were made using agglomerated powders from Sigma Aldrich.

To obtain the samples, powders were first pressed with binders in a uniaxial die (2.5 cm inner diameter) at 350 MPa pressure to obtain the compressed green bodies, which were then sintered at 1450˚C for 5 hours and 30 minutes to obtain the dense bodies. The densities of the sintered samples were measured by the Archimedes technique using water as the buoyant medium. The sintered samples were fine polished using alumina paste to a 1 μm finish prior to the hot corrosion tests.

To perform an accelerated high-temperature hot corrosion test on samples, a mixture of 50wt% Na_2SO_4 + 50wt% V_2O_5 deposit was spread evenly onto the surfaces of the specimens with a salt amount of 20 mg/cm^2. Figure 5.1 shows surface of an as received specimen charged with the salt at beginning of each hot corrosion cycle.

Based on hot corrosion chemical reaction formulas, the amount of corrosive salt charged in the tests (20 mg/cm^2 per cycle) was enough to react with the entire YSZ and TaYSZ samples. The specimens were then set in an electric furnace with an ambient atmosphere under a maximum temperature of 1100˚C for 4 h.

Although hot corrosion temperature (1100˚C) is more than melting points of V_2O_5(Tm~690˚C), Na_2SO_4(Tm~884˚C) and $NaVO_3$(Tm~640˚C), the penetration and reaction rate of $NaVO_3$ is much faster than volatilization of it. Figure 5.2 shows surface of YSZ sample after hot corrosion at 1100˚C, as it is clear from Figure 5.2, the color of the surface is completely changed which shows occurring some chemical reactions.

After each 4 h of testing at 1100˚C, the samples were allowed to cool down inside the furnace, and then the samples were inspected both visually and with an optical microscope for possible crack initiation. To repeat the test, the samples were recoated with the Na_2SO_4 + V_2O_5 salt mixture and the heating profile was repeated until failure of the samples. Failure of samples occurred when the cracked area exceeded 15% of the sample surface area.

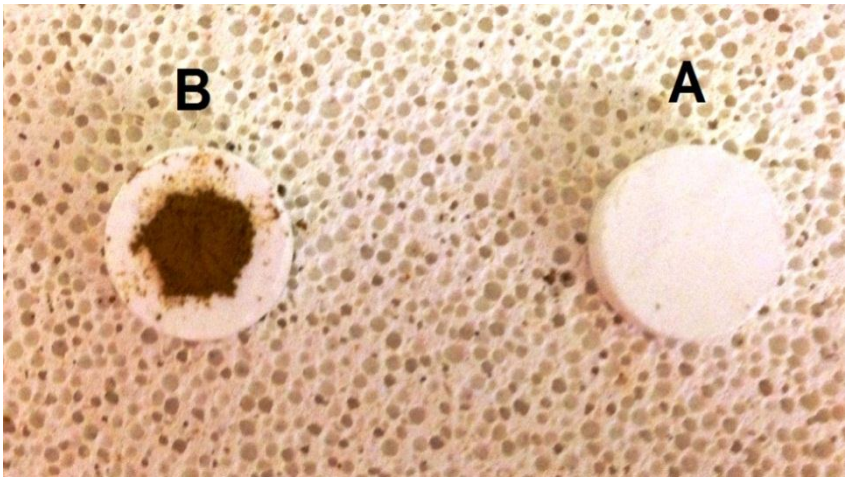

Figure 5.1 Surface of as received specimen A) before and B) after charging with salt mixuture for hot corrosion

Figure 5.2 Surface of YSZ sample after hot corrosion in Na_2SO_4 + V_2O_5 at 1100˚C after 40 hours

The morphology and microstructure of the as received samples and the samples after the hot corrosion tests were examined using field emission scanning electron microscopy (Quanta3D^{TM} FEG, FEI Company, USA). For surface morphology studies using SEM, a thin Pt layer was sputtered onto the samples to improve the electrical conductivity. X-ray diffraction (MiniFlex XRD, Rigaku Corporation, Japan) with Cu Kα radiation λ = 1.54178Å at a scan speed of 1˚/min was used to establish the phase composition of the specimen.

5.4 Results and Discussion

X-ray diffraction patterns of the as-received sintered YSZ and TaYSZ samples are shown in Figure 5.3. It can be seen that the major phase of the sintered YSZ is tetragonal zirconia. In the TaYSZ sample, zirconium tantalum oxide forms as the result of sintering 50 wt. % YSZ and 50 wt. % Ta_2O_5 mixture at high temperature. Two compounds are identified to contribute the XRD patterns of TaYSZ, $Zr_{0.66}Y_{0.17}Ta_{0.17}O_2$ tetragonal and $TaZr_{2.75}O_8$ orthorhombic. Weak peaks of orthorhombic Ta_2O_5 are detected too.

However, only based on the XRD patterns shown in Figure 5.3, the presence of a pure ZrO_2 phase cannot be ruled out. This is because although the peaks at 2θ=30.2, 50.3 and 59.8° correspond to the solid solutions of $TaZr_{2.75}O_8$ and $Zr_{0.66}Y_{0.17}Ta_{0.17}O_2$, the tetragonal ZrO_2 peak also appears at 2θ =30.2°. Previous investigations showed similar results [36, 44, 77, 106]. For the ZrO_2 (Y_2O_3)-Ta_2O_5 system, due to the strong interaction of Y^{3+} and Ta^{5+} cations in tetragonal ZrO_2 matrix, and also due to the high Ta_2O_5 content (50 wt %) in the system, complex Zirconium Tantalum oxides such as $TaZr_{2.75}O_8$ and $Zr_{0.66}Y_{0.17}Ta_{0.17}O_2$ are formed. Figure 5.4 shows the XRD patterns obtained from the YSZ and TaYSZ samples after the hot corrosion test using the Na_2SO_4 + V_2O_5 salt mixture at 1100˚C. Comparing the patterns of the as-received sintered

samples, most of the tetragonal zirconia in the YSZ sample has been changed to the monoclinic phase and YVO_4 is formed as a major hot corrosion product. In the TaYSZ case, after hot corrosion only a small quantity of rod-shaped crystals were formed. These crystals can be identified as $NaTaO_3$, $TaVO_5$ and TaV_9O_{25}.

Typical surface morphologies of the YSZ specimen after hot corrosion tests are presented in Figure 5.5, with the apparent formation of new crystals. Apart from XRD analysis (Figure 5.4), Energy Dispersive Spectroscopy (EDS) analysis was performed at different regions of the samples to confirm the chemical compositions of the hot corrosion products.

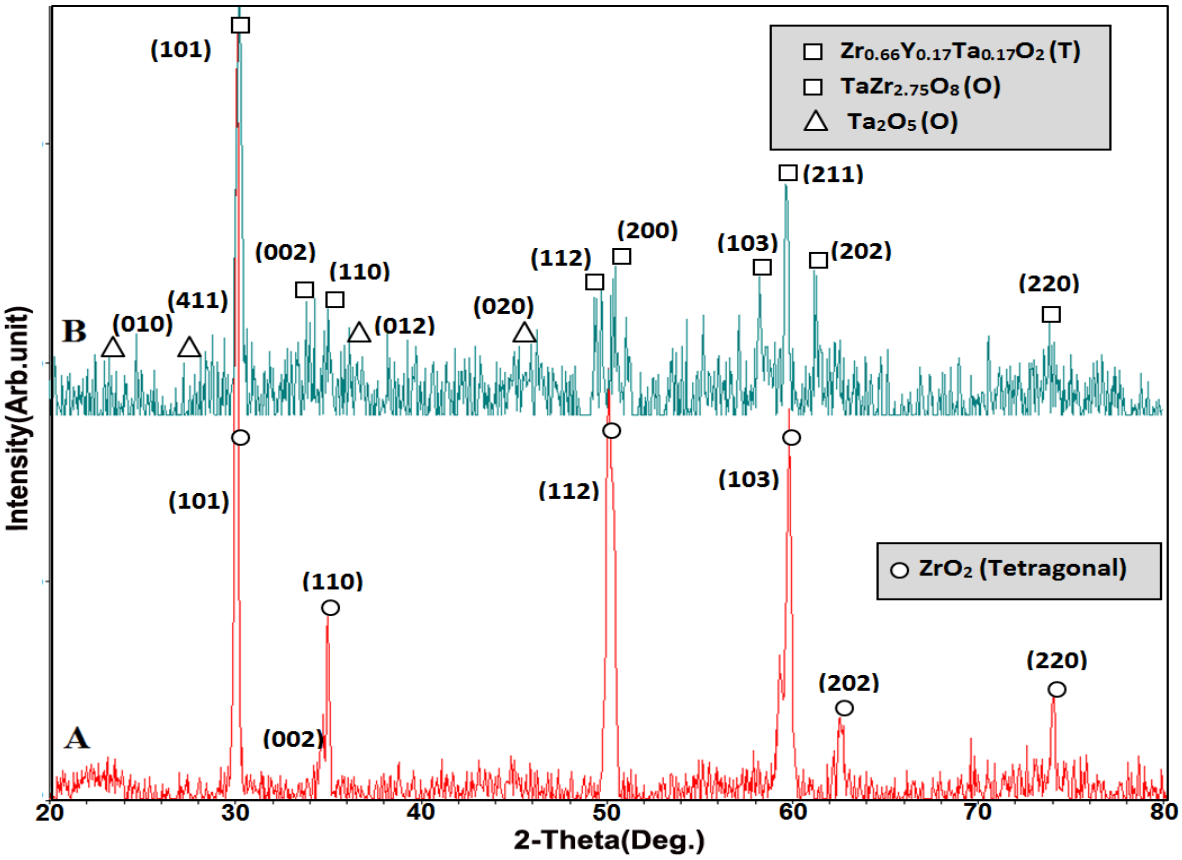

Figure 5.3 XRD patterns of as-received (A) YSZ, (B) TaYSZ.

For crystals in Figure 5.5A, EDS analysis demonstrated that these crystals were composed of yttrium, vanadium, and oxygen. Further analysis confirmed these crystals were YVO_4. These images in Figure 5.5 show the formation and growth of YVO_4 crystals during the hot corrosion tests. A great deal of research has been done on the corrosion behavior of YSZ in molten salts containing vanadium and sulfur [21, 22, 31, 37, 41, 54, 55].

The main mechanism is the dissolution of YSZ in the melt followed by re-precipitation of both YVO_4 and Y-depleted monoclinic zirconia. For the YSZ sample, after hot corrosion tests for 40 h at a peak temperature of 1100˚C (ten 4-h cycles), serious degradation and cracking occurred, Figure 5.5D. Due to the damage caused by $Na_2SO_4 + V_2O_5$, a porous layer was formed on the YSZ sample. Phase analysis results on these porous areas showed that a large amount of tetragonal zirconia on the surfaces of the YSZ had transformed to monoclinic phase due to the depletion of yttria. In addition, a large quantity of rod/plate shaped hot corrosion reaction product, YVO_4, was detected on the surface of the YSZ sample.

Similar findings have been reported by other researchers [21, 22, 37, 41, 54, 55]. YVO_4 ribbons were first detected on the surface of the sample after the second hot corrosion cycle (after two 4-h cycles) and then these YVO_4 crystals changed to dendritic shape and continued to grow and became rod-shape as time progressed (Figure 5.5). After exposure to molten salt at 1100˚C for 40 h (ten 4-h cycles), the YSZ sample developed spallation and delamination. Chemical degradation of the YSZ sample can be classified as successive occurrence of related chemical reactions during the hot corrosion tests.

During the exposure of V_2O_5 and Na_2SO_4 salt mixture at a high temperature (1100˚C), $NaVO_3$ will be formed.

$$V_2O_5 + Na_2SO_4 \rightarrow 2(NaVO_3) + SO_3 \quad (1)$$

Then, $NaVO_3$, having a melting point of 610˚C, reacts with yttria from the YSZ solid solution to form YVO_4:

$$ZrO_2\ (Y_2O_3) + 2(NaVO_3) \rightarrow ZrO_2 + 2(YVO_4) + Na_2O \quad (2)$$

Also Na_2O can react with V_2O_5 directly to form $NaVO_3$:

$$Na_2O\ (\text{base}) + V_2O_5\ (\text{acid}) \rightarrow 2NaVO_3\ (\text{salt}) \quad (3)$$

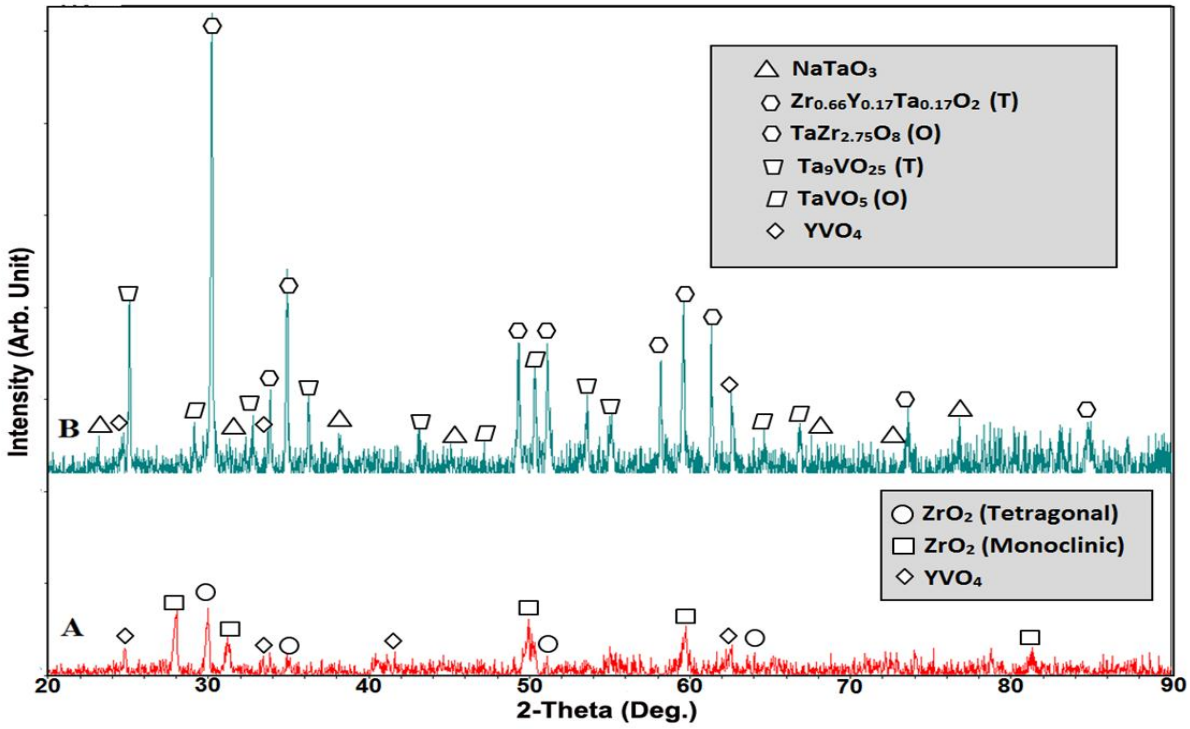

Figure 5.4 XRD patterns of samples after hot corrosion in $Na_2SO_4 + V_2O_5$ at 1100˚C (A) YSZ, after 40 hours and (B) TaYSZ, after 80 hours.

For the YSZ sample, after hot corrosion tests, thin rod/plate like YVO_4 crystals of various sizes are found covering most of the sample surfaces, Figure 5.5. The Y^{3+} in the lattice of YSZ has the mobility to migrate preferentially toward the reaction interface due to the high V concentration presented on the sample surfaces[24]. The molten $NaVO_3$ is also reported to increase the atom

mobility, hence further promote the depletion of yttria from YSZ and the growth of YVO_4 crystals [17, 24, 31, 54]. Increasing the reaction time (multiple hot corrosion cycles) enlarges the corroded zones and consequently increases the hot corrosion products. The previously formed YVO_4 crystals may act as nucleation locations for the formation of new crystals, similar to the role of grain boundaries in the nucleation and growth process. Likewise, the repeated charging of molten salts in the hot corrosion tests promotes the formation and growth of the corrosion products due to the increased amount of corrosive species available to react with the sample (Figure 5.5 A to D). After losing Y_2O_3, the transformation of tetragonal zirconia to monoclinic zirconia during the cooling stage of thermal cycling is accompanied by a 3–5% volume expansion, leading to cracking and spallation of samples.

SEM images of the TaYSZ specimen after hot corrosion tests are presented in Figure 5.6. Based on these SEM images, the TaYSZ sample appears to have very minor reactions with the corrodent salt. Apart from XRD analysis, (Figure 5.4), EDS analysis was performed at different regions of the TaYSZ sample to confirm the chemical compositions of the hot corrosion products (Figure 5.7). Crystals in Figure 5.6A contain sodium, tantalum and oxygen and with considering the XRD pattern, they are found to be $NaTaO_3$; for regions A and B in Figure 5.6B, the EDS spectra confirm the presence of $NaTaO_3$ (region A) and Ta_9VO_{25} (region B); the crystals in Figure 5.6C are Ta_9VO_{25}. The matrix in Figure 5.6C contains tantalum, zirconium, yttrium and oxygen. It is determined to be tantalum zirconium oxides, $Zr_{0.66}Y_{0.17}Ta_{0.17}O_2$ and $TaZr_{2.75}O_8$, which remain perfectly intact after exposure to molten salts during hot corrosion.

As described earlier, Na_2SO_4 and V_2O_5 would first react and form $NaVO_3$, then, the possible reactions that would have produced those identified reaction products include [37, 40, 44]:

$$TaYSZ\ (Ta_2O_5)\ (s) + NaVO_3\ (l) \rightarrow NaTaO_3(s) + TaVO_5(s) \quad (4)$$

$$TaYSZ\ (5Ta_2O_5)\ (s) + NaVO_3\ (l) \rightarrow NaTaO_3(s) + Ta_9VO_{25}(s) \quad (5)$$

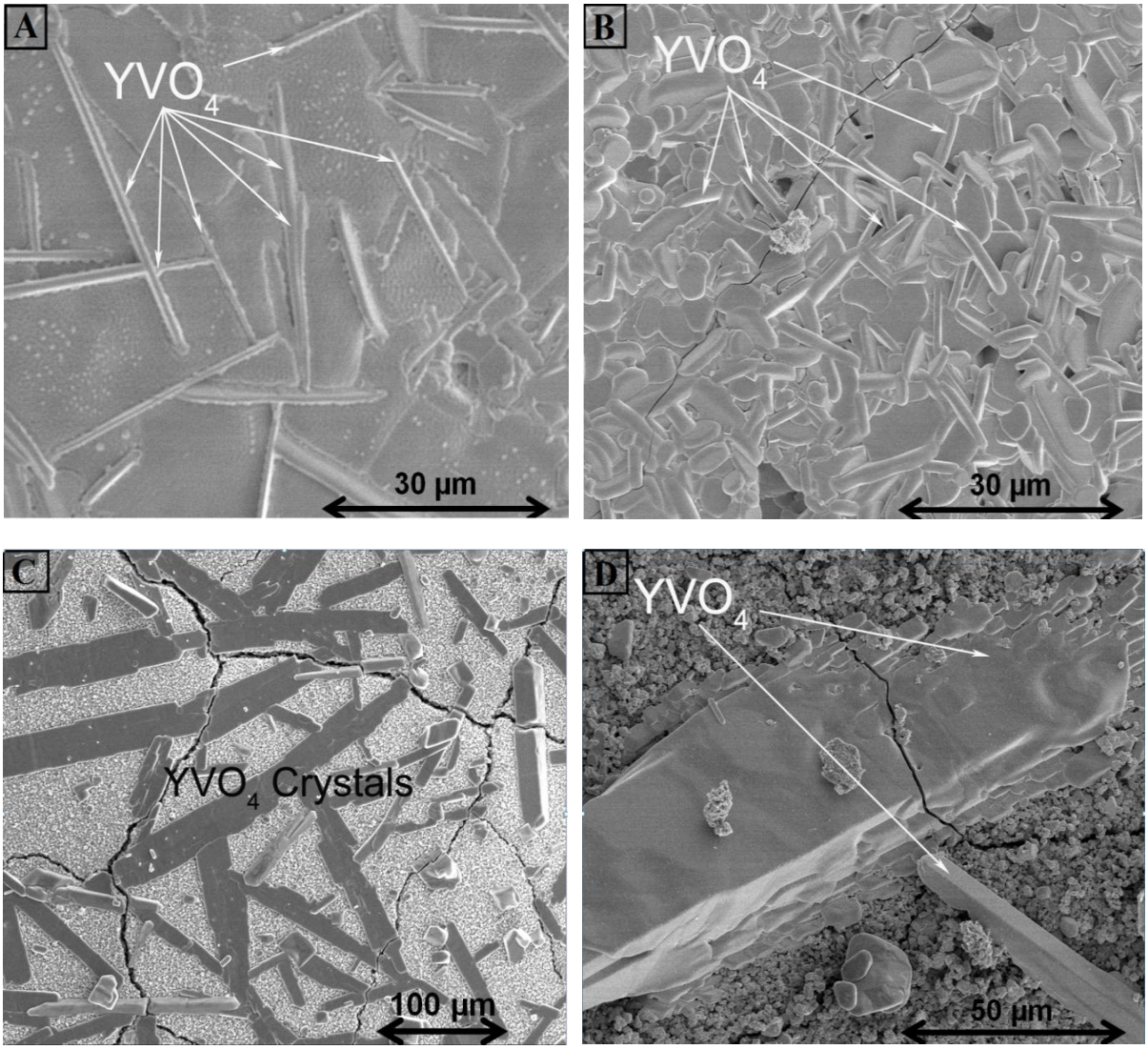

Figure 5.5 SEM surface images of YSZ A) after 2 cycles, B) after 5 cycles, C) after 7 cycles, D) after 10 cycles, hot corrosion in $Na_2SO_4 + V_2O_5$ at 1100˚C

V_2O_5 may also react with Ta_2O_5 directly at elevated temperature and the products could be $TaVO_5$ or VTa_9O_{25}. According to Ta_2O_5-V_2O_5 phase diagram in temperatures lower than 1200˚C two possible components are $TaVO_5$ and Ta_9VO_{25}, as described below[37, 92]

$$V_2O_5\ (l) + TaYSZ\ (Ta_2O_5)\ (s) \rightarrow 2TaVO_5\ (s) \quad (6)$$

$$V_2O_5\ (l) + 9\ TaYSZ\ (Ta_2O_5)\ (s) \rightarrow 2Ta_9VO_{25}\ (s) \quad (7)$$

According to the XRD patterns of the as-received TaYSZ, weak peaks of Ta_2O_5 were detected. After 80 hours (twenty 4-h cycles) at 1100˚C with Na_2SO_4 + V_2O_5, in contrast to the hot corrosion behavior of the YSZ sample, only very weak $NaTaO_3$, TaV_9O_{25} , $TaVO_5$ and YVO_4 XRD peaks could be detected on the surface of the TaYSZ sample. Since vast areas of $Zr_{0.66}Y_{0.17}Ta_{0.17}O_2$ and $TaZr_{2.75}O_8$ were identified intact after hot corrosion and the excess Ta_2O_5 peaks in the as-received sample disappeared after the hot corrosion, it is more likely that the excess Ta_2O_5 in the sample would react with the molten salt to form the above mentioned products. No spallation of the sample was found even after 80 hours (twenty 4-h cycles) of testing at 1100˚C, which is twice the YSZ test duration. Thus the amount of Ta_2O_5 stabilizer inside the TaYSZ sample is high enough to keep zirconium tantalum oxide stabilized.

The detection of tetragonal $Zr_{0.66}Y_{0.17}Ta_{0.17}O_2$ and orthorhombic $TaZr_{2.75}O_8$ by XRD and EDS over a vast surface area of the TaYSZ sample after hot corrosion suggests that both phases are stable to the molten salt attack.

No evidences from the XRD patterns indicate direct chemical interactions between Na_2SO_4 with YSZ and TaYSZ, thus the chemical reactions between Na_2SO_4 and YSZ and TaYSZ are believed to be minimum at the elevated temperature of 1100˚C. For the YSZ sample, YVO_4 forms throughout the entire surface of the sample. Apart from the stresses induced by the ZrO_2 phase transfer due to the depletion of Y_2O_3, as foreign objects, the corrosion product (YVO_4) could impose extra stresses, which can easily initiate cracks and damage the coating [31, 41, 54]. For the TaYSZ sample, after 80 h of accelerated hot corrosion testing, many regions in the TaYSZ sample are still intact and the original $Zr_{0.66}Y_{0.17}Ta_{0.17}O_2$ and $TaZr_{2.75}O_8$ phases exist. On the surface of the TaYSZ samples, the amount of hot corrosion products is significantly less than the amount of hot corrosion products found on the YSZ sample. Although XRD shows very

weak peaks of YVO_4, no YVO_4 was observed in the SEM images. The strong interaction between Y and Ta in the solid solution of TaYSZ leads to formation of a highly stable phase which has lower tendency to react with V in the melt, thus no YVO_4 formed after hot corrosion. It is evident that the TaYSZ composition has significantly higher corrosion resistance than the standard YSZ.

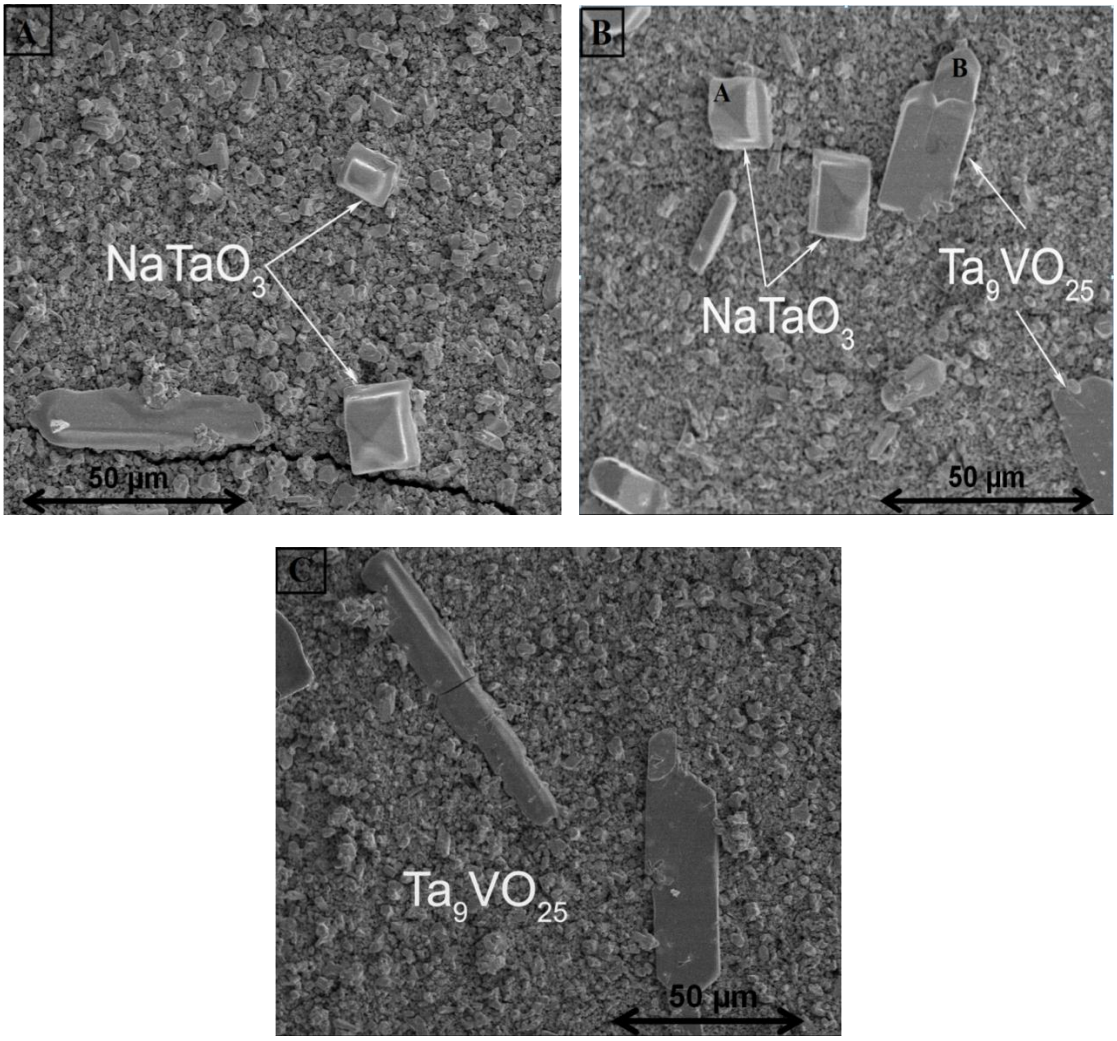

Figure 5.6 SEM surface images of TaYSZ after hot corrosion in $Na_2SO_4 + V_2O_5$ at 1100˚C after 80 hours.

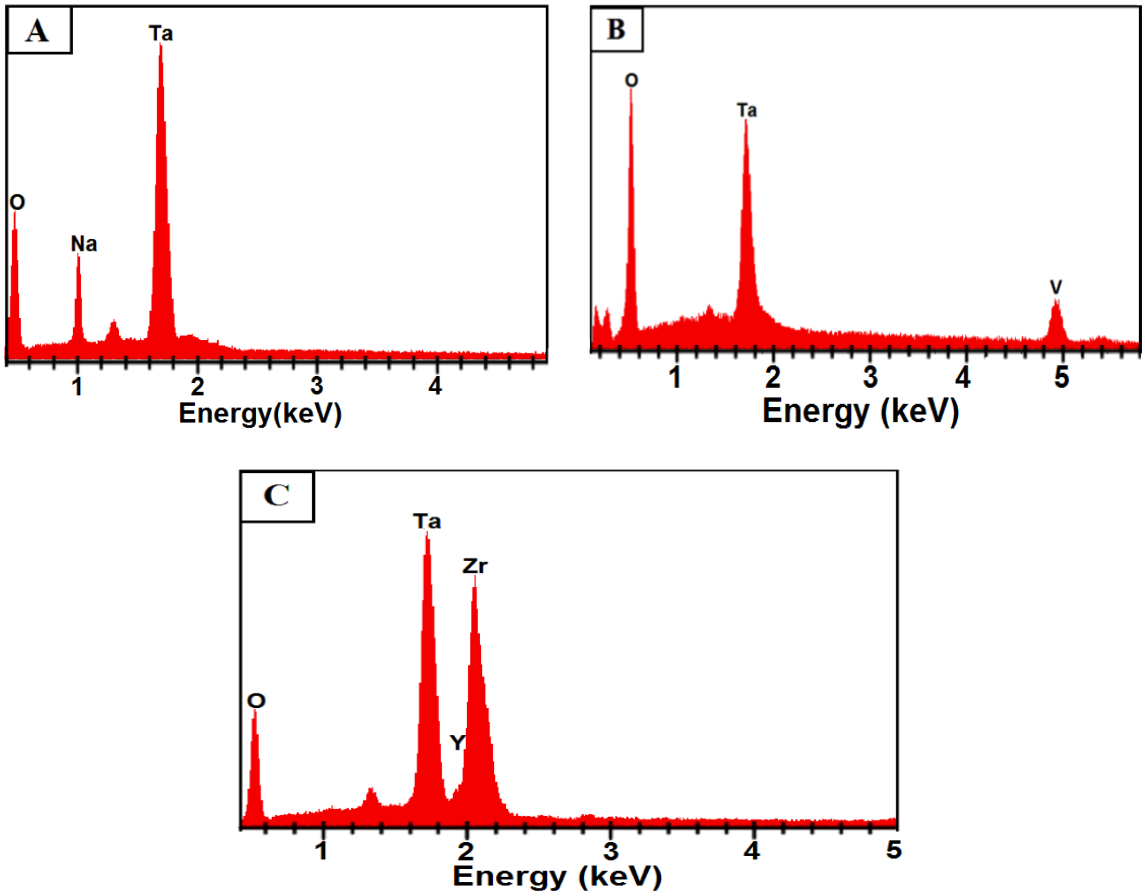

Figure 5.7 EDS spectra from the surface of TaYSZ after hot corrosion in Na_2SO_4 + V_2O_5 at 1100˚C after 80 hours (Figure 5.6) (A) crystal at region A in Figure 5.6B, (B) crystal at region B in Figure 5.6B, and (C) matrix in Figure 5.6C.

5.5 Conclusions

The hot corrosion resistances of YSZ and TaYSZ samples to Na_2SO_4 + V_2O_5 mixtures were studied. Under a typical gas turbine component surface temperature of 1100˚C, the reactions between yttria (Y_2O_3) and $V_2O_5/NaVO_3$ produce YVO_4, leaching Y_2O_3 from the YSZ and causing progressive tetragonal to monoclinic destabilization transformation. After 40 h (10 cycles) of hot corrosion test at 1100˚C, visible cracks formed on the surface of the YSZ sample and it failed. For the TaYSZ sample, molten Na_2SO_4 + V_2O_5 mixture reacts weakly with the sample to form $NaTaO_3$, $TaVO_5$ and Ta_9VO_{25} after 80 h (20 cycles) of hot corrosion testing. On

the surface of the TaYSZ, hot corrosion products are significantly smaller (about 10μm in length) than the large plate shaped YVO_4 found in the YSZ sample (about 60 μm in length). Based on the degradation rate, the corrosive layer thickness, and the general status of the coating after hot corrosion, TaYSZ has a better hot corrosion resistance at a temperature of 1100˚C than that of YSZ. Thus TaYSZ offers good opportunities for developing novel TBC compositions with improved resistance to corrosion by sulfate/vanadate melts.

5.6 Disclaimer

This report was prepared as an account of work sponsored by an agency of the United States Government. Neither the United States Government nor any agency thereof, nor any of their employees, makes any warranty, express or implied, or assumes any legal liability or responsibility for the accuracy, completeness, or usefulness of any information, apparatus, product, or process disclosed, or represents that its use would not infringe privately owned rights. Reference herein to any specific commercial product, process, or service by trade name, trademark, manufacturer, or otherwise does not necessarily constitute or imply its endorsement, recommendation, or favoring by the United States Government or any agency thereof. The views and opinions of authors expressed herein do not necessarily state or reflect those of the United States Government or any agency thereof.

5.7 Acknowledgments

This publication is based upon work supported by the US Department of Energy National Energy Technology Laboratory under Award Number DE-FE0004734 and NASA-EPSCoR program (Grant NNX09AP72A).

6 Evolution of Hot Corrosion Behavior of YSZ-Ta_2O_5 Composites with Different YSZ/Ta_2O_5 Ratios[4]

6.1 Abstract

This study compares the hot corrosion performance of yttria stabilized zirconia (YSZ)-Ta_2O_5 composite mixtures (TaYSZ) in the presence of molten mixture of Na_2SO_4 + V_2O_5 at 1100˚C. The tested compositions vary from pure YSZ (0TaYSZ) to a Ta_2O_5 dominating (70 wt%Ta_2O_5+ balance YSZ, 70TaYSZ) composite mixture with a gradual increase of Ta_2O_5. 50TaYSZ (50 wt% Ta_2O_5 + balance YSZ) sample forms a highly stable zirconium tantalum oxide. 50TaYSZ is more stable, both thermally and chemically in Na_2SO_4+V_2O_5 media at 1100˚C, than other tested YSZ-Ta_2O_5 (TaYSZ) composites, and shows a good hot corrosion resistance.

6.2 Introduction

To increase thermal conversion efficiency, advanced gas-turbines are being developed for high operating temperatures. Ceramic thermal barrier coatings (TBCs) are extensively used as insulation materials protecting the underlying metallic structure of gas turbine components under severe operating temperatures and enhancing the engine efficiencies [17, 29, 95, 107-110].

Currently, yttria stabilized zirconia (YSZ), especially zirconia containing 8 wt. % yttria coatings are the mostly used TBCs for gas turbines. YSZ has a low thermal diffusivity (2.5 W/m K at 1273 K) as well as a good coefficient of thermal expansion ($\sim 10^{-5}$/˚C). These characteristics naturally make it a good material for use as a TBC. However, the reliability of

[4] Chapter 6 previously appeared as [Hamed Habibi and Shengmin Guo, Evolution of Hot Corrosion Behavior of YSZ-Ta_2O_5 Composites with Different YSZ/Ta_2O_5 Ratios, *International Journal of Applied Ceramic Technology,* 1–9 (2014)]. It is reprinted by permission of *International Journal of Applied Ceramic Technology* (See Appendix A)

YSZ coatings can be weakened easily due to its phase transformation and sintering or densification behavior at high operating temperatures under corrosive environments [32, 35, 59, 111-113]. Hot corrosion on oxide coatings usually results from the presence of salt contaminants such as Na_2SO_4, NaCl and V_2O_5 [11, 15, 60, 65, 67, 114, 115], mainly due to the environment and the use of low quality fuels. There are numerous earlier studies on the hot corrosion behavior of YSZ coatings against foremost corrosive materials such as vanadium pentoxide (V_2O_5), sodium sulfate (Na_2SO_4) etc. at elevated temperatures [21, 22, 38, 41, 74, 115-118].

To enhance the stability of YSZ beyond 1200˚C, many researchers have tried further doping of the YSZ system, for example, with bigger or smaller cations of rare-earth elements [36]. A comparative analysis of various stabilizers including MgO, Y_2O_3, Sc_2O_3, In_2O_3, CeO_2, SmO_2 and TiO_2 appeared in [37]. Such studies have shown that the YSZ is attacked by pure $NaVO_3$, resulting in the removal of yttria as YVO_4 and the destabilization of the tetragonal to the monoclinic phase. Scandia- and india-stabilized zirconia have proven more resistant than yttria-stabilized zirconias to corrosion by vanadia [21, 38-41, 74]. This behavior shows that an oxide whose cation is more acidic than yttrium, such as scandium and indium, would be thermodynamically less prone to react with acidic oxides. Thus, when stabilized with such oxides the zirconia would be more resistant to hot corrosion by acidic oxides [37, 39, 40].

An alternate approach to YSZ TBC improvement is using Ta_2O_5 as a co-doped stabilizer. The solubility of Ta^{5+} in ZrO_2 is quite modest, but there is a strong synergism when co-doping with Y^{3+} so that the solubility of $YTaO_4$ in tetragonal ZrO_2 is much higher than that of Y^{3+} or Ta^{5+} alone. This strong interaction between Y^{3+} and Ta^{5+} in solid solution suggests that their activities are mutually reduced, which implies that the tendency of Y^{3+} to react with V^{5+} in the melt could be substantially lower than in the YSZ [40, 43-45, 76, 77].

Data in literature indicate defect association between the larger Y^{3+} ion (Y^{3+} ionic radius = 104 pm) and the smaller Ta^{5+} ion (Ta^{5+} ionic radius = 78 pm) in zirconia matrix (Zr^{2+} ionic radius = 86 pm), leading to decreased chemical potential and diffusivity of these ions [40]. The strong interaction between the Y^{3+} and Ta^{5+} ions can also reduce the individual activities of cations and hence make the Y^{3+} cations less susceptible to react with foreign ions such as V^{5+}(V^{5+} ionic radius = 54 pm). According to S. Raghavan et. al. [76]. the Y_2O_3-Ta_2O_5 co-doped zirconia is more resilient to the $NaVO_3$ attack. Ta-doped YSZ, which is stable up to 1500˚C and has a low thermal conductivity and a comparable coefficient of thermal expansion, has been reported as one prospective TBC.

With sufficiently high levels of dopants, the synergistic effect of the local distortions associated with the substitution of larger Y^{3+} and smaller Ta^{5+} cations for Zr^{4+} result in stabilization of the single phase even in the absence of anion vacancies [36, 40, 44, 45, 76]. Along with the good phase stability and mechanical properties, the Y_2O_3-Ta_2O_5 co-doped zirconia system was also found to be suitable for plasma spraying [76]. Air plasma spray (APS) coatings of the same material were also reported to show promising durability in burner rig testing [76]. However, previous reports on Y_2O_3-Ta_2O_5 co-doped zirconia systems mainly have a focus on the system stability and on the study of associated thermal properties. The investigated compositions generally have a low Ta_2O_5 content of less than 20 wt%.

To better understand the effect of doping of different amount of Ta_2O_5 in YSZ on hot corrosion behavior of YSZ-Ta_2O_5 systems, in this paper, YSZ-Ta_2O_5 composite mixtures (0 to 70 wt%Ta_2O_5) are made, and the phase stability and hot corrosion behaviors of YSZ-Ta_2O_5 composites in Na_2SO_4+V_2O_5 at 1100˚C are presented.

There are many publications on the hot corrosion study of alloys. Apart from SEM, EDS, and XRD, the measurement of weight gain/loss is a direct indication of the hot corrosion process [109, 119-124]. For alloys, NiCrAlY was found to be one of the most protective materials against hot corrosion due to the formation of a continuous, protective, and adherent alumina scale. The hot corrosion process typically has three stages [125]; (1) the initial weight gain is mainly due to the oxidation and formation of thermally grown oxide (TGO); (2) the minimum weight change period. In this stage, oxidation rate and spallation due to cracking and dissolution of oxide scale in the salt would be equal; and (3) weight loss period due to spallation and dissolving of TGO in the molten salt. By examine the hot corrosion of NiCoCrAlTaY coated superalloy, Mei et al. [126] reported a parabolic ‘‘diffusion controlled’’ region I at a rate of $4.6x10^{-6}$ mg^2 cm^{-4} s^{-1}, the combination of parabolic and linear ‘‘reaction–diffusion controlled’’ region II at rate of 2.28 $x10^{-5}$ mg^2 cm^{-4} s^{-1} and 4.35 $x10^{-5}$ mg^2 cm^{-2} s^{-1}, and finally the complete ‘‘reaction controlled’’ region III at the rate of 3.92 $x10^{-4}$ mg^2 cm^{-2} s^{-1} . The ‘‘diffusion controlled’’ region I is related to growth of the protective oxide scales, mainly dense and continuous α-Al_2O_3; The ‘‘reaction–diffusion controlled’’ region II is related to reactions of major alloy elements with O_2 and Na_2SO_4 diffused inward through the discontinuous net-like structured Al_2O_3; and the ‘‘reaction controlled’’ region III is related to direct reactions of major alloy elements with O_2 and Na_2SO_4 after complete failure of the protective scales. The spallation of the scales by the rapid scale growth and thermal stress is the main reason for weight loss.

Ceramic oxides generally have a much better hot corrosion resistance than most alloys. Cho et al. [127] studied the hot corrosion of the bare and YSZ coated IN713LC samples in LiCl–3 wt.% Li_2O at 675 °C for 216 h. It’s found that the YSZ coated IN713LC sample has a weight loss (0.5 wt%) about one tenth of the bare IN713 sample. Ramachandran et al. [128] reported the study of

cyclic hot corrosion behavior of atmospheric plasma sprayed Lanthanum Zirconate based coatings in contact with a mixture of sodium sulphate and vanadate salts. After 100 one-hour cycles at 1000 °C, the base metal, Inconel 738, has a weight gain of 36 mg/cm^2, while the best ceramic coating, a Lanthanum Zirconate/ Yttria Stabilized Zirconia layered structure, has a weight gain of only 4 mg/cm^2.

In this study, by altering the YSZ-Ta_2O_5 compositions, a highly stable zirconium tantalum oxide is formed, As the zirconium tantalum oxide is much more stable than YSZ, both thermally and chemically in Na_2SO_4+V_2O_5 media, the weight change is expected to be very small. To accurately measure the sample weight changes, the salt vapor pressure over the test specimens ideally should be maintained, to compensate the weight loss due to the possible salt vaporization. This could be done by using a stream of carrying gas partially carrying water vapor through a bubble bottle and then a crucible filled with salt, with a careful calibration to find out the salt vapor pressure.

The major focus of this paper is on the reaction chemistry of YSZ-Ta_2O_5 composites with molten salts. SEM, EDS, and XRD give enough information to draw the conclusions based on this comparative study. Thus in this study, the constant salt vapor pressure was not implemented, and the sample weight change was not measured.

6.3 Experimental Procedure

Hot corrosion studies using Na_2SO_4 and V_2O_5 mixture were conducted on YSZ-Ta_2O_5 composite samples at 1100˚C in air. For the salt mixture, 95% Na_2SO_4 and 99.9% V_2O_5 from Sigma Aldrich were used. Eight YSZ-Ta_2O_5 composite samples were made. The compositions of the tested samples are listed in Table 6.1. These samples were made using agglomerated powders

from Sigma Aldrich. To obtain the samples, powders were first pressed with binders in a uniaxial die (2.5 cm inner diameter) at 350 MPa pressure to obtain the compressed green bodies, which were then sintered at 1450˚C for 5 hours and 30 minutes to obtain the dense bodies.

The densities of the sintered samples were measured by the Archimedes technique using water as the buoyant medium. To perform an accelerated high-temperature hot corrosion test on samples, a mixture of 50wt% Na_2SO_4 + 50wt% V_2O_5 deposit was spread evenly onto the surfaces of the specimens with a salt amount of 20 mg/cm^2.

Table 6.1. The compositions of tested samples

Sample	Composition	Name
1	100 wt% YSZ	0TaYSZ
2	90 wt%YSZ + 10 wt% Ta_2O_5	10TaYSZ
3	80 wt%YSZ + 20 wt% Ta_2O_5	20TaYSZ
4	70 wt%YSZ + 30 wt% Ta_2O_5	30TaYSZ
5	60 wt%YSZ + 40 wt% Ta_2O_5	40TaYSZ
6	50 wt%YSZ + 50 wt% Ta_2O_5	50TaYSZ
7	40 wt%YSZ + 60 wt% Ta_2O_5	60TaYSZ
8	30 wt%YSZ + 70 wt% Ta_2O_5	70TaYSZ

The specimes were then set in an electric furnace with an ambient atmosphere under a maximum temperature of 1100˚C for 4 h. After each 4 h of testing at 1100˚C, the samples were allowed to cool down inside the furnace, and then the samples were inspected both visually and with an optical microscope for possible crack initiation. To repeat the test, the samples were

recoated with the Na_2SO_4 + V_2O_5 salt mixture and the heating profile was repeated. The morphology and microstructure of the as received samples and the samples after the hot corrosion tests were examined using field emission scanning electron microscopy (Quanta^{TM}3D FEG, FEI Company, USA). For surface morphology studies using SEM, a thin Pt layer was sputtered onto the samples to improve the electrical conductivity. X-ray diffraction (MiniFlex XRD, Rigaku Corporation, Japan) with Cu Kα radiation λ = 1.54178 Å at a scan speed of 1˚/min was used to establish the phase composition of the specimen.

6.4 Phase Stability and Hot Corrosion Behavior of 0TaYSZ, 10TaYSZ, 20TaYSZ and 30TaYSZ

Figure 6.1 reveals the X-ray diffraction patterns for the as-received 0TaYSZ, 10TaYSZ, 20TaYSZ and 30TaYSZ specimens. As indicated by the XRD patterns, all four compositions of YSZ-Ta_2O_5 had a tetragonal zirconia crystal structure. For these compositions, the amount of Ta_2O_5 addition is not high enough to form complex tantalum zirconium or tantalum yttrium zirconium oxides. Instead, tetragonal zirconia is found to be the only phase formed, with Ta_2O_5–Y_2O_3 dopants in the ZrO_2 matrix. For the four samples shown in Figure 6.1, the highest Ta_2O_5 mol% (in 30TaYSZ) is 11%. Similar findings are reported in previous studies [26, 77, 78]. For the ZrO_2–Ta_2O_5–Y_2O_3 system, many published studies used equal co-doping of Ta_2O_5/Y_2O_3 into ZrO_2 [36, 40, 44]. It was reported that tetragonal ZrO_2 based solid solution was a single phase and non-transformable, with up to 22 mol% of Ta_2O_5/Y_2O_3 as dopants[26, 77]. When the amount of Ta_2O_5 and Y_2O_3 is not equal in a ZrO_2–Ta_2O_5–Y_2O_3 system, the formed phases after sintering at high temperature could be tetragonal zirconia, orthorhombic zirconia, and $YTaO_4$. According to ZrO_2–Ta_2O_5–Y_2O_3 phase diagram [26, 44, 77], with around 20 mol% of Ta_2O_5, a complex

tantalum zirconium oxide may form at high temperature but upon cooling tetragonal or orthorhombic zirconia can be formed.

Figure 6.2 shows XRD patterns of 0TaYSZ, 10TaYSZ, 20TaYSZ and 30TaYSZ specimens after hot corrosion at 1100˚C in Na_2SO_4+V_2O_5 salt for 40 hours. Comparing the patterns of the as-received sintered specimen, most of the tetragonal zirconia in the 0TaYSZ sample has been changed to the monoclinic phase and YVO_4 was formed as a major hot corrosion product.

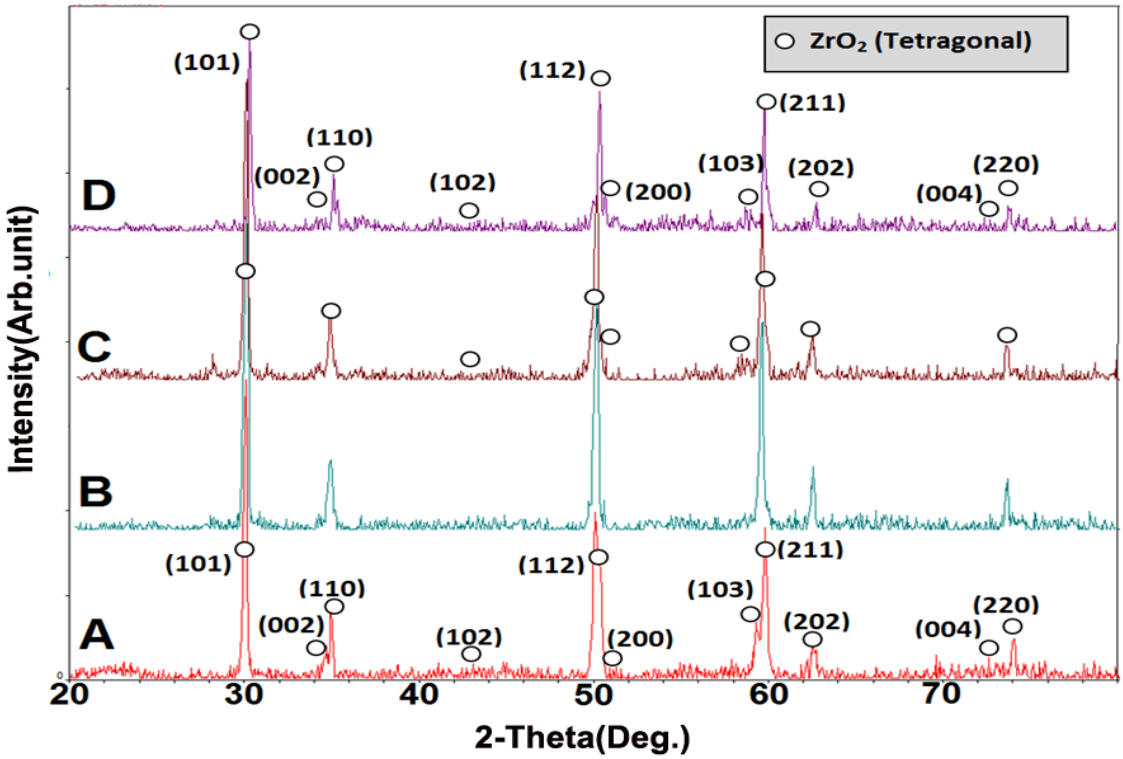

Figure 6.1 XRD patterns of as-received A) 0TaYSZ, B) 10TaYSZ, C) 20TaYSZ and D) 30TaYSZ

For 10TaYSZ and 20TaYSZ samples, the same transformation happened and a portion of the tetragonal zirconia changed to monoclinic zirconia.

The fraction of monoclinic phase in the sample (M%) was estimated by the following equation:

$$M\% = (M1 + M2) / (M1 + M2 + T) \quad (1)$$

where T is the intensity of tetragonal ZrO_2 (2θ=30.271) peak, M1 the intensity of monoclinic ZrO_2 (2 θ =28.218) peak and M2 is the intensity of monoclinic ZrO_2 (2θ =31.502) peak in XRD patterns after hot corrosion tests [54]. The quantities of monoclinic zirconia phase (M%) are presented in Table 6.2. Table 6.2 shows that the portion of monoclinic phase is decreased from 60% in 0TaYSZ sample to 26% in 30TaYSZ and the portion of monoclinic zirconia in both 10TaYSZ and 20TaYSZ is about 30% which are well below the 0TaYSZ case. The co-doping of Ta_2O_5 and Y_2O_3 reduced the tendency of zirconia transformation from tetragonal to monoclinic phase upon cooling. Also YVO_4 formed on all of these specimens after hot corrosion. This shows that up to 30 wt. % of Ta_2O_5 as the dopant for YSZ is not enough to stabilize the tetragonal phase of zirconia completely and it is not enough to form a new complex Tantalum Zirconium compound.

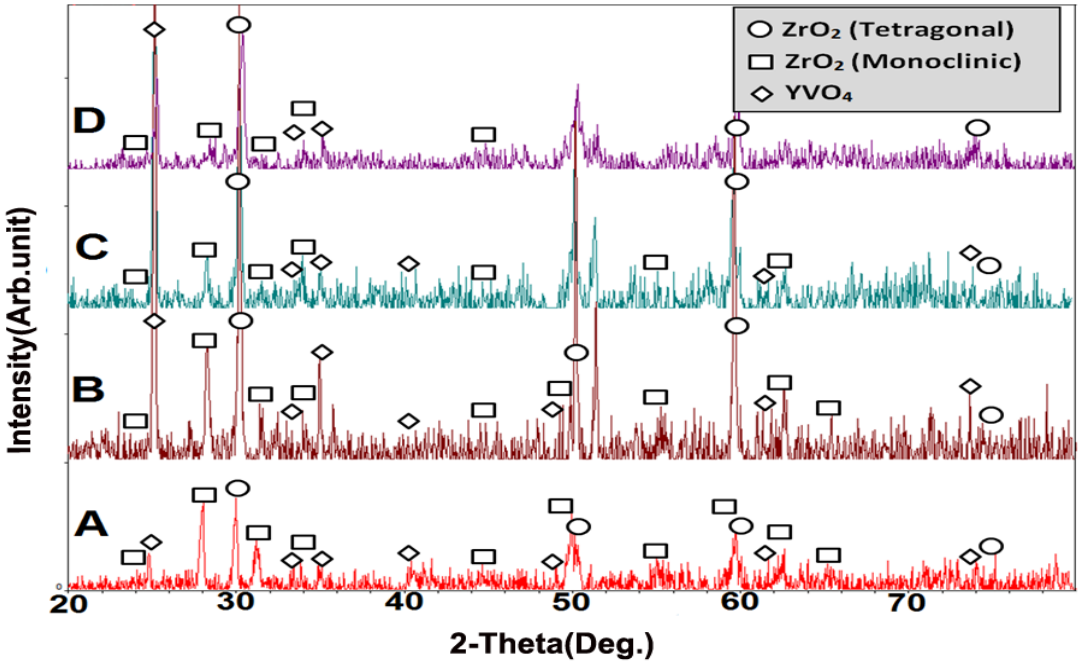

Figure 6.2 XRD patterns of A) 0TaYSZ, B) 10TaYSZ, C) 20TaYSZ and D) 30TaYSZ after hot corrosion in Na_2SO_4 + V_2O_5 at 1100˚C for 40 hours

Typical surface morphologies of the 0TaYSZ, 10TaYSZ, 20TaYSZ and 30TaYSZ specimens after hot corrosion tests are presented in Figure 6.3. Apart from XRD analysis (Figure 6.2), Energy Dispersive Spectroscopy (EDS) analysis was performed at different regions of the specimen to confirm the chemical compositions of the hot corrosion products. For crystals in Figure 6.3A, EDS analysis demonstrated that these crystals were composed of yttrium, vanadium, and oxygen. Further analysis confirmed these crystals were YVO_4. Corrosion products had a layered morphology with an outermost layer of YVO_4, followed by an inner layer of monoclinic zirconia.

Table 6.2. The fraction of monoclinic zirconia in the coatings after hot corrosion tests.

Sample	Composition	Name	Monoclinic Zirconia (%)
A	100 wt% YSZ	0TaYSZ	60
B	90 wt%YSZ + 10 wt% Ta_2O_5	10TaYSZ	30
C	80 wt%YSZ + 20 wt% Ta_2O_5	20TaYSZ	29
D	70 wt%YSZ + 30 wt% Ta_2O_5	30TaYSZ	26

For 10TaYSZ, the hot corrosion products were also found to be YVO_4 and they grow into the dendiritic shape. Dendiritic growing of crystals, which covered the entire surface, shows that reaction rate is considerable (Figure 6.3B). For 20TaYSZ (Figure 6.3C) and 30TaYSZ (Figure 6.3D), the YVO_4 crystals were rod shaped and covered a large portion of the surface area.

Although the 20TaYSZ and 30TaYSZ samples were degraded, the hot corrosion rate was considered to be less than the 0TaYSZ and 10TaYSZ cases. Ta_2O_5 might react with molten salt

and form new crystals; however no XRD peaks of any tantalum were found in 0TaYSZ, 10TaYSZ, 20TaYSZ, and 30TaYSZ samples.

6.5 Phase Stability and Hot Corrosion Behavior of 40TaYSZ, 50TaYSZ, 60TaYSZ and 70TaYSZ

Figure 6.4 shows the X-ray diffraction patterns for the as-received 40TaYSZ, 50TaYSZ, 60TaYSZ and 70TaYSZ specimens. For 40TaYSZ specimen (Figure 6.4E) only diffraction peaks corresponding to tetragonal zirconia can be distinguished.

The addition of Ta_2O_5 brings about the gradual stabilization of tetragonal zirconia or forming a new complex material. In the 50TaYSZ and 60TaYSZ specimens (Figure 6.4F and 6.4G), zirconium tantalum oxide forms as the result of sintering YSZ and Ta_2O_5 mixture at high temperature. Two compounds are identified to contribute the XRD patterns of 50TaYSZ and 60TaYSZ, $Zr_{0.66}Y_{0.17}Ta_{0.17}O_2$ tetragonal and $TaZr_{2.75}O_8$ orthorhombic. Weak peaks of orthorhombic Ta_2O_5 are also detected in these two samples, with slightly higher Ta_2O_5 peaks in 60TaYSZ; However, only based on the XRD patterns shown in Figure 6.4, the presence of a pure ZrO_2 phase (with Ta_2O_5–Y_2O_3 dopants) cannot be ruled out. This is because although the peaks at 2θ=30.2, 50.3 and 59.8° correspond to the solid solutions of $TaZr_{2.75}O_8$ and $Zr_{0.66}Y_{0.17}Ta_{0.17}O_2$, the tetragonal ZrO_2 peak also appears at 2θ =30.2°. Previous investigations showed similar results [36, 44, 77, 106]. XRD pattern of 70TaYSZ (Figure 6.4H) sample is different from the patterns of 50TaYSZ and 60TaYSZ. In the 70TaYSZ case, more intense peaks contributing to orthorhombic Ta_2O_5 can be distinguished.

Figure 6.5 shows XRD patterns of 40TaYSZ, 50TaYSZ, 60TaYSZ and 70TaYSZ specimens after hot corrosion at 1100˚C in Na_2SO_4+V_2O_5 salt for 40 hours. SEM images of the 40TaYSZ,

50TaYSZ, 60TaYSZ and 70TaYSZ specimen after hot corrosion tests are presented in Figure 6.6. For 40TaYSZ sample, comparing to the patterns in Figure 6.2 A to D, although less tetragonal zirconia changed to monoclinic zirconia and less YVO_4 crystals formed as hot corrosion products, this specimen degraded and corroded like previous specimens. The YVO_4 crystals had a rod-shape and they didn't grow into clusters. The extent of the attack is much smaller in comparison to the 0TaYSZ to 30TaYSZ specimens.

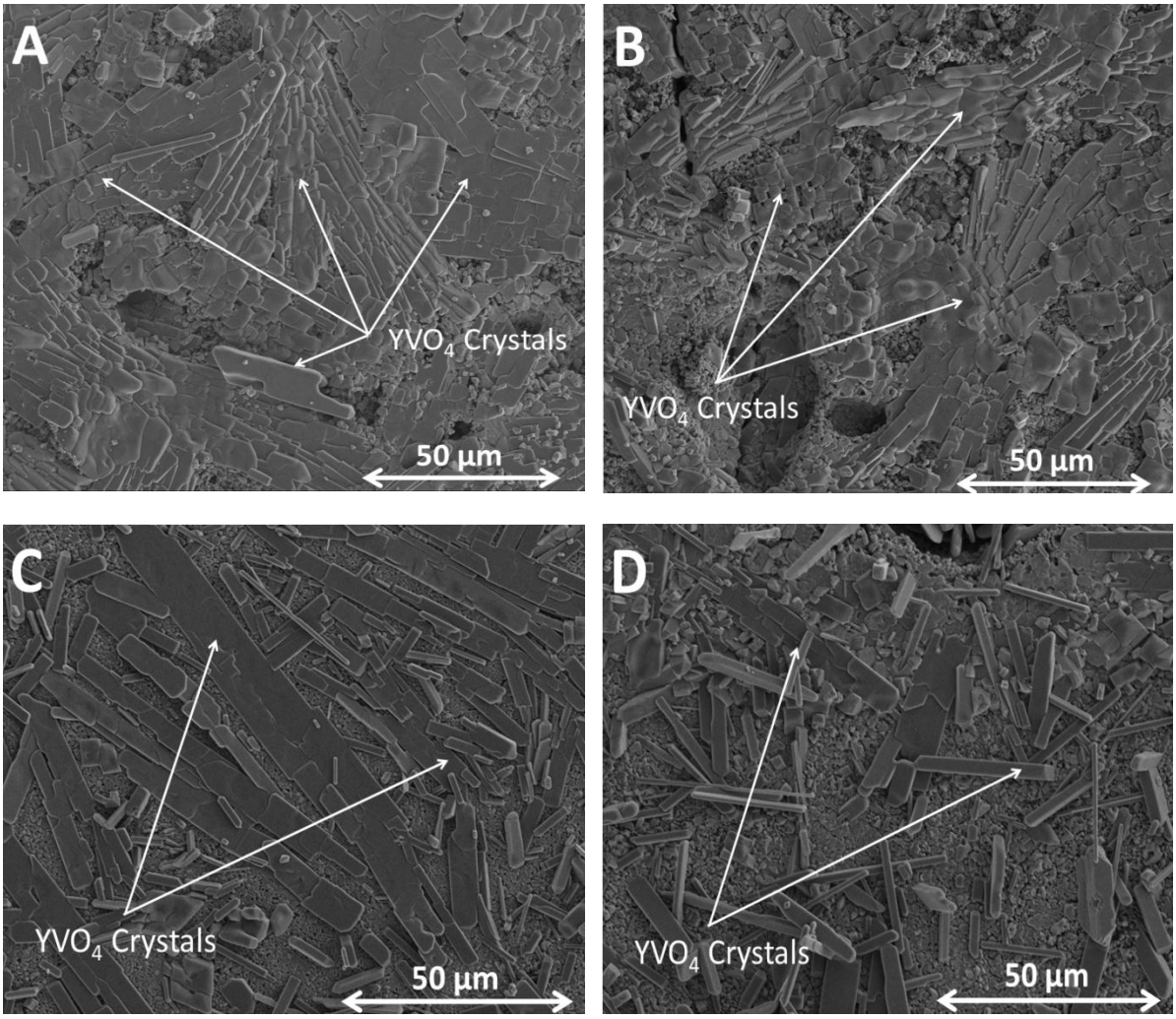

Figure 6.3 SEM surface images of A) 0TaYSZ, B)10TaYSZ, C) 20TaYSZ, D) 30TaYSZ, hot corrosion in $Na_2SO_4 + V_2O_5$ at 1100˚C for 40 hours

Based on SEM images, the 50TaYSZ sample appears to have very minor reactions with the corrodent salt. After hot corrosion, only a small quantity of rod-shaped crystals was formed.

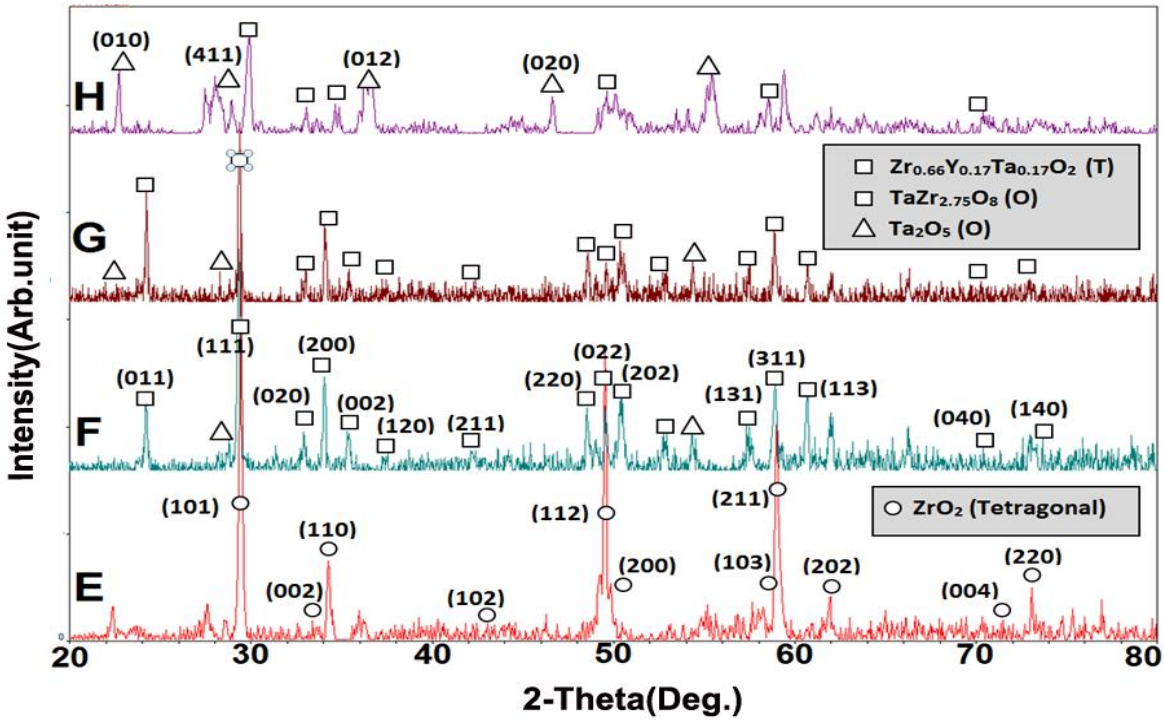

Figure 6.4 XRD patterns of as-received E) 40TaYSZ, F) 50TaYSZ, G) 60TaYSZ and H) 70TaYSZ

Crystals in Figure 6.6B contain sodium, tantalum and oxygen and with considering the XRD pattern, they are found to be $NaTaO_3$. The matrix in Figure 6.6B contains tantalum, zirconium, yttrium and oxygen. It is determined to be tantalum zirconium oxides, $Zr_{0.66}Y_{0.17}Ta_{0.17}O_2$ and $TaZr_{2.75}O_8$, which remain perfectly intact after exposure to molten salts during hot corrosion tests. The EDS spectra confirm the presence of $TaVO_5$ and Ta_9VO_{25} on the surface of 60TaYSZ specimen. Crystals in Figure 6.6D are Ta_9VO_{25}. In 60TaYSZ and 70TaYSZ samples, besides TaV_9O_{25}, strong peaks contributed to pure Ta_2O_5 and $TaVO_5$ were also detected. Considering peaks intensity, the reaction rate for 70TaYSZ is higher than the 60TaYSZ.

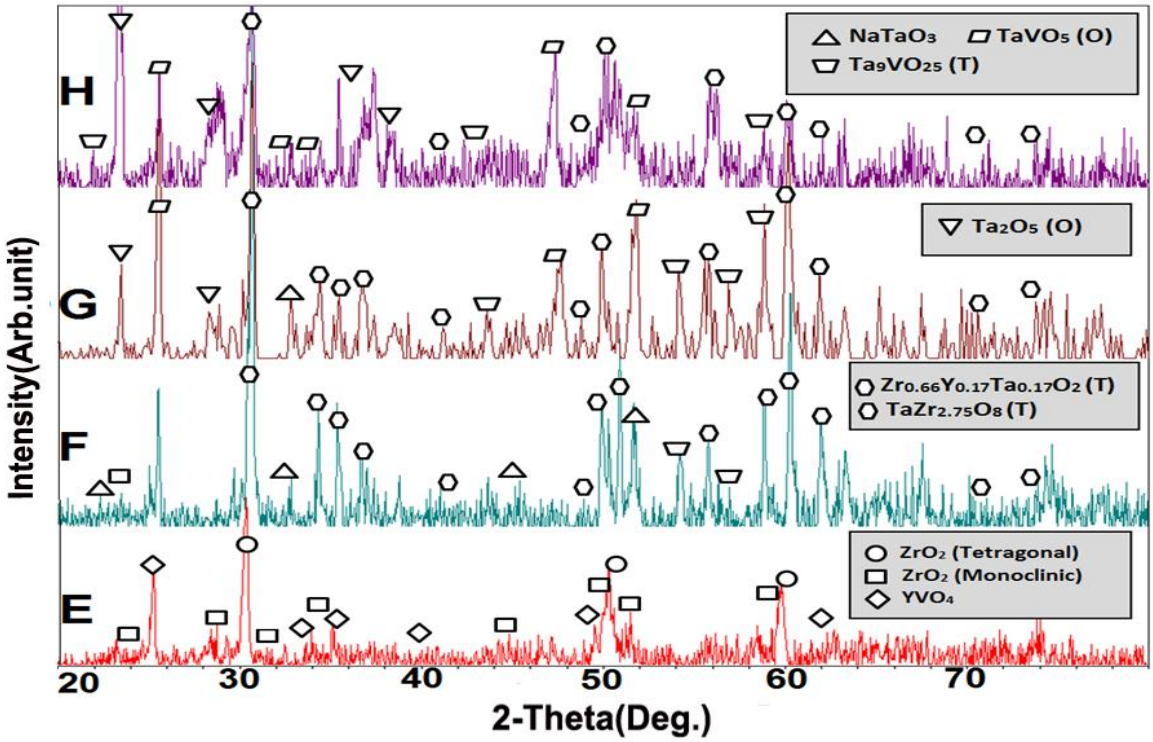

Figure 6.5 XRD patterns of E) 40TaYSZ, F) 50TaYSZ, G) 60TaYSZ and H) 70TaYSZ after hot corrosion in Na_2SO_4 + V_2O_5 at 1100˚C for 40 hours

Although matrix of these samples are $TaZr_{2.75}O_8$ and $Zr_{0.66}Y_{0.17}Ta_{0.17}O_2$, the amount of corrosion products states a weaker performance than 50TaYSZ. Considering the XRD patterns of 60TaYSZ and 70TaYSZ samples, large amount of Ta_2O_5 was detected in these samples. The formation of considerable amount of $TaVO_5$ and Ta_9VO_{25} crystals in these samples can be due to the faster reaction rate of excess Ta_2O_5 with the molten salt. For comparison, the 50TaYSZ sample is mainly formed by $TaZr_{2.75}O_8$ with very few excess Ta_2O_5. With high original Ta_2O_5 contents, exposure to Na_2SO_4+V_2O_5 salt does not cause destabilization of zirconium tantalum oxide in 50TaYSZ, 60TaYSZ, and 70TaYSZ to monoclinic phase, seen for the low Ta_2O_5 content TaYSZ samples.

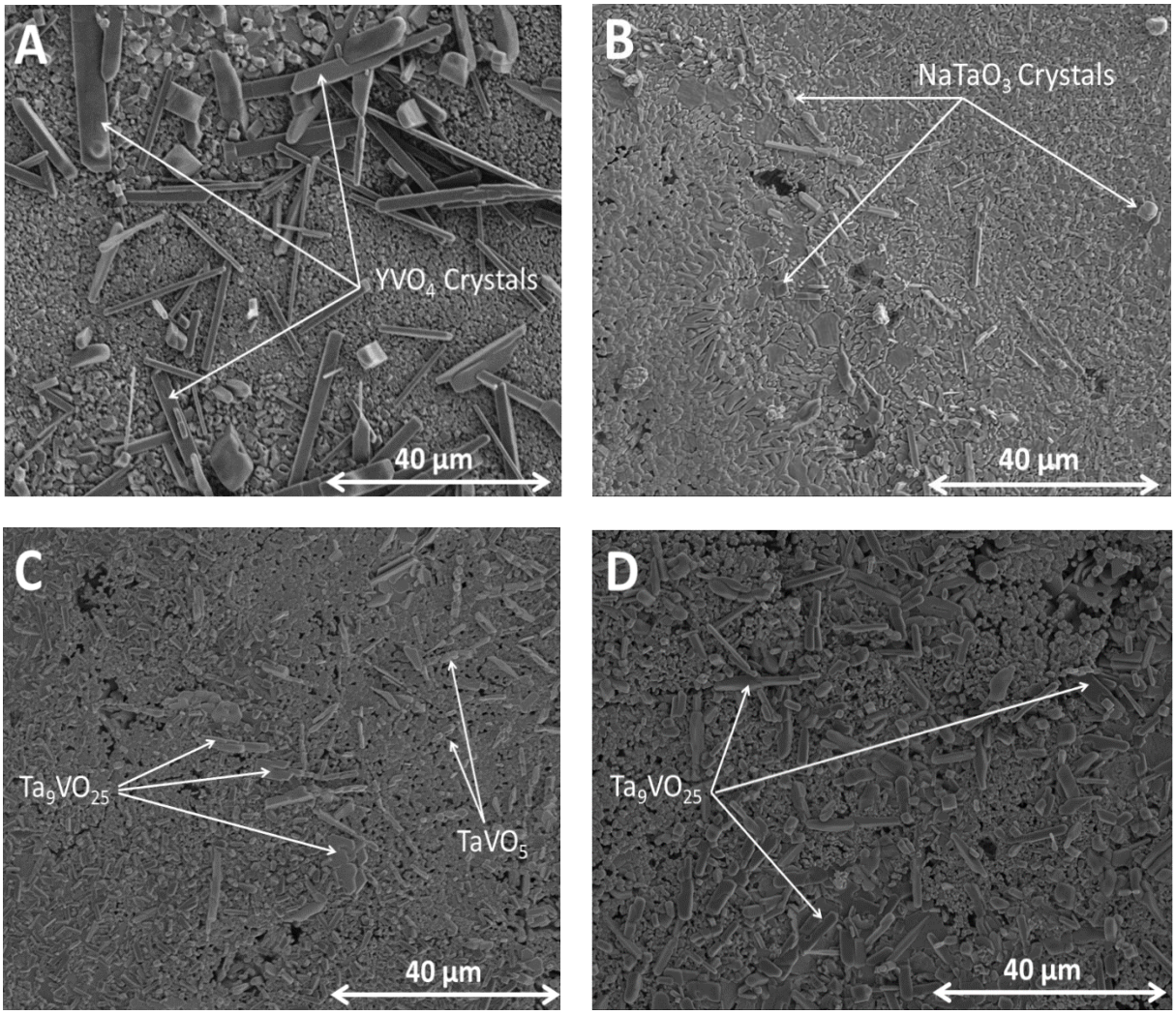

Figure 6.6 SEM surface images of A) 40TAYSZ, B) 50TaYSZ, C) 60TaYSZ, D) 70TaYSZ, after hot corrosion in Na_2SO_4 + V_2O_5 at 1100˚C for 40 hours

Substantial amount of research have been done on the corrosion behavior of YSZ in molten salts containing vanadium and sulfur [21, 22, 31, 41, 55]. The main mechanism is the dissolution of YSZ in the melt followed by re-precipitation of both YVO_4 and Y-depleted monoclinic zirconia. Attack by chemical reaction is characterized by the presence of an identifiable reaction product and usually by the ability to postulate a specific reaction. The laws of stoichiometry and thermodynamics apply. After exposure to molten salt at 1100˚C for 40 h (ten 4-h cycles), 0TaYSZ, 10TaYSZ, 20TaYSZ, 30TaYSZ and 40TaYSZ samples demonstrated the improvement

of hot corrosion resistance with the increase of Ta_2O_5. Chemical degradation of zirconia based samples stabilized with Y_2O_3, can be classified as successive occurrence of related chemical reactions during the hot corrosion tests. During the exposure of V_2O_5 and Na_2SO_4 salt mixture at a high temperature (1100˚C), $NaVO_3$ will be formed.

$$V_2O_5 + Na_2SO_4 \rightarrow 2(NaVO_3) + SO_3 \quad (2)$$

Then, $NaVO_3$, having a melting point of 610˚C, reacts with yttria from the YSZ solid solution to form YVO_4:

$$ZrO_2\ (Y_2O_3) + 2(NaVO_3) \rightarrow ZrO_2 + 2(YVO_4) + Na_2O \quad (3)$$

Also Na_2O can react with V_2O_5 directly to form $NaVO_3$:

$$Na_2O\ (base) + V_2O_5\ (acid) \rightarrow 2NaVO_3\ (salt) \quad (4)$$

For the 0TaYSZ, 10TaYSZ, 20TaYSZ, 30TaYSZ, and 40TaYSZ samples, after hot corrosion tests, thin rod/plate like YVO_4 crystals of various sizes are found covering most of the sample surfaces, Figures 6.3 and 6.6. In these samples Ta_2O_5 are not enough to act as co-dopant to stabilize zirconia. Because Y_2O_3 is more active and less stable than Ta_2O_5, it reacts with molten salt at a considerable rate. The Y^{3+} in the lattice of YSZ has the mobility to migrate preferentially toward the reaction interface due to the high V concentration presented on the sample surfaces [24]. The molten $NaVO_3$ is also reported to increase the atom mobility, hence further promote the depletion of yttria from YSZ and the growth of YVO_4 crystals. After losing Y_2O_3, the transformation of tetragonal zirconia to monoclinic zirconia during the cooling stage of thermal cycling is accompanied by a 3–5% volume expansion, leading to cracking and spallation of samples. For 50TaYSZ, 60TaYSZ and 70 TaYSZ, as described earlier, Na_2SO_4 and V_2O_5 would

first react and form $NaVO_3$, then, the possible reactions that would have produced those identified reaction products include [37, 40, 44]:

$$\text{TaYSZ } (Ta_2O_5)\ (s) + NaVO_3\ (l) \rightarrow NaTaO_3(s) + TaVO_5(s) \quad (5)$$

$$\text{TaYSZ } (5Ta_2O_5)\ (s) + NaVO_3\ (l) \rightarrow NaTaO_3(s) + Ta_9VO_{25}(s) \quad (6)$$

V_2O_5 may also react with Ta_2O_5 directly at elevated temperature. According to Ta_2O_5-V_2O_5 phase diagram in temperatures lower than 1200˚C two possible components are $TaVO_5$ and Ta_9VO_{25}, as described below [37, 92]

$$V_2O_5\ (l) + \text{TaYSZ } (Ta_2O_5)\ (s) \rightarrow 2TaVO_5\ (s) \quad (7)$$

$$V_2O_5\ (l) + 9\ \text{TaYSZ } (Ta_2O_5)\ (s) \rightarrow 2Ta_9VO_{25}\ (s) \quad (8)$$

After 40 hours (ten 4-h cycles) at 1100˚C with $Na_2SO_4 + V_2O_5$, in contrast to the hot corrosion behavior of the low Ta_2O_5 samples, only very weak $NaTaO_3$ and TaV_9O_{25} XRD peaks could be detected on the surface of the 50TaYSZ sample. Since vast areas of $Zr_{0.66}Y_{0.17}Ta_{0.17}O_2$ and $TaZr_{2.75}O_8$ were identified intact after hot corrosion and the excess Ta_2O_5 peaks in the as-received sample disappeared after the hot corrosion, it is more likely that the excess Ta_2O_5 in the sample would react with the molten salt to form the above mentioned products. This is further confirmed by the tests on samples 60TaYSZ and 70TaYSZ, which increasingly have more excess Ta_2O_5. No spallation was found on the 50TaYSZ sample even after 80 hours (twenty 4-h cycles) of testing at 1100˚C. The detection of tetragonal $Zr_{0.66}Y_{0.17}Ta_{0.17}O_2$ and orthorhombic $TaZr_{2.75}O_8$ by XRD and EDS over a vast surface area of the 50TaYSZ sample after hot corrosion suggests that both phases are stable to the molten salt attack. No evidences from the XRD patterns indicate direct chemical interactions between Na_2SO_4 with TaYSZ, thus the chemical reactions between Na_2SO_4 and YSZ and TaYSZ are believed to be minimum at the elevated temperature of 1100˚C.

Comparing all samples tested in this study, hot corrosion resistance of 50TaYSZ is the best. On ZrO_2-Y_2O_3-Ta_2O_5 phase diagram at high temperatures, 50TaYSZ is chemically equivalent to the combination of orthorhombic $TaZr_{2.75}O_8$ and tetragonal $Zr_{0.66}Y_{0.17}Ta_{0.17}O_2$. This study confirms that orthorhombic $TaZr_{2.75}O_8$ /tetragonal $Zr_{0.66}Y_{0.17}Ta_{0.17}O_2$ which are formed as the result of co-doping of zirconia with Y_2O_3 and Ta_2O_5, is highly stable in high temperatures and resistant to hot corrosion attack in molten salts.

6.6 Summary and Conclusion

The hot corrosion resistances of different compositions of YSZ and Ta_2O_5 composite samples to Na_2SO_4 + V_2O_5 mixture were studied. Under a typical gas turbine component surface temperature of 1100˚C, the reactions between yttria (Y_2O_3) and V_2O_5/$NaVO_3$ produce YVO_4, leaching Y_2O_3 from the YSZ and causing progressive tetragonal to monoclinic destabilization transformation. After 40 h (10 cycles) of hot corrosion test at 1100˚C, visible cracks formed on the surface of the 0TaYSZ sample and it failed. Among YSZ-Ta_2O_5 composite samples, with different amount of Ta_2O_5 (0 Wt. % to 70 Wt.%), the sample 50TaYSZ (50 wt% Ta_2O_5+ balance YSZ) showed the best hot corrosion resistance against molten mixture of Na_2SO_4 + V_2O_5 at 1100 ˚C, based on the degradation rate, the corrosive layer thickness, and the general status of the coatings after the hot corrosion tests. For the 50TaYSZ sample, molten Na_2SO_4 + V_2O_5 mixture reacts weakly with the sample to form $NaTaO_3$ and Ta_9VO_{25} after 40 h (10 cycles) of hot corrosion testing. On the surface of the 50TaYSZ, hot corrosion products are significantly smaller (about 10 μm in length) than the large plate shaped YVO_4 found in the 0TaYSZ sample (about 50 to 90 μm in length). The strong interaction between Y^{3+} and Ta^{5+} in the solid solution of 50TaYSZ leads to the formation of a highly stable zirconium tantalum oxide which has lower

tendency to react with V in the melt. 50TaYSZ offers good opportunities for developing novel TBC compositions with good resistance to corrosion by sulfate/vanadate melts.

6.7 Disclaimer

This report was prepared as an account of work sponsored by an agency of the United States Government. Neither the United States Government nor any agency thereof, nor any of their employees, makes any warranty, express or implied, or assumes any legal liability or responsibility for the accuracy, completeness, or usefulness of any information, apparatus, product, or process disclosed, or represents that its use would not infringe privately owned rights. Reference herein to any specific commercial product, process, or service by trade name, trademark, manufacturer, or otherwise does not necessarily constitute or imply its endorsement, recommendation, or favoring by the United States Government or any agency thereof. The views and opinions of authors expressed herein do not necessarily state or reflect those of the United States Government or any agency thereof.

6.8 Acknowledgments

This publication is based upon work supported by the US Department of Energy National Energy Technology Laboratory under Award Number DE-FE0004734 and NASA-EPSCoR program (Grant NNX09AP72A).

7 The Hot Corrosion Behavior of Plasma Sprayed Zirconia Coatings Stabilized with Yttria, Ceria, and Titania in Na_2SO_4+V_2O_5[5]

7.1 Abstract

This paper compares the hot corrosion performance of yttria stabilized zirconia (ZrO_2-3-4Y_2O_3, YSZ), ceria stabilized zirconia (ZrO_2-24CeO_2-2.5Y_2O_3, CSZ), and titania stabilized zirconia (ZrO_2-18TiO_2-10Y_2O_3, TiSZ) coatings in the presence of molten mixture of Na_2SO_4+V_2O_5 at 1050°C. These coatings were prepared by air plasma spray (APS). Characterizations using X-ray diffraction (XRD) and scanning electron microscope (SEM) indicate that in the case of YSZ, the reaction between $NaVO_3$ and Y_2O_3 produces YVO_4 and leads to the transformation of tetragonal ZrO_2 to monoclinic ZrO_2. For the CSZ coatings, by the formation of $CeVO_4$, the amount of YVO_4 formed on the CSZ coating is significantly reduced, thus the amount of monoclinic phase in the TBC coating is substantially reduced. For TiSZ coating, although some minor reactions happened and some $TiVO_4$ ribbons formed on the surface of coating, tetragonal zirconia was stable after hot corrosion test and no monoclinic zirconia was formed. Comparing to YSZ and CSZ under a temperature of 1050˚C, TiSZ coating is found to be more stable, both thermally and chemically, and exhibits a better hot corrosion resistance.

7.2 Introduction

Thermal barrier coating (TBC) systems typically consist of a metallic oxidation protection layer, the so called bond coat, and an isolative ceramic topcoat. TBCs are powerful tools to enhance engine efficiency and performance, in terms of higher operating temperatures and/or

[5] Chapter 7 previously appeared as [M. H. Habibi and S. M. Guo, The Hot Corrosion Behavior of Plasma Sprayed Zirconia Coatings Stabilized with Yttria, Ceria, and Titania in Na_2SO_4+V_2O_5, *Journal of Materials and Corrosion*, 1–8 (2013)]. It is reprinted by permission of *Journal of Materials and Corrosion* (See Appendix A)

reduced cooling air flow, as well as lower emissions and lower fuel consumption[96, 129-131]. A common TBC bond coat is the MCrAlY (M=Co and/or Ni) type, which has two major functions, 1, enhances the bonding between the substrate and the topcoat; and 2, protects the underlying substrate from corrosion and oxidation [71, 101, 131]. The topcoat is usually applied either by an air plasma spray (APS) or electron beam physical vapor deposition (EB-PVD) process. APS method offers the possibility to deposit thick layers at an affordable price [17, 59, 132]. The primary industrially used thermal barrier coating material is zirconia stabilized with 3.2–4.2 mol% (6–8 wt. %) yttria (3–4YSZ). A major disadvantage of yttria-stabilized zirconia (YSZ) is the limited operation temperature (<1200°C) for long-term applications. At higher temperatures, phase transformations from the tetragonal to tetragonal and cubic and then, upon cooling, to monoclinic occur, giving rise to the formation of cracks in the coating[26, 133].

TBC is essential to safeguard gas turbines for high-temperature operations. Among the various life-limiting factors, one key durability issue of TBCs is their resistance to environmental degradation due to molten deposits arising from the aggressive combustion environment [17, 37, 94]. Vanadium and sodium are common impurities in low grade petroleum fuels. Molten sodium salts of vanadium and sulfur oxides condensed on to the TBC in the 600–1050˚C temperature range are extremely corrosive [15, 38, 40, 95].

Extensive efforts have been made to enhance the phase stability and hot corrosion resistance of the traditional zirconia material by doping new metal oxides [36, 72, 73]. A comparative analysis of various stabilizers including MgO, Y_2O_3, Sc_2O_3, In_2O_3, SmO_2 and Gd_2O_3 appeared in [37]. Many studies have shown that the YSZ is attacked by pure $NaVO_3$ or V_2O_5 resulting in the removal of yttria as YVO_4 and the destabilization of the tetragonal to the monoclinic phase. Scandia- and india-stabilized zirconia proved to be more resistant than yttria-stabilized zirconia

to corrosion by vanadia [21, 38-41, 74]. Studies reveal that ZrO_2–CeO_2 system may exhibit the formation of $CeVO_4$ in media with fuels contaminated with high levels of S and V [37, 41, 74]. However, ceria stabilized zirconia coating has many advantages, such as good phase stability at high temperature, improved thermal insulation, higher coefficient of thermal expansion, good thermal shock resistance etc. [25, 47, 73].

An alternate approach to YSZ TBC improvement is using TiO_2 as a stabilizer. ZrO_2-TiO_2 binary system was found to be inferior [134, 135]. However, tetragonal compositions in the zirconia-rich corner of TiO_2–$YO_{1.5}$–ZrO_2 ternary system are of interest because of their potential for enhancing the material toughness through the improved tetragonality of the structure. TiO_2 is one of a small number of dopants that increase the tetragonality of the zirconia solid solution without compromising its phase stability[135, 136]. [137] reported that ZrO_2-Y_2O_3-TiO_2 samples contained a higher concentration of the tetragonal phase than the ZrO_2-Y_2O_3 samples. Moreover, suitable co-doping with Y^{3+} and Ti^{4+} yields compositions that do not transform to monoclinic even after decomposition of the metastable solid solution into its equilibrium assemblage of t + c phases[137]. It has been found that fully or nearly fully tetragonal poly crystals within a wide range of compositions (Y_2O_3 from 0.5 to 3 mol% and TiO_2 from 3 to 28 mol %)[136].

Previous reports mainly investigated hot corrosion properties of ZrO_2-Y_2O_3 and ZrO_2-CeO_2. However, studies on hot corrosion properties of ZrO_2-Y_2O_3-TiO_2 systems are very limited. In this study, the hot corrosion behavior of zirconia doped with both Y_2O_3 and TiO_2 (TiSZ) is compared with YSZ and CSZ samples in Na_2SO_4+V_2O_5 at 1050˚C.

7.3 Experimental Procedure

Nickel-based super alloy (Inconel 738) disks of Φ25×1.5mm were employed as the substrates. TBCs composed of a ceramic top coating and a NiCrAlY bond coat (Amdry 9625, Sulzer Metco, with particle size 45~75 μm) were deposited onto the superalloy substrates by the atmospheric plasma spray (APS) process. Three types of samples using Sulzer Metco agglomerated powders, 3-4YSZ, ZrO_2-18TiO_2-10Y_2O_3 (TiSZ) and ZrO_2-24CeO_2-2.5Y_2O_3 (CSZ) (mol%), were made with the APS method. The plasma spraying was carried out using a Sulzer-Metco 9M plasma spray system with an Ar/H_2 gas mixture. The spraying parameters are given in Table 7.1.

Hot corrosion studies using Na_2SO_4 and V_2O_5 mixtures were conducted on samples at 1050˚C in air. For the above mixtures, 95% Na_2SO_4 and 99.9% V_2O_5 from Sigma Aldrich were used. To perform an accelerated high-temperature hot corrosion test on TBCs, a mixture of 50wt% Na_2SO_4 + 50wt% V_2O_5 deposit was spread onto the surfaces of the TBC specimens with a total salt amount of 20 mg/cm^2. The specimens were then set in an electric furnace with an ambient atmosphere under a maximum temperature of 1050˚C for 4 h. After each 4 h of testing at 1050˚C, the samples were allowed to cool down inside the furnace, and then the samples were inspected both visually and with an optical microscope for possible crack initiation. To repeat the test, the samples were recoated with the Na_2SO_4 + V_2O_5 salt mixture and the heating profile was repeated. The morphology and microstructure of the as-sprayed TBC coatings and the coatings after the hot corrosion tests were examined using field emission scanning electron microscopy (Quanta 3D FEG, FEI Company, USA). For surface morphology studies, a thin Pt coating was evaporated onto the coating samples for electrical conductivity before they were examined by SEM. To obtain a cross-section, the specimens were first mounted in an epoxy resin. The mounted specimens were then sectioned with a slow speed diamond cutter and subjected to

polishing using a diamond paste (1 μm). X-ray diffraction (MiniFlex XRD, Rigaku Corporation, Japan) with Cu K_α radiation λ=1.54178Å at a scan speed of 1^o/min was used to establish the phase composition of the coatings.

Table 7.1. Plasma spraying parameters

Layer	Arc current (A)	Coating distance (mm)	Plasma gas Ar/H_2 (SCFH)	Carrier gas Ar (SCFH)	Powder feed rate (g/min)
Bond coat	500	130	96/15	8	40
YSZ	600	80	90/15	8.4	40
CSZ	400	80	80/15	13.5	38
TiSZ	600	70	84/17	13.5	38

7.4 Results

The cross-sectional microstructure SEM images of the as-received YSZ, CSZ and TiSZ TBC specimens are shown in Figure 7.1. All top layers of the as-sprayed specimens show similar microstructures with a certain level of porosity without any visible cracks under optical microscopes. For the as-sprayed TBC samples, no delamination can be found along the YSZ / CSZ / TiSZ top layer and the NiCrAlY bond coat interface.

XRD measurement results of the as-received YSZ, CSZ and TiSZ TBC specimens are illustrated in Figure 7.2. It can be seen that the major phase of the APS coated YSZ and CSZ is tetragonal zirconia as expected. Previous publications showed the same results[31, 41]. For the TiSZ system, it also shows a tetragonal zirconia. It is reported that zirconia is a stable phase for zirconia doped with both Y_2O_3 and TiO_2 , with a Y_2O_3 concentration in the range of 0.5 to 3 mol% and with a TiO_2 concentration from 3 to 28 mol% [135-137].

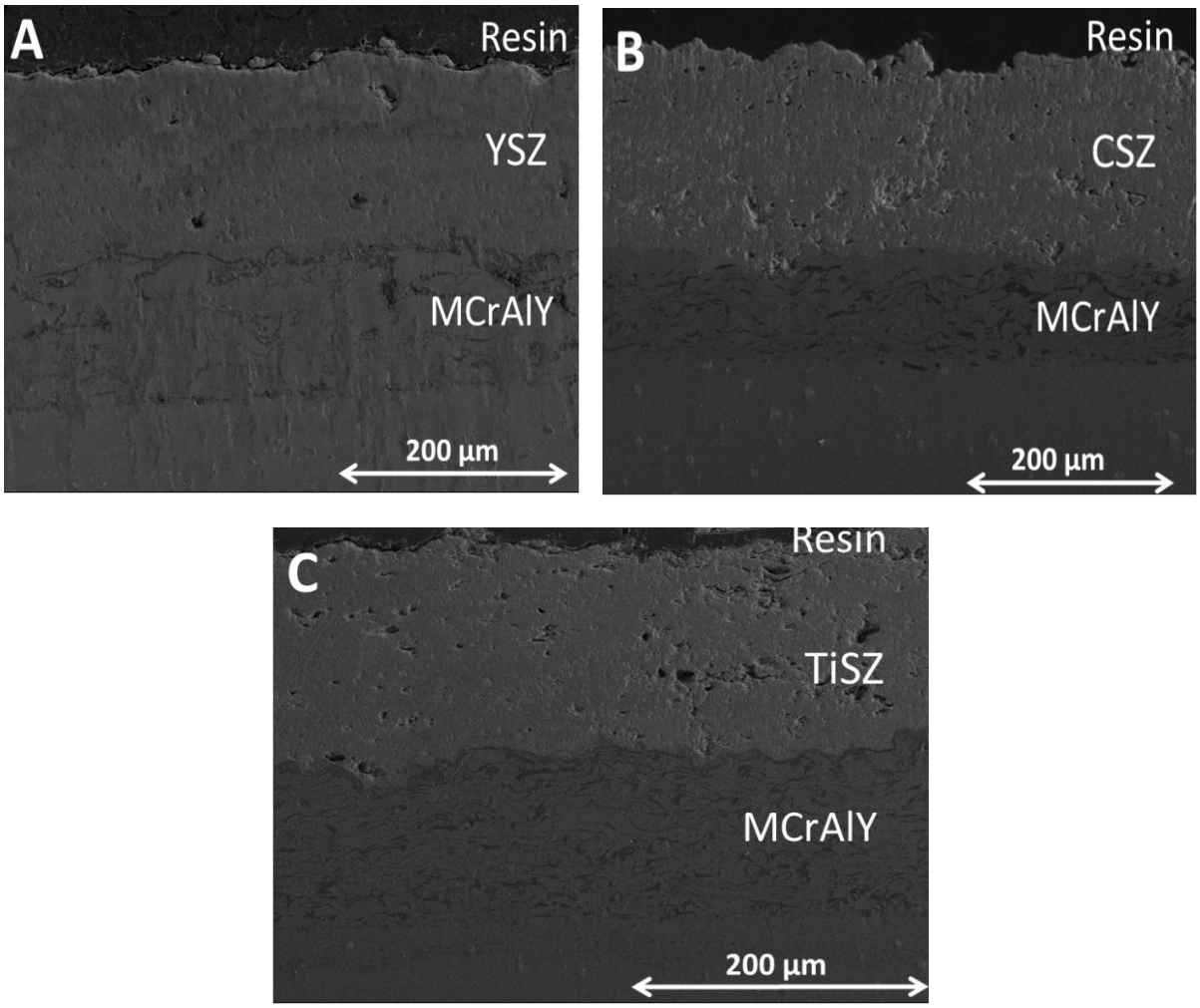

Figure 7.1 Cross-section SEM images of as received APS coatings A) YSZ, B) CSZ, C) TiSZ

Figure 7.3 shows the XRD patterns obtained from the YSZ, CSZ and TiSZ coatings after the hot corrosion test with the Na_2SO_4+V_2O_5 salt mixture at 1050ºC. Comparing the patterns of the as-sprayed YSZ TBC sample, most of the tetragonal zirconia in the YSZ sample has changed to the monoclinic phase and YVO_4 is formed as a hot corrosion product, while for the CSZ specimen, besides monoclinic ZrO_2 and YVO_4, the newly evolved peaks are related to $CeVO_4$. For the TiSZ sample, monoclinic zirconia isn't detected. It means either all zirconia is still in tetragonal phase or the amount of monoclinic zirconia is still negligible which can't be detected with XRD.

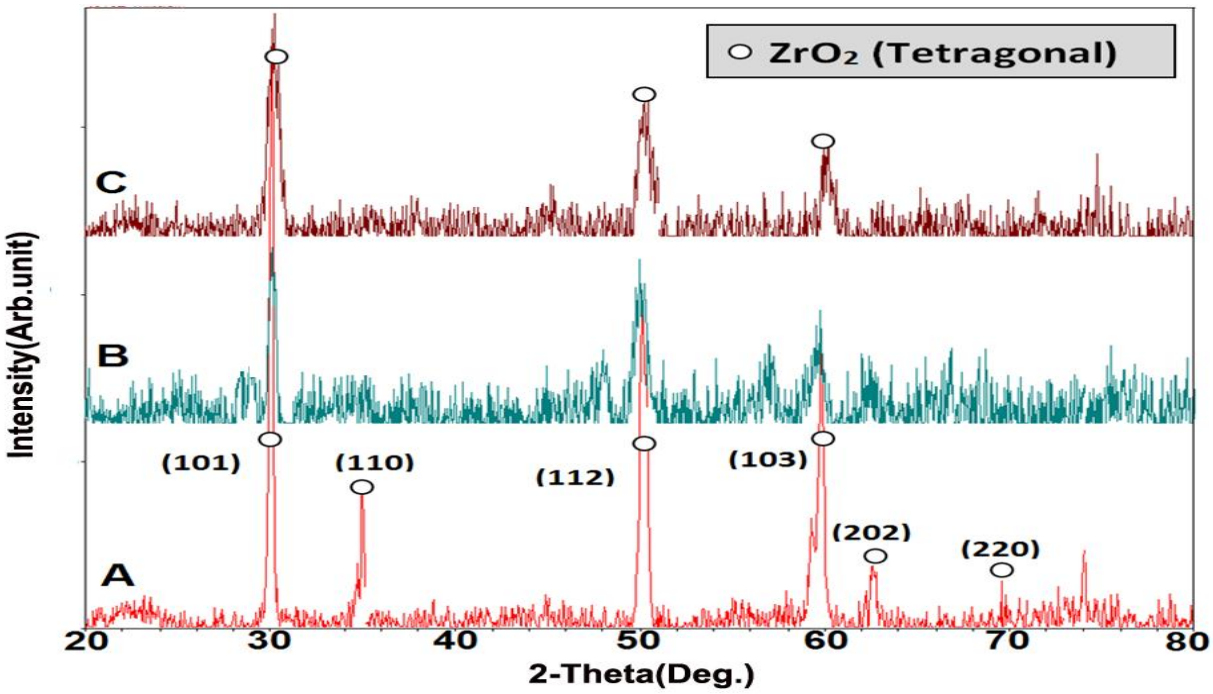

Figure 7.2 XRD patterns of as-received A) YSZ, B) CSZ, C) TiSZ

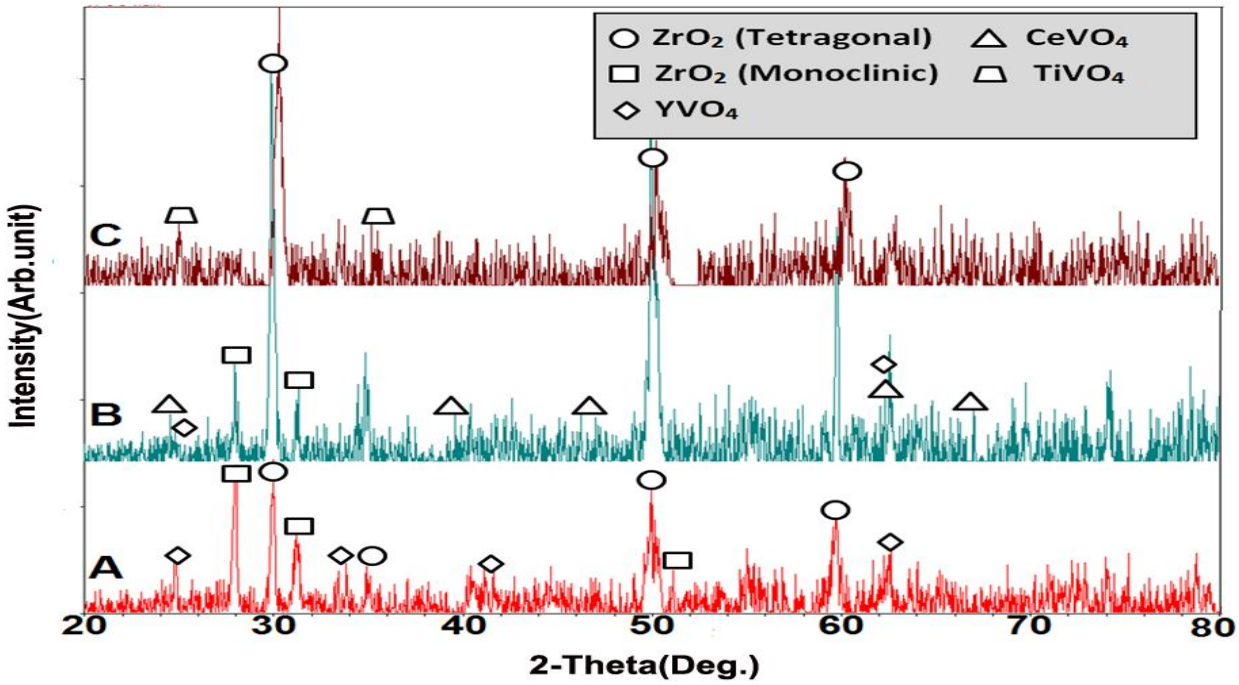

Figure 7.3 XRD patterns of A) YSZ after 20 h, B) CSZ after 28 h, C) TiSZ after 40 h, hot corrosion in Na_2SO_4+V_2O_5 at 1050ºC

Some new peaks contributed to $TiVO_4$ was detected at the surface of sample after 40 hours of hot corrosion, however, the lack of monoclinic zirconia after hot corrosion shows that TiSZ is more corrosion resistant at high temperature than both YSZ and CSZ.

YSZ sample spalled and degraded after 20 hours (five 4-h cycle) with transvers cracks and surface covered with rod shaped hot corrosion products, while for CSZ samples degradation happened after 28 hours (seven 4-h cycle). Typical surface SEM images of YSZ, CSZ specimens after hot corrosion tests in Na_2SO_4+V_2O_5 at 1050ºC after 5 and 7 cycles, respectively, are presented in Figure 7.4, with the apparent formation of new crystals. Apart from XRD analysis, Energy Dispersive Spectroscopy (EDS) analysis was performed at different regions of the TBC surfaces to confirm the chemical compositions of the hot corrosion products. EDS analysis on crystals in Figure 7.4A demonstrated that the crystals were composed of yttrium, vanadium and oxygen, and then they were identified by XRD analysis to be YVO_4. The EDS spectra obtained on crystals in Figure 7.4B confirmed the presence of elements consistent with the formation of $CeVO_4$ besides some YVO_4 crystals. YVO_4 crystals are smaller on CSZ than those on the YSZ sample, and the amount of hot corrosion products on CSZ is also less which shows the better hot corrosion resistance of CSZ.

SEM surface images of TiSZ sample after hot corrosion test in Na_2SO_4+V_2O_5 at 1050ºC are showed in Figure 7.5. $TiVO_4$ ribbons were first detected on the sample surface after the fifth hot corrosion cycle (after five 4-h cycles, Figure 7.5A) and then these $TiVO_4$ crystals changed to dendritic shape and continued to grow and became dendritic-shape as time progresses. Figure 7.5B shows the surface image of TiSZ sample after 40 hour of hot corrosion. Increasing the reaction time (multiple hot corrosion cycles) enlarges the corroded zones and consequently increases the hot corrosion products.

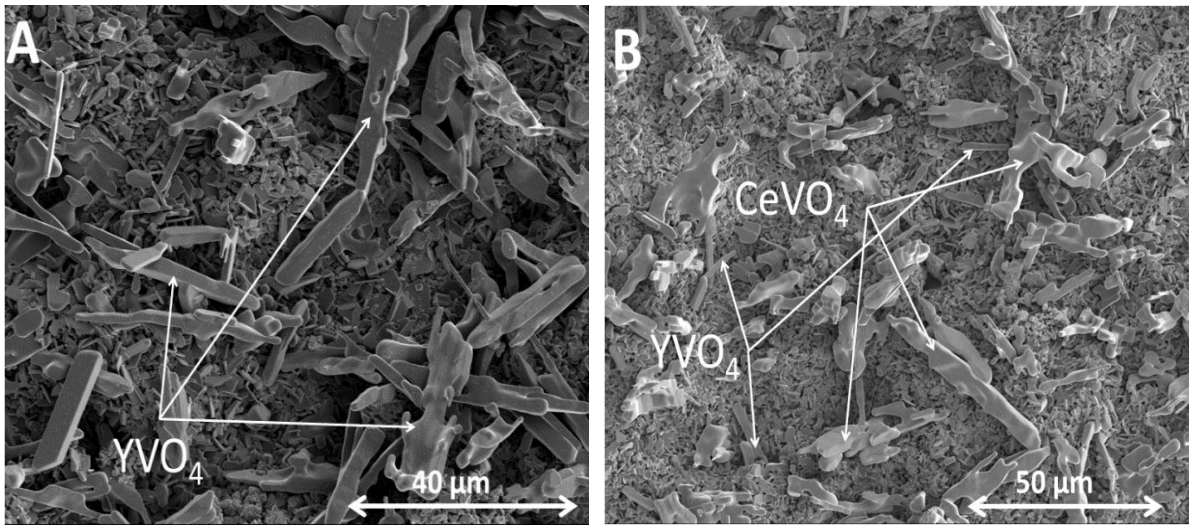

Figure 7.4 SEM surface images of A) YSZ after 5 cycles and B) CSZ after 7 cycles, hot corrosion in Na_2SO_4+V_2O_5 at 1050ºC

The previously formed $TiVO_4$ crystals may act as nucleation locations for the formation of new crystals, similar to the role of grain boundaries in the nucleation and growth process. Likewise, the repeated charging of molten salts in the hot corrosion tests promotes the formation and growth of the corrosion products due to the increased amount of corrosive species available to react with the sample.

As it can be seen in Figure 7.5B, this sample didn't degrade significantly even after 40 hour of hot corrosion test. In Figures 7.5A and 7.5B, it is obvious that some regions are perfectly intact and the major phase in these areas is still tetragonal zirconia. Compare to YVO_4 and $CeVO_4$, the $TiVO_4$ crystals are much smaller in size and quantity and they have a unique dendrite shape. Based on the test results, TiSZ is highly stable at high temperature and TiSZ sample is more resistant against molten salt at high temperature than YSZ and CSZ.

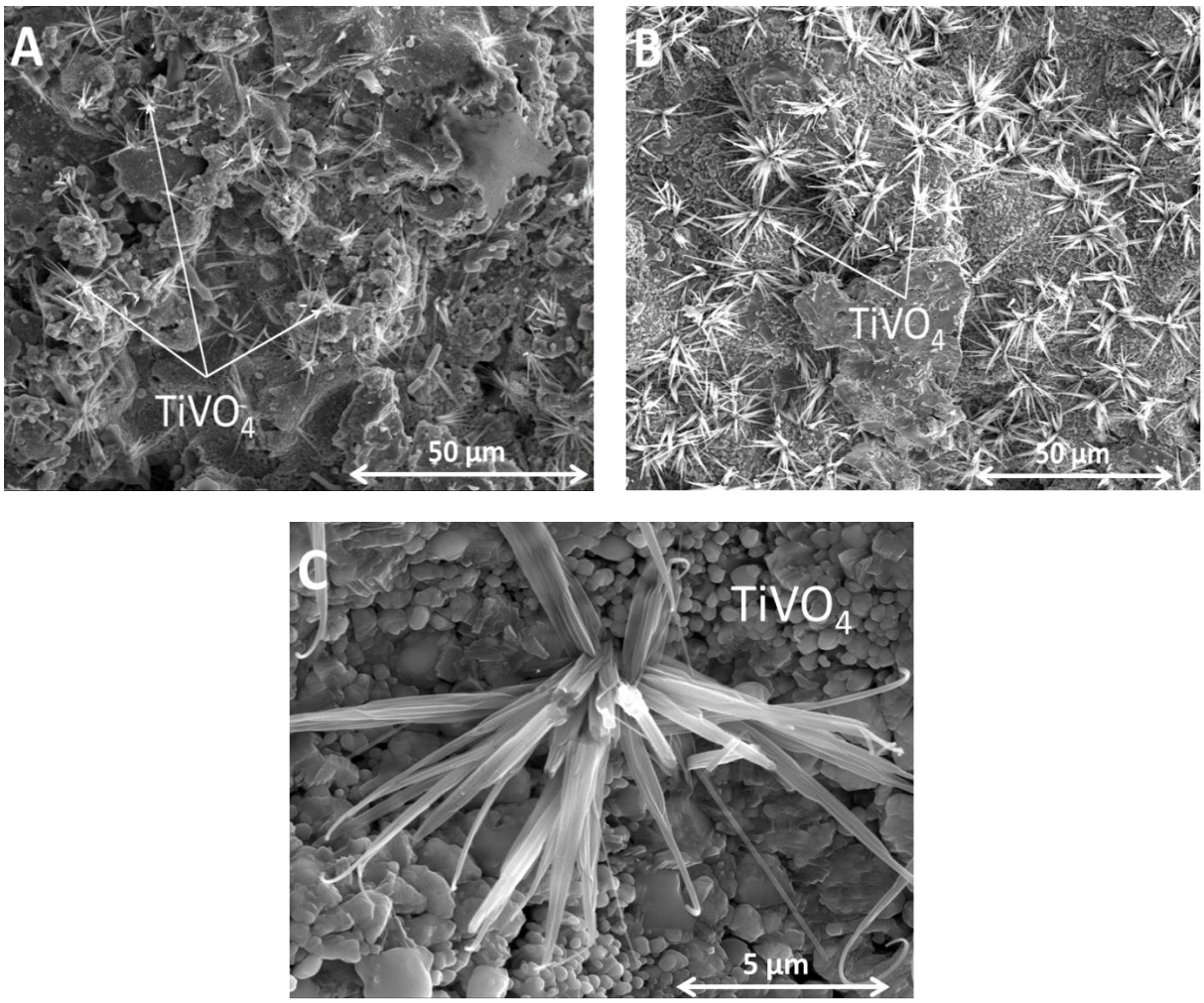

Figure 7.5 SEM surface images of TiSZ A) after 5 cycles, B) 10 cycles and C) 10 cycles (higher magnification), hot corrosion in $Na_2SO_4 + V_2O_5$ at 1050˚C

7.5 Discussion

Many research have been done on the corrosion behavior of YSZ in molten salts containing vanadium and sulfur [21, 22, 31, 41, 55]. The main mechanism is the dissolution of YSZ in the melt followed by re-precipitation of both YVO_4 and Y-depleted monoclinic zirconia. CSZ sample also undergo some chemical reactions and YVO_4 and $CeVO_4$ formed on the sample. Chemical degradation of zirconia-based samples stabilized with Y_2O_3 and CeO_2, can be classified as successive occurrence of related chemical reactions during the hot corrosion tests.

During the exposure of V_2O_5 and Na_2SO_4 salt mixture at a high temperature, $NaVO_3$ will be formed.

$$V_2O_5 + Na_2SO_4 \rightarrow 2(NaVO_3) + SO_3 \quad (1)$$

For YSZ case, $NaVO_3$, having a melting point of 610˚C, reacts with yttria from the YSZ solid solution to form YVO_4:

$$ZrO_2\,(Y_2O_3) + 2(NaVO_3) \rightarrow ZrO_2\,(\text{monoclinic}) + 2(YVO_4) + Na_2O \quad (2)$$

Also Na_2O can react with V_2O_5 directly to form $NaVO_3$:

$$Na_2O\ (\text{base}) + V_2O_5\ (\text{acid}) \rightarrow 2NaVO_3\ (\text{salt}) \quad (3)$$

For CSZ sample, $NaVO_3$ reacts with both Y_2O_3 and CeO_2 and YVO_4 and $CeVO_4$ form.

$$ZrO_2\,(CeO_2) + 2(NaVO_3) \rightarrow ZrO_2\,(\text{monoclinic}) + CeVO_4 + Na_2O \quad (4)$$

In the case of CSZ TBCs, in comparison with YSZ, both the monoclinic transformation of zirconia layer and the formation of hot corrosion products were much retarded. No visible cracks were formed inside the zirconia layer after 28h of hot corrosion test. This resistivity against molten salt can be due to the strong acidity and high content of CeO_2 (25 mol. %). This result is supported by the fact that CeO_2 is more resistant to chemical attacks by salts such as sulfates and vanadates [15, 17, 105]. Formation of $CeVO_4$ can partially consume vanadium in molten salt and vanadium is less available to react with Y_2O_3 and consequently less YVO_4 formed and thus less tetragonal monoclinic transformed to monoclinic zirconia.

Zirconia in the TiSZ sample is stabilized with 18 mol. % of TiO_2 and 10 mol. % Y_2O_3. The amount of Y_2O_3 in TiSZ is more than that in YSZ and CSZ; therefore the chance of producing YVO_4 should be higher in TiSZ sample. In CSZ, although the content of Y_2O_3 is less, significant

amount of YVO_4 was formed after 20 hours of hot corrosion. However, no YVO_4 was formed on TiSZ even after 40 hours of hot corrosion. The formation of $TiVO_4$ on TiSZ is based on the following chemical reactions:

The $NaVO_3$ which is the result of chemical reaction between V_2O_5 and Na_2SO_4 can react with TiSZ sample:

$$TiSZ\,(2TiO_2) + (2NaVO_3) \rightarrow 2TiVO_4 + Na_2O + 1/2\ O_2 \quad (4)$$

V_2O_5 may also react with TiSZ directly at elevated temperature to form $TiVO_4$.

$$TiSZ\,(2TiO_2) + V_2O_5\,(l) \rightarrow 2TiVO_4\,(s) + 1/2\ O_2 \quad (5)$$

The cross-sectional microstructure of YSZ, CSZ and TiSZ TBC specimens after hot corrosion tests are shown in Figure 7.6. After hot corrosion tests of 20 h, very porous areas damaged by $NaVO_3$ corrodents were observed in the YSZ sample. As shown in Figure 7.6A, large harmful horizontal cracks have formed inside the YSZ layer throughout the thickness of coating. Transverse cracks are clearly visible in the YSZ coating, Figure 7.6A.

In certain regions, the cracks divided the YSZ layer into several sub-layers, implying the initiation of delamination and spallation of the YSZ coating. Some large cracks have propagated and extended deep into the ceramic coat and even reached the top-coat/bond-coat interface, which would be susceptible to cause the debonding of the ceramic coat from the bond coat.

As shown in Figure 7.6B, after 28 h of hot corrosion test, the damaged areas of CSZ TBCs are much less than those of YSZ TBCs'. Figure 7.6C shows a TiSZ coating cross-section, which has no significant degradation and spallation after 40h of hot corrosion test. Although some pores appear near bond coat, no visible degradation around the pores is observed. The cross-section image of the TiSZ coating shows less porosity than the YSZ and CSZ. This further confirms that

the TiSZ based coating exhibits a good hot corrosion resistance and good durability. This result clearly demonstrates that TiSZ TBCs have a better resistance than YSZ and CSZ TBCs in terms of overall hot corrosion damage behavior.

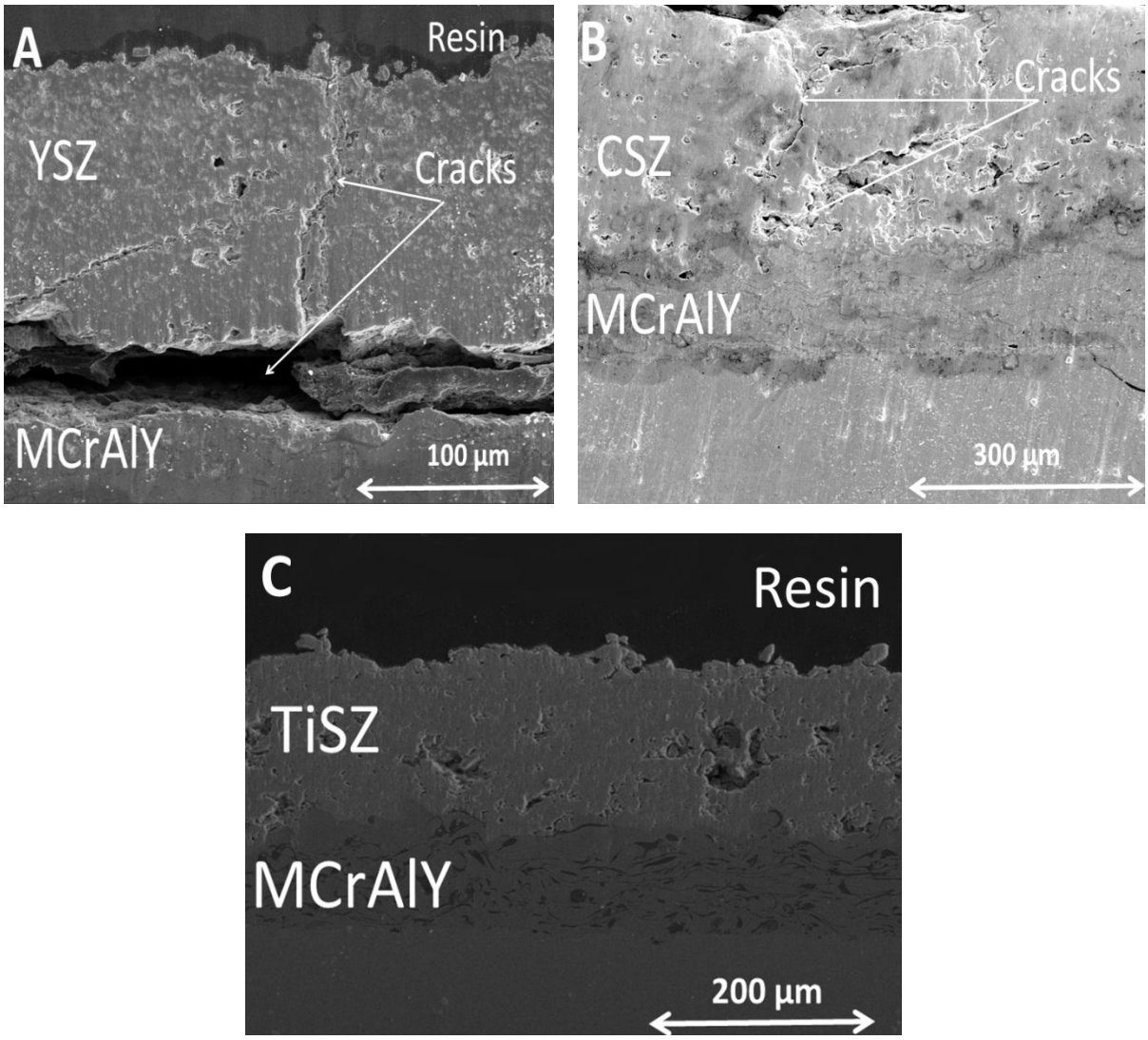

Figure 7.6 Cross-section SEM Images of APS coatings (A) YSZ, (B) CSZ, (C) TiSZ after hot corrosion in $Na_2SO_4 + V_2O_5$ at 1050˚C

Failure of YSZ and CSZ TBCs may occur by gradual loss of zirconia coats from the surface in real applications under hot corrosion environments. Because the monoclinic phase transformation is induced by a depletion of tetragonal stabilizers in zirconia, this result indicates

that $NaVO_3$ salt penetrated deep into the zirconia top layer within a short period of hot corrosion test. The phase transformation to monoclinic phase in the zirconia layer, which is harmful to thermal shock resistance of TBC systems, may be initiated from the early stage of hot corrosion even near the bond layer. If hot corroded YSZ TBCs are to be thermally shocked as in real operation conditions, it is expected that premature failure of TBCs will occur by formation of horizontal cracks near the interface far before macroscale spalling of the damaged areas by salt attacks alone.

For TiSZ coating, according to ZrO_2-TiO_2 phase diagram in [136], in area with around 20 mol. % TiO_2 and at a temperature higher than 1000˚C, stable phase is tetragonal zirconia. When this composition cools down to room temperature, zirconia changes to monoclinic and the other compounds such as $ZrTiO_4$ and TiO_2 may form[136].

When Zirconia stabilized with both Y_2O_3 and TiO_2, this tetragonal to monoclinic phase transformation can be suppressed. A maximum of 16% TiO_2 can be substituted for ZrO_2 in 7YSZ while staying within the t + f two-phase field. Single-phase tetragonal zirconia can dissolve a maximum of 4% $YO_{1.5}$ and 16% TiO_2 in equilibrium[136].

In this study, a synthetized powder containing $18TiO_2$ and $10Y_2O_3$ has been used and deposited as TBC on super alloy testing samples. XRD confirmed that at room temperature, the phase is tetragonal zirconia, which proves zirconia can dissolve 18% TiO_2 and $10Y_2O_3$. Hot corrosion experiment showed that this composition is chemically stable against molten salt attack at temperature as high as 1050˚C. This confirms that co-doping of zirconia with appropriate amount of TiO_2 and Y_2O_3 has the potential for thermal barrier application under corrosive environment. Further investigations are undergoing to optimize the composition in TiO_2-$YO_{1.5}$-ZrO_2 system.

7.6 Conclusions

In the present study, hot corrosion properties of YSZ, CSZ and TiSZ TBCs under a Na_2SO_4 + V_2O_5 salt environment at 1050˚C were compared. The reactions between yttria (Y_2O_3) and V_2O_5/$NaVO_3$ produce YVO_4, leaching Y_2O_3 from the YSZ and causing progressive tetragonal to monoclinic destabilization transformation. After 20 h (5 cycles) of hot corrosion test at 1050˚C, the failure of the YSZ TBCs has initiated and propagated throughout the entire top coat, and led to the top coat delamination and spallation near the top coat–bond coat interface.

CSZ coating degraded after 28 h of hot corrosion test. In CSZ coating, the formation of $CeVO_4$ crystals possibly postponed the formation of YVO_4 and transformation of tetragonal zirconia to monoclinic. The hot corrosion products are much smaller than the YSZ case and monoclinic zirconia portion is less than YSZ sample. For TiSZ coating, molten Na_2SO_4 + V_2O_5 mixture reacts with TiSZ to form $TiVO_4$ but no monoclinic ZrO_2 was formed after 40 hours of testing. On the surface of the TiSZ coating, $TiVO_4$ crystals are significantly smaller (about 5μm in length) than the large plate shaped YVO_4 and $CeVO_4$ found on the YSZ and CSZ samples. Under this accelerated hot corrosion test, TiSZ coating started to degrade after 40 h of hot corrosion testing (10 cycles), which is much better than the YSZ case, which failed after 5 cycles. Based on the degradation rate, the corrosive layer thickness, and the general status of the coating after hot corrosion, TiSZ coating was found to have a better hot corrosion resistance at a temperature of 1050˚C than both YSZ and CSZ coatings.

7.7 Disclaimer

employees, makes any warranty, express or implied, or assumes any legal liability or responsibility for the accuracy, completeness, or usefulness of any information, apparatus, product, or process disclosed, or represents that its use would not infringe privately owned rights. Reference herein to any specific commercial product, process, or service by trade name, trademark, manufacturer, or otherwise does not necessarily constitute or imply its endorsement, recommendation, or favoring by the United States Government or any agency thereof. The views and opinions of authors expressed herein do not necessarily state or reflect those of the United States Government or any agency thereof.

7.8 Acknowledgments

This publication is based upon work supported by the US Department of Energy National Energy Technology Laboratory under Award Number DE-FE0004734 and NASA-EPSCoR program (Grant NNX09AP72A).

8 Summary and Conclusions

Ceramic thermal barrier coatings (TBCs) are commonly used gas turbine engines. The current material of choice (YSZ) degrades when it contacts with impurities arise from low quality fuels such vanadium and sulfur. YSZ cannot be used in temperature higher than 900˚C. Higher efficiency and performance of gas turbine engines will require a new generation of thermal barrier coatings (TBCs).

The aim of this research is finding novel candidate for next generation thermal barrier coatings. The first step is studying potential ceramic materials characteristics with regard to their availability. Samples had been made with either with Air Plasma Spray method or conventional pressing and sintering method. Only sprayable powders can be fed in plasma spray chambers.

To start with, hot corrosion studies of YSZ coatings by sulfate and vanadate melts were performed. For YSZ case, the reaction between $NaVO_3$ and Y_2O_3 produces YVO_4 and leads to the transformation of tetragonal ZrO_2 to monoclinic ZrO_2. A clear understanding of hot corrosion reactions by which YSZ and MCrAlY coatings degrade by molten deposits would help as a basic theory for development of protective coatings for gas turbine applications. With a motivation to identify promising engineering materials that withstand severe high temperature environments, various ceramic oxides were reviewed. In this work, some new candidates for replacing YSZ are introduced. In current work, hot corrosion behavior of $Gd_2Zr_2O_7$, ZrO_2 stabilized with Ta_2O_5, zirconia stabilized with both Ta_2O_5 and Y_2O_3 and zirconia stabilized with CeO_2 and TiO_2 is investigated.

An alternate material to zirconia based top coats is $A_2B_2O_7$-type rare-earth zirconate ceramic, such as $La_2Zr_2O_7$, $Nd_2Zr_2O_7$, $Gd_2Zr_2O_7$ and $Sm_2Zr_2O_7$, have been shown recently to have lower thermal conductivity, higher melting points, relatively higher thermal expansion coefficients

(TEC), higher stability, and better ability to accommodate defects than YSZ. Thus $Gd_2Zr_2O_7$ was selected and phase stability and high temperature reactivity of $Gd_2Zr_2O_7$ and composite $Gd_2Zr_2O_7$+YSZ have been studied. Molten salt is also found to react with $Gd_2Zr_2O_7$ to form $GdVO_4$. Comparing to YSZ, under a temperature of 1050 °C, $Gd_2Zr_2O_7$ is found to be more stable, both thermally and chemically, than YSZ, and exhibits a better hot corrosion resistance.

There are several oxides which can be used as stabilizer of zirconia rather than yttria. Literature review reveals that previous researchers investigated various stabilizers including MgO, Y_2O_3, Sc_2O_3, In_2O_3, CeO_2, and SmO_2. An alternate approach to YSZ TBC improvement is using Ta_2O_5 as a co-doped stabilizer. Ta_2O_5 has a melting point over 1800˚C. On heating it undergoes a phase transformation at 1360˚C which is well above the typical turbine surface temperatures. Data in literature indicate defect association between the larger oxide of Y and the smaller oxide of Ta in YSZ. According to acid-base Lewis chemical reactions, by virtue of Ta's position in the periodic table, tantalum is more acidic than vanadium. Thus, the ZrO_2-Ta_2O_5 is expected to be substantially more resistant to corrosion by the acidic oxides than ZrO_2-Y_2O_3. So, first Ta_2O_5 was used as single stabilizer of zirconia and then Zirconia samples doped with both yttria and tantalum oxide have been made and phase stability and hot corrosion behavior of ZrO_2-Ta_2O_5 and ZrO_2-Ta_2O_5-Y_2O_3 were studied.

To examine the effect of stabilizing zirconia with tantalum oxide, different compositions of ZrO_2-Ta_2O_5 samples in the presence of molten mixture of Na_2SO_4 + V_2O_5 at 1100˚C were tested. Hot corrosion results show that orthorhombic zirconium-tantalum oxide is more stable, both thermally and chemically in Na_2SO_4+V_2O_5 media at 1100˚C, and shows a better hot corrosion resistance than the tetragonal phase. When zirconia stabilized with yttria and tantalum oxide, due to synergic effect of Y and Ta, the resulted compound expects to be stable in high temperatures

and can be considered a good candidate for TBC application. Hot corrosion behavior of YSZ-Ta_2O_5 (TaYSZ) composite samples in the presence of molten mixture of Na_2SO_4 + V_2O_5 at 1100˚C is studied. In TaYSZ sample, minor amounts of $NaTaO_3$, $TaVO_5$ and Ta_9VO_{25} are formed as the hot corrosion products with only traceable amounts of YVO_4. Due to the synergic effect of doping of zirconia with both Y_2O_3 and Ta_2O_5, the TaYSZ sample has a much better hot corrosion resistance than YSZ.

In zirconia stabilized with CeO_2 coating, the formation of $CeVO_4$ crystals possibly postponed the formation of YVO_4 and transformation of tetragonal zirconia to monoclinic. On surface of zirconia stabilized with TiO_2 coating, $TiVO_4$ crystals are significantly smaller (about 5µm in length) than the large plate shaped YVO_4 and $CeVO_4$ found on the YSZ and CSZ samples. TiSZ coating was found to have a better hot corrosion resistance at a temperature of 1050˚C than both YSZ and CSZ coatings.

The important issue in investigating hot corrosion behavior of TBCs is to understand chemical reactions and physical changes that occur at the molten salt/TBC and bondcoat/topcoat interfaces. The chemical properties of contaminant salts are important to gain a fundamental understanding of how these salts react with TBC top coats with engineered chemistry. This understanding is eventually going to be used to create and develop TBCs that are resistant to hot corrosion degradation. In this research, new candidates for thermal barrier coating applications have been introduced and developed. Hot corrosion behavior and phase stability of new candidates have been studied and the appropriate hot corrosion mechanisms have been presented.

References

1. Bose S., High Temperature Coatings. 2007, Elsevier Science & Technology Books.

2. Rajendran R., Gas turbine coatings – An overview. Engineering Failure Analysis, 2012.

3. Feuerstein A., et al., Technical and Economical Aspects of Current Thermal Barrier Coating Systems for Gas Turbine Engines by Thermal Spray and EBPVD: A Review. Journal of Thermal Spray Technology, 2008. 17 (2): p. 199-213.

4. Eliaz N., Hot corrosion in gas turbine components. Engineering Failure Analysis, 2002. 9: p. 13.

5. Padture N., et al., Thermal barrier coatings for gas-turbine engine applications. Science, 2002. 296. p. 280-284.

6. Ahmadi-Pidani R., et al., Laser surface modification of plasma sprayed CYSZ thermal barrier coatings. Ceramics International, 2013. 39 (3): p. 2473-2480.

7. Xie X., et al., Hot Corrosion Behavior of Double-ceramic-layer $LaTi_2Al_9O_{19}$/YSZ Thermal Barrier Coatings. Chinese Journal of Aeronautics, 2012. 25(1): p. 137-142.

8. Drexler J.M., et al., Plasma sprayed gadolinium zirconate thermal barrier coatings that are resistant to damage by molten Ca–Mg–Al–silicate glass. Surface and Coatings Technology, 2012. 206(19-20): p. 3911-3916.

9. Karaoglanli A.C., et al., Thermal Shock and Cycling Behavior of Thermal Barrier Coatings (TBCs) Used in Gas Turbines. Progress in Gas Turbine Performance. 2013.

10. Wu J., et al., Evaluation of plasma sprayed YSZ thermal barrier coatings with the CMAS deposits infiltration using impedance spectroscopy. Progress in Natural Science: Materials International, 2012. 22(1): p. 40-47.

11. Wang L., et al., Thermal shock behavior of 8YSZ and double-ceramic-layer $La_2Zr_2O_7$/8YSZ thermal barrier coatings fabricated by atmospheric plasma spraying. Ceramics International, 2012. 38(5): p. 3595-3606.

12. Begley M.R., et al., Delamination resistance of thermal barrier coatings containing embedded ductile layers. Acta Materialia, 2012. 60(6-7): p. 2497-2508.

13. Schulz U., et al., EB-PVD Y_2O_3 - and CeO_2/Y_20_3-stabilized zirconia thermal barrier coatings-crystal habit and phase composition. Surface and Coatings Technology, 1995. 82: p. 11.

14. Jamali H., et al., Comparison of thermal shock resistances of plasma-sprayed nanostructured and conventional yttria stabilized zirconia thermal barrier coatings. Ceramics International, 2012. 38(8): p. 6705-6712.

15. Ahmadi-Pidani R., et al., Evaluation of hot corrosion behavior of plasma sprayed ceria and yttria stabilized zirconia thermal barrier coatings in the presence of $Na_2SO_4+V_2O_5$ molten salt. Ceramics International, 2012. 38(8): p. 6613-6620.

16. Hass D.D., et al., Multi-scale pore morphology in directed vapor deposited yttria-stabilized zirconia coatings. Materials Science and Engineering: A, 2010. 527(23): p. 6270-6282.

17. Jones R.L., Some aspects of the hot corrosion of thermal barrier coatings. Journal of Thermal Spray Technology, 1997. 6(1): p. 8.

18. Jones R.L., Vanadate-sulfate Melt Thermochemistry Relating to Hot Corrosion of Thermal Barrier Coatings. . Naval Research Laboratory, 1997: p. 23.

19. Jones R.L. et al., Reaction of Vanadium Compounds with Ceramic Oxides. Journal of Electrochemechal Society: Solid-State Science and Technology, 1986. 133(1): p. 4.

20. Chen X., et al., Hot corrosion behaviour of plasma sprayed YSZ/$LaMgAl_{11}O_{19}$ composite coatings in molten sulfate–vanadate salt. Corrosion Science, 2011. 53(6): p. 2335-2343.

21. Chen Z., et al., Degradation of plasma-sprayed yttria-stabilized zirconia coatings via ingress of vanadium oxide. Journal of the European Ceramic Society, 2009. 29(9): p. 1647-1656.

22. Chen Z., et al., Investigation of reactions between vanadium oxide and plasma-sprayed yttria-stabilized zirconia coatings. Journal of the European Ceramic Society, 2009. 29(8): p. 1403-1411.

23. Hong-song Z., et al., Investigation about thermal conductivities of $La_2Ce_2O_7$ doped with calcium or magnesium for thermal barrier coatings. Journal of Alloys and Compounds, 2012. 537: p. 141-146.

24. Hertl W., Vanadia reaction with yttria stabilized zirconia. Journal of applied physics, 1988. 63: p. 6.

25. Ramaswamya P., et al. , Evaluation of $CaO \pm CeO_2 \pm$partially stabilized zirconia thermal barrier coatings. Ceramics International, 1999. 25: p. 8.

26. Kim D. J. et al., Phase Stability and Physical Properties of Cubic and Tetragonal ZrO_2 in the System ZrO_2-Y_2O_3-Ta_2O_5. Journal of American Ceramin Society, 1991. 74(12): p. 5.

27. Xu Z., et al., Evolution of high temperature corrosion behavior of $La_2(Zr0.7Ce0.3)_2O_7$ with the addition of Y_2O_3 thermal barrier coatings in contacts with vanadate–sulfate salts. Journal of Alloys and Compounds, 2012. 536: p. 106-112.

28. Yugeswaran S., et al., Initial phase hot corrosion mechanism of gas tunnel type plasma sprayed thermal barrier coatings. Materials Science and Engineering: B, 2012. 177(7): p. 536-542.

29. Li, S., et al.Growth of $YbVO_4$ crystals evolved from hot corrosion reactions of $Yb_2Zr_2O_7$ against V_2O_5 and Na_2SO_4+V_2O_5. Applied Surface Science, 2013. 276: p. 653-659.

30. Huang, H., et al., Evaluation of microstructural evolution of thermal barrier coatings exposed to Na_2SO_4 using impedance spectroscopy. Corrosion Science, 2011. 53(4): p. 1369-1374.

31. Habibi M.H., et al., Evolution of hot corrosion resistance of YSZ, $Gd_2Zr_2O_7$, and $Gd_2Zr_2O_7$+YSZ composite thermal barrier coatings in Na_2SO_4+V_2O_5 at 1050°C. Journal of the European Ceramic Society, 2012. 32(8): p. 1635-1642.

32. Yugeswaran S., et al., Hot corrosion behaviors of gas tunnel type plasma sprayed $La_2Zr_2O_7$ thermal barrier coatings. Journal of the European Ceramic Society, 2012. 32(4): p. 823-834.

33. Xiang J., et al., Synthesis kinetics and thermophysical properties of $La_2(Zr0.7Ce0.3)_2O_7$ ceramic for thermal barrier coatings. Journal of Rare Earths, 2012. 30(3): p. 228-232.

34. Xiang J., et al., Phase structure and thermophysical properties of co-doped $La_2Zr_2O_7$ ceramics for thermal barrier coatings. Ceramics International, 2012. 38(5): p. 3607-3612.

35. Hong-song Z., et al., Influence of Gd_2O_3 addition on thermophysical properties of $La_2Ce_2O_7$ ceramics for thermal barrier coatings. Journal of the European Ceramic Society, 2012. 32(14): p. 3693-3700.

36. Bhattachaya A., et al., Effect of 7YSZ on the long-term stability of $YTaO_4$ doped ZrO_2 system. Journal of the European Ceramic Society, 2011. 31(15): p. 2897-2901.

37. Jones R.L., Vanadate-sulfate Melt Thermochemistry Relating to Hot Corrosion of Thermal Barrier Coatings. Naval Research Laboratory, 1997.

38. Mohan P., et al., Degradation of Yttria-Stabilized Zirconia Thermal Barrier Coatings by Vanadium Pentoxide, Phosphorous Pentoxide, and Sodium Sulfate. Journal of the American Ceramic Society, 2007. 90(11): p. 3601-3607.

39. Habibi, M.H., et al., An Investigation on hot corrosion resistance of plasma sprayed composite YSZ-$Gd_2Zr_2O_7$ and $Gd_2Zr_2O_7$ thermal barrier coayings in simulated turbine environment at 1050 °C, in 12th ASME 2012 International Mechanical Engineering Congress. 2012, ASME: Houston,Texas.

40. Mayo S.R. et. al., The hot corrosion resistance of 20 mol% $YTaO_4$ stabilized tetragonal zirconia and 14 mol% Ta_2O_5 stabilized orthorhombic zirconia for thermal barrier coating applications. Surface and Coating technology, 2002. 160: p. 10.

41. Park S.Y., et al., Microscopic observation of degradation behavior in yttria and ceria stabilized zirconia thermal barrier coatings under hot corrosion. Surface and Coatings Technology, 2005. 190(2-3): p. 357-365.

42. Moldovan M., et al., Tantalum Oxide Coatings as Candidate Environmental Barriers. Journal of Thermal Spray Technology, 2004. 13(1): p. 51-56.

43. Raghavan S. et al. thermal properties of zirconi co-doped with trivalet and pentavalent oxides. Acta Materialia, 2001. 49: p. 11.

44. Pitek F.M. et al.,Opportunities for TBCs in the ZrO_2–$YO_{1.5}$–$TaO_{2.5}$ system. Surface and Coatings Technology, 2007. 201(12): p. 6044-6050.

45. Shen Y., et al., Low thermal conductivity without oxygen vacancies in equimolar $YO_{1.5}$+$TaO_{2.5}$- and $YbO_{1.5}$+$TaO_{2.5}$-stabilized tetragonal zirconia ceramics. Acta Materialia, 2010. 58(13): p. 4424-4431.

46. Schulz U., et al., Some recent trends in research and technology of advanced thermal barrier coatings. Aerospace Science and Technology, 2003. 7: p. 8.

47. Lee J.H., Microstructure and thermal cyclic performance of laser-glazed plasma-sprayed ceria–yttria-stabilized zirconia thermal barrier coatings. Surface and Coatings Technology, 2008. 202(22-23): p. 5607-5612.

48. Han Z., et al., A comparison of thermal shock behavior between currently plasma spray and supersonic plasma spray CeO_2–Y_2O_3–ZrO_2 graded thermal barrier coatings. Surface and Coatings Technology, 2007. 201(9-11): p. 5253-5256.

49. Mohan P., et al., Degradation of free-standing air plasma sprayed CoNiCrAlY coatings by vanadium and phosphorus pentoxides. Surface and Coatings Technology, 2008. 203(5-7): p. 427-431.

50. Chen, Z., et al., Effect of Al_2O_3 overlay on hot-corrosion behavior of yttria-stabilized zirconia coating in molten sulfate-vanadate salt. Thin Solid Films, 2003. 443(1-2): p. 46-52.

51. Rahaman M., et al., Phase stability, sintering, and thermal conductivity of plasma-sprayed ZrO_2–Gd_2O_3 compositions for potential thermal barrier coating applications. Acta Materialia, 2006. 54(6): p. 1615-1621.

52. Xu Q., et al., Rare-Earth Zirconate Ceramics with Fluorite Structure for Thermal Barrier Coatings. Journal of the American Ceramic Society, 2006. 89(1): p. 340-342.

53. Liu Z.G., et al., Densification, Structure, and Thermophysical Properties of Ytterbium-Gadolinium Zirconate Ceramics. International Journal of Applied Ceramic Technology, 2009. 6(4): p. 485-491.

54. Afrasiabi A., et al., A comparative study on hot corrosion resistance of three types of thermal barrier coatings: YSZ, YSZ+Al_2O_3 and YSZ/Al_2O_3. Materials Science and Engineering: A, 2008. 478(1-2): p. 264-269.

55. JoneR.L.,et. al., Hot corrosion studies of zirconia ceramics. Surface and Coatings Technology, 1987. 32(1–4): p. 349-358.

56. Tsai, P.C., at al., High temperature corrosion resistance and microstructural evaluation of laser-glazed plasma-sprayed zirconia/MCrAlY thermal barrier coatings. Surface and Coatings Technology, 2004. 183(1): p. 29-34.

57. Gong, W.B., et al., Microstructures and thermal insulation capability of plasma-sprayed nanostructured ceria stabilized zirconia coatings. Surface and Coatings Technology, 2006. 201(6): p. 3109-3115.

58. Xu Z., et al., Hot corrosion behavior of $La_2Zr_2O_7$ with the addition of Y_2O_3 thermal barrier coatings in contacts with vanadate–sulfate salts. Journal of Alloys and Compounds, 2010. 504(2): p. 382-385.

59. Xu Z., et al., Hot corrosion behavior of rare earth zirconates and yttria partially stabilized zirconia thermal barrier coatings. Surface and Coatings Technology, 2010. 204(21-22): p. 3652-3661.

60. Li S., et al., Hot corrosion behaviour of $Yb_2Zr_2O_7$ ceramic coated with V_2O_5 at temperatures of 600–800°C in air. Corrosion Science, 2010. 52(10): p. 3568-3572.

61. Liu Z.G., et al., High-temperature hot corrosion behavior of gadolinium zirconate by vanadium pentoxide and sodium sulfate in air. Journal of the European Ceramic Society, 2010. 30(12): p. 2707-2713.

62. Liu, Z.G., et al., Hot corrosion behavior of V_2O_5-coated $Gd_2Zr_2O_7$ ceramic in air at 700–850°C. Journal of the European Ceramic Society, 2009. 29(11): p. 2423-2427.

63. Krämer S., et al., Infiltration-Inhibiting Reaction of Gadolinium Zirconate Thermal Barrier Coatings with CMAS Melts. Journal of the American Ceramic Society, 2008. 91(2): p. 576-583.

64. Carre A. et al., Study of Acid/Base Properties of Oxide, Oxide Glass, and Glass-Ceramic Surfaces. Journal of colloid interface science, 1992. 154(1): p. 10.

65. Li, S., et al., Ouyang, Study on hot corrosion reactions between $SmYbZr_2O_7$ ceramic and vanadium pentoxide at temperatures of 600–1000°C in air. Materials Chemistry and Physics, 2011. 130(3): p. 1134-1138.

66. Li S., et al., Hot Corrosion of $(Sm1{-}xYbx)_2Zr_2O_7$ (x=0, 0.5, 1.0) Ceramics Against V_2O_5 Molten Salt in Air at 800°C. International Journal of Applied Ceramic Technology, 2012. 9(1): p. 149-158.

67. Marple B.R., et al., Hot Corrosion of Lanthanum Zirconate and Partially Stabilized Zirconia Thermal Barrier Coatings. Journal of Engineering for Gas Turbines and Power, 2006. 128(1): p. 144.

68. Raghavan C., et al., Synthesis, spheroidization and spray deposition of lanthanum zirconate using thermal plasma process. Surface and Coatings Technology, 2012. 206(13): p. 3017-3035.

69. Yugeswaran, S., et al., Influence of critical plasma spraying parameter (CPSP) on plasma sprayed Alumina–Titania composite coatings. Ceramics International, 2010. 36(1): p. 141-149.

70. Fritsch M., et al., Corrosion of selected ceramic materials in hot gas environment. Journal of the European Ceramic Society, 2006. 26(16): p. 3557-3565.

71. Raghavan C., et al., Thermal cycling behaviour of plasma sprayed lanthanum zirconate based coatings under concurrent infiltration by a molten glass concoction. Ceramics International, 2012.

72. Schulz U., et al., Klaus Fritscher, Christoph Leyens, Review on Advanced EB-PVD Ceramic Topcoats for TBC Applications. International Joutnal of Applied Ceramic Technology , 2004. 1(4): p. 15.

73. Girolamo G., et al., Structure and thermal properties of heat treated plasma sprayed ceria–yttria co-stabilized zirconia coatings. Ceramics International, 2010. 36(3): p. 961-968.

74. Saremi M., et al., An Investigation on Hot Corrosion Resistance of Plasma Sprayed YSZ-Ceria TBC in Na_2SO_4+V_2O_5 at 1050°C, in Supplemental Proceedings. 2011, John Wiley & Sons, Inc. p. 429-437.

75. Brandon J.R., et al.,Thermal properties of ceria and yttria partially stabilized zirconia thermal barrier coatings. Surface and Coatings Technology, 1989. 39–40, Part 1(0): p. 143-151.

76. Srinivasan R., et al. , Ta_2O_5/Nb_2O_5 and Y_2O_3 Co-doped Zirconias for Thermal Barrier Coatings. Journal of American Ceramic Society, 2004. 87(3): p. 7.

77. Bhattacharya A.K., et al., Ta_2O_5–Y_2O_3–ZrO_2 system: Experimental study and preliminary thermodynamic description. Journal of the European Ceramic Society, 2011. 31(3): p. 249-257.

78. Gritzner G. et al.,V_2O_5, Nb_2O_5 and Ta_2O_5 doped zirconia ceramics. Journal of the European Ceramic Society, 1994. 13(5): p. 387-394.

79. Technology,N.I.O.S.A. NIST,Chemical Kinetics Database, http://kinetics.nist.gov/janaf/. 2013.

80. Barin, I., et al., Thermochemical properties of inorganic substances. First ed. 1973: Springer.

81. Luthra K. L., et al., Impurity deposits in gas turbines from fuels coating sodium and vanadium. Journal of Electrochemechal Society:Solid-State Science and technology, 1982. 129(3): p. 8.

82. H. Yokokawa, N.S., T. Kawada, M. Dokiya, Chemical potential diagrams for rare earth-transition metal-oxygen systems :Ln-V-O and Ln-Mn-O systems. Journal of American Ceramic Society, 1990. 73(3): p. 9.

83. Mah A.D., Thermodynamic properties of vanadium and its compounds. Report of investigations / United States Department of the Interior, Bureau of Mines, Number 6727,, 1966.

84. Woo Y. L. , Na_2SO_4-Induced corrosion of Si_3N_4 coated with chemically vapor deposited Ta_2O_5. Journal of American Ceramic Society, 1995. 78(7): p. 4.

85. Hinden J.A. , Etude des systems Na_3AlF_6-Ta_2O_5 ET Na_3AlF_6-$NaTaO_3$. Electrochemical Acta, 1975. 20: p. 5.

86. Kresse G., et al., Ab initio molecular dynamics for liquid metals,. Physical Review B, 1993. 47: p. 4.

87. Furthmüller G.K., et al., Efficiency of ab-initio total energy calculations for metals and semiconductors using a plane-wave basis set. Computational Materials Science, 1996. 6: p. 36.

88. Furthmüller, G.K. et al., Efficient iterative schemes for ab initio total-energy calculations using a plane-wave basis set. physical Review B, 1996. 84: p. 17.

89. VASP 2013 manual, see: http://cms.mpi.univie.ac.at/vasp/.

90. Blöchl P.E., Projector augmented-wave method. physical Review B, 1994. 50: p. 27.

91. Kresse G., at al., From ultrasoft pseudopotentials to the projector augmented-wave method,. Physical Review B, 1999. 59: p. 18.

92. Schadowh H. et al., Investigations on the Quasi-binary system V_2O_5-Ta_2O_5. Crystal recourse technology, 1992. 27: p. 5.

93. Rabiei A. et al., Failure mechanisms associated with the thermally grown oxide in plasma-sprayed thermal barrier coatings. Acta Materialia, 2000. 48: p. 14.

94. Ahmaniemi S., et al., Modified thick thermal barrier coatings: microstructural characterization. Journal of the European Ceramic Society, 2004. 24(8): p. 2247-2258.

95. Cao X.Q., et al., Ceramic materials for thermal barrier coatings. Journal of the European Ceramic Society, 2004. 24(1): p. 1-10.

96. Levi C.G., Emerging materials and processes for thermal barrier systems. Current Opinion in Solid State and Materials Science, 2004. 8(1): p. 77-91.

97. Xie L., et al., Properties and Performance of High-Purity Thermal Barrier Coatings. Journal of Thermal Spray Technology, 2007. 16(5-6): p. 804-808.

98. Ahmaniemi S., et al., Thermal cycling resistance of modified thick thermal barrier coatings. Surface and Coatings Technology, 2005. 190(2-3): p. 378-387.

99. Sreedhar G., et al., Hot corrosion of YSZ/Al_2O_3 dispersed NiCrAlY plasma-sprayed coatings in Na_2SO_4–10 wt.% NaCl melt. Corrosion Science, 2010. 52(8): p. 2592-2602.

100. Haynes J.A., et al., Thermal Cycling Behavior of Plasma-Sprayed Thermal Barrier Coatings with Various MCrAIX Bond Coats. Journal of Thermal Spray Technology, 2000. 9(1): p. 11.

101. Raghavan C., et al., Influence of the intermixed interfacial layers on the thermal cycling behaviour of atmospheric plasma sprayed lanthanum zirconate based coatings. Ceramics International, 2012. 38(5): p. 4081-4096.

102. Braue, W., Environmental stability of the YSZ layer and the YSZ/TGO interface of an in-service EB-PVD coated high-pressure turbine blade. Journal of Materials Science, 2009. 44(7): p. 1664-1675.

103. Afrasiabi A., et al., Hot corrosion control in plasma sprayed YSZ coating by alumina layer with evaluation of microstrcuture and nanoindentation data (H, E). Vacuum, 2012.

104. Yugeswaran S., et al., Hot corrosion behaviors of gas tunnel type plasma sprayed $La_2Zr_2O_7$ thermal barrier coatings. Journal of the European Ceramic Society, 2011: p. 12.

105. Brandon J.R., et al., Phase stability of zirconia-based thermal barrier coatings part II. Zirconia-ceria alloys. Surface and Coatings Technology, 1991. 46(1): p. 91-101.

106. Samaranch B., et al., Synthesis and Characterization of Ta_2O_5-ZrO_2 Systems: Structure,Surface Acidity, and Catalytic Properties. Chemical material, 2007. 19: p. 7.

107. Chen H., et al., Design, Preparation, and Characterization of Graded YSZ/$La_2Zr_2O_7$ Thermal Barrier Coatings. Journal of the American Ceramic Society, 2010.

108. Zhu L., et al., Hot corrosion behaviour of a Ni+CrAlYSiN composite coating in Na_2SO_4–25wt.% NaCl melt. Applied Surface Science, 2013. 268: p. 103-110.

109. Srivastava, M., et al., High temperature oxidation and corrosion behaviour of Ni/Ni–Co–Al composite coatings. Applied Surface Science, 2012. 263: p. 597-607.

110. Huang W., et al., Fabrication of novel thermal barrier coating on polymer composites via the combined sol–gel/sealing treatment process. Applied Surface Science, 2012. 258(22): p. 9058-9066.

111. Fourmond, C., et al., Characterisation of thermal barrier coatings and ultra high temperature composites deposited in a low pressure plasma reactor. Journal of the European Ceramic Society, 2011. 31(13): p. 2295-2302.

112. Keyvani A., et al., Oxidation resistance of YSZ-alumina composites compared to normal YSZ TBC coatings at 1100°C. Journal of Alloys and Compounds, 2011. 509(33): p. 8370-8377.

113. Wang J., et al., The structure, thermal expansion coefficient and sintering behavior of Nd_3+-doped $La_2Zr_2O_7$ for thermal barrier coatings. Journal of Alloys and Compounds, 2009. 476(1-2): p. 89-91.

114. Morks M.F., et al., Microscopic observation of laser glazed yttria-stabilized zirconia coatings. Applied Surface Science, 2010. 256(21): p. 6213-6218.

115. Vourlias G., et al., Plasma-sprayed YSZ coatings: Microstructural features and resistance to molten metals. Journal of Alloys and Compounds, 2009. 483(1-2): p. 382-385.

116. Drexler J.M., et al., Air-plasma-sprayed thermal barrier coatings that are resistant to high-temperature attack by glassy deposits. Acta Materialia, 2010. 58(20): p. 6835-6844.

117. Keyvani, A., et al., An investigation on oxidation, hot corrosion and mechanical properties of plasma-sprayed conventional and nanostructured YSZ coatings. Surface and Coatings Technology, 2011. 206(2-3): p. 208-216.

118. Mahdipoor M.S., et al., Comparative Study of Hot Corrosion Behavior of Plasma Sprayed Yittria and Ceria Stabilized Zirconia Thermal Barrier Coatings in Na_2SO_4+V_2O_5 at 1050°C, in Supplemental Proceedings. 2011, John Wiley & Sons, Inc. p. 715-723.

119. Goyal G., et al., Effect of superficially applied ZrO_2 inhibitor on the high temperature corrosion performance of some Fe-, Co- and Ni-base superalloys. Applied Surface Science, 2008. 254(20): p. 6653-6661.

120. Tsaur, C.-C., et al., The hot corrosion of 310 stainless steel with pre-coated $NaCl/Na_2SO_4$ mixtures at 750°C. Materials Chemistry and Physics, 2005. 89(2-3): p. 445-453.

121. Singh H., et al., Some studies on hot corrosion performance of plasma sprayed coatings on a Fe-based superalloy. Surface and Coatings Technology, 2005. 192(1): p. 27-38.

122. Bala N., et al., Accelerated hot corrosion studies of cold spray Ni–50 Cr coating on boiler steels. Materials & Design, 2010. 31(1): p. 244-253.

123. Gurappa I., et al., Protection of titanium alloy components against high temperature corrosion. Materials Science and Engineering: A, 2003. 356(1-2): p. 372-380.

124. Bhatia R., et al., Hot Corrosion Studies of HVOF-Sprayed Coating on T-91 Boiler Tube Steel at Different Operating Temperatures. Journal of Materials Engineering and Performance, 2013.

125. Mohammadi M., et al., Characterization and hot corrosion performance of LVPS and HVOF-CoNiCrAlYSi coatings. Vacuum, 2012. 86(10): p. 1458-1464.

126. Mei H., et al., Corrosion mechanism of a NiCoCrAlTaY coated Mar-M247 superalloy in molten salt vapour. Corrosion Science, 2012. 55: p. 201-204.

127. Cho S.H., et al., Corrosion behaviour of Y_2O_3–ZrO_2 coatings on IN713LC in a LiCl–Li_2O molten salt. Corrosion Science, 2010. 52(7): p. 2353-2364.

128. Ramachandran C.S., et al., On the cyclic hot corrosion behaviour of atmospheric plasma sprayed Lanthanum Zirconate based coatings in contact with a mixture of sodium sulphate and vanadate salts: A comparison with the traditional YSZ duplex and NiCrAlY coated samples. Vacuum, 2013. 97: p. 81-95.

129. Vassen R., et al., Recent Developments in the Field of Thermal Barrier Coatings. Journal of Thermal Spray Technology, 2009. 18(2): p. 181-186.

130. Stöver D., et al., New Material Concepts for the Next Generation of Plasma-Sprayed Thermal Barrier Coatings. Journal of Thermal Spray Technology, 2004. 13(1): p. 76-83.

131. Vaben R., et al., New thermal barrier coatings based on pyrochlore/YSZ double-layer systems. International Journal of Ceramic Technology., 2004. 1(4): p. 11.

132. Xu, Z., et al., Thermal barrier coatings of rare earth materials deposited by electron beam-physical vapor deposition. Journal of Alloys and Compounds, 2010. 508(1): p. 94-98.

133. Cao X. Q., et al., Thermal Stability of Lanthanum Zirconate Plasma-Sprayed Coating. Journal of American Ceramic Society, 2001. 84(9): p. 5.

134. Pyda W., et al., A study on preparation of Tetragonal Zirconia Polycrystals (TZP) in the TiO_2+Y_2O_3+ZrO_2 system. Ceramics International, 1992. 18(5): p. 321-326.

135. Diaz P., et al., Microstructural changes and phase transformations in a plasma-sprayed zirconia-yttria-titania thermal barrier coating. Surface and Coating technology, 1996. 82: p. 7.

136. Schaedler, T.A., et al., Phase equilibria in the TiO_2–$YO_{1.5}$–ZrO_2 system. Journal of the European Ceramic Society, 2008. 28(13): p. 2509-2520.

137. Díaz P., et al., Transmission Electron Microscope Characterization of a Plasma-Sprayed ZrO_2-Y_2O_3-TiO_2Thermal Barrier Coating. Material Characterization, 1998. 41: p. 13.

Appendix A: Letters of Permission to Use Published Material

The Permissions from Springer and Elsevier publishing companies are presented in the following pages:

Copyright Clearance Center RightsLink®

Home | Account Info | Help

Title: Evolution of hot corrosion resistance of YSZ, Gd2Zr2O7, and Gd2Zr2O7+YSZ composite thermal barrier coatings in Na2SO4+V2O5at 1050°C
Author: M.H. Habibi,Li Wang,S.M. Guo
Publication: Journal of the European Ceramic Society
Publisher: Elsevier
Date: July 2012
Copyright © 2012, Elsevier

Logged in as:
Mohammad Hamed habibi
LOGOUT

Order Completed

Thank you very much for your order.

This is a License Agreement between Mohammad Hamed habibi ("You") and Elsevier ("Elsevier"). The license consists of your order details, the terms and conditions provided by Elsevier, and the payment terms and conditions.

Get the printable license.

License Number	3298371361042
License date	Dec 29, 2013
Licensed content publisher	Elsevier
Licensed content publication	Journal of the European Ceramic Society
Licensed content title	Evolution of hot corrosion resistance of YSZ, Gd2Zr2O7, and Gd2Zr2O7+YSZ composite thermal barrier coatings in Na2SO4+V2O5at 1050°C
Licensed content author	M.H. Habibi,Li Wang,S.M. Guo
Licensed content date	July 2012
Licensed content volume number	32
Licensed content issue number	8
Number of pages	8
Type of Use	reuse in a thesis/dissertation
Portion	full article
Format	both print and electronic
Are you the author of this Elsevier article?	Yes
Will you be translating?	No
Title of your thesis/dissertation	HOT CORROSION BEHAVIOUR OF NEW CANDIDATES FOR THERMAL BARRIER COATINGS APPLICATION IN TURBINE SIMULATED ENVIRONMENTS
Expected completion date	May 2014
Estimated size (number of pages)	130
Elsevier VAT number	GB 494 6272 12
Permissions price	0.00 USD
VAT/Local Sales Tax	0.00 USD / 0.00 GBP
Total	0.00 USD

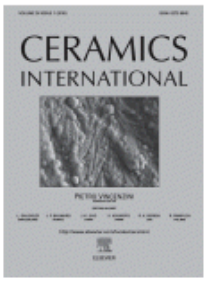

Title: Phase stability and hot corrosion behavior of ZrO2–Ta2O5compound in Na2SO4–V2O5mixtures at elevated temperatures

Author: M.H. Habibi,Shizhong Yang,S.M. Guo

Publication: Ceramics International

Publisher: Elsevier

Date: April 2014

Order Completed

Thank you very much for your order.

This is a License Agreement between Mohammad Hamed habibi ("You") and Elsevier ("Elsevier"). The license consists of your order details, the terms and conditions provided by Elsevier, and the payment terms and conditions.

Get the printable license.

License Number	3298370761005
License date	Dec 29, 2013
Licensed content publisher	Elsevier
Licensed content publication	Ceramics International
Licensed content title	Phase stability and hot corrosion behavior of ZrO2–Ta2O5compound in Na2SO4–V2O5mixtures at elevated temperatures
Licensed content author	M.H. Habibi,Shizhong Yang,S.M. Guo
Licensed content date	April 2014
Licensed content volume number	40
Licensed content issue number	3
Number of pages	7
Type of Use	reuse in a thesis/dissertation
Portion	full article
Format	both print and electronic
Are you the author of this Elsevier article?	Yes
Will you be translating?	No
Title of your thesis/dissertation	HOT CORROSION BEHAVIOUR OF NEW CANDIDATES FOR THERMAL BARRIER COATINGS APPLICATION IN TURBINE SIMULATED ENVIRONMENTS
Expected completion date	May 2014
Estimated size (number of pages)	130
Elsevier VAT number	GB 494 6272 12
Permissions price	0.00 USD
VAT/Local Sales Tax	0.00 USD / 0.00 GBP
Total	0.00 USD

Order Completed

Thank you very much for your order.

This is a License Agreement between Mohammad Hamed habibi ("You") and Elsevier ("Elsevier"). The license consists of your order details, the terms and conditions provided by Elsevier, and the payment terms and conditions.

Get the printable license.

License Number	3298370986760
License date	Dec 29, 2013
Licensed content publisher	Elsevier
Licensed content publication	Corrosion Science
Licensed content title	An investigation on hot corrosion behavior of YSZ-Ta2O5in Na2SO4+V2O5salt at 1100°C
Licensed content author	M.H. Habibi,Li Wang,Jiandong Liang,S.M. Guo
Licensed content date	October 2013
Licensed content volume number	75
Number of pages	6
Type of Use	reuse in a thesis/dissertation
Portion	full article
Format	both print and electronic
Are you the author of this Elsevier article?	Yes
Will you be translating?	No
Title of your thesis/dissertation	HOT CORROSION BEHAVIOUR OF NEW CANDIDATES FOR THERMAL BARRIER COATINGS APPLICATION IN TURBINE SIMULATED ENVIRONMENTS
Expected completion date	May 2014
Estimated size (number of pages)	130
Elsevier VAT number	GB 494 6272 12
Permissions price	0.00 USD
VAT/Local Sales Tax	0.00 USD / 0.00 GBP
Total	0.00 USD

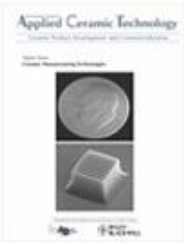

Title: Evolution of Hot Corrosion Behavior of YSZ-Ta2O5 Composites with Different YSZ/Ta2O5 Ratios

Author: Hamed Habibi,Shengmin Guo

Publication: International Journal of Applied Ceramic Technology

Publisher: John Wiley and Sons

Date: Jan 21, 2014

Order Completed

Thank you very much for your order.

This is a License Agreement between Mohammad Hamed habibi ("You") and John Wiley and Sons ("John Wiley and Sons"). The license consists of your order details, the terms and conditions provided by John Wiley and Sons, and the payment terms and conditions.

Get the printable license.

License Number	3332590320807
License date	Feb 19, 2014
Licensed content publisher	John Wiley and Sons
Licensed content publication	International Journal of Applied Ceramic Technology
Licensed content title	Evolution of Hot Corrosion Behavior of YSZ-Ta2O5 Composites with Different YSZ/Ta2O5 Ratios
Licensed copyright line	© 2014 The American Ceramic Society
Licensed content author	Hamed Habibi,Shengmin Guo
Licensed content date	Jan 21, 2014
Start page	n/a
End page	n/a
Type of use	Dissertation/Thesis
Requestor type	Author of this Wiley article
Format	Print and electronic
Portion	Full article
Will you be translating?	No
Title of your thesis / dissertation	HOT CORROSION BEHAVIOUR OF NEW CANDIDATES FOR THERMAL BARRIER COATINGS APPLICATION IN TURBINE SIMULATED ENVIRONMENTS
Expected completion date	May 2014
Expected size (number of pages)	130
Total	0.00 USD

Copyright Clearance Center RightsLink®

Home | Account Info | Help

Title: The hot corrosion behavior of plasma sprayed zirconia coatings stabilized with yttria, ceria, and titania in sodium sulfate and vanadium oxide

Author: M. H. Habibi,S. M. Guo

Publication: Materials and Corrosion

Publisher: John Wiley and Sons

Date: Dec 21, 2013

Logged in as:
Mohammad Hamed habibi
Account #:
3000734103

LOGOUT

Order Completed

Thank you very much for your order.

This is a License Agreement between Mohammad Hamed habibi ("You") and John Wiley and Sons ("John Wiley and Sons"). The license consists of your order details, the terms and conditions provided by John Wiley and Sons, and the payment terms and conditions.

Get the printable license.

License Number	3298380376644
License date	Dec 29, 2013
Licensed content publisher	John Wiley and Sons
Licensed content publication	Materials and Corrosion
Licensed content title	The hot corrosion behavior of plasma sprayed zirconia coatings stabilized with yttria, ceria, and titania in sodium sulfate and vanadium oxide
Licensed copyright line	© 2013 WILEY-VCH Verlag GmbH & Co. KGaA, Weinheim
Licensed content author	M. H. Habibi,S. M. Guo
Licensed content date	Dec 21, 2013
Start page	n/a
End page	n/a
Type of use	Dissertation/Thesis
Requestor type	Author of this Wiley article
Format	Print and electronic
Portion	Full article
Will you be translating?	No
Total	0.00 USD

Vita

Mohammad Hamed Habibi was born in Shiraz, Iran in March 1984. He received his BS in Material Science and Engineering in 2007. Then he continued his education as graduate student in Materials/Corrosion Engineering and he received his MS from university of Tehran in 2010. He worked as material engineer for Supplier of Automotive Part Company (SAPCO) in Tehran, Iran. He joined Turbine Innovation and Energy Research Center (TIER), Mechanical Engineering Department, Louisiana State University, Baton Rouge, LA, USA where he started his Ph.D. research under the supervision of Dr. Shengmin Guo in 2010. Mohammad Hamed Habibi has made technical contributions in several Materials Engineering areas, including advanced materials selection, high temperature corrosion and thermal barrier coatings (TBC) and he has authored 5 scientific articles in internationally peer-reviewed journals. He also attended several academic conferences and presented several papers. He is a member of American Society of Mechanical Engineers (AMSE), American society of Materials Engineers (ASM), NACE International corrosion Institute, Phi Kappa Phi honor society and Gold Key International honor society.

Mohammad Hamed Habibi is expected to receive his Doctor of Philosophy degree at the 2014 Spring Commencement.